HYDROGEN AND MERCURY EMBRITTLEMENT OF SELECTED NICKEL-BASED ALLOYS

By

JAMES ARTHUR MORRIS

Bachelor of Science

Oklahoma State University

Stillwater, Oklahoma

1982

Submitted to the Faculty of the Graduate College
of the Oklahoma State University
in partial fulfillment of the requirements
for the Degree of
MASTER OF SCIENCE
May, 1984

HYDROGEN AND MERCURY EMBRITTLEMENT OF

SELECTED NICKEL-BASED ALLOYS

Thesis Approved:

C E Price
Thesis Adviser

James K. Good

R F Lowery

Norman N Durham
Dean of the Graduate College

ACKNOWLEDGMENTS

I would like to express my appreciation to those who have helped during this study. Special thanks to Dr. C. E. Price, my major adviser, for his guidance and encouragement throughout my undergraduate and graduate studies at Oklahoma State University. Without his wisdom and willing ear, this study would not have been possible. Thanks to Dr. Keith Good and Dr. Richard Lowery for graciously serving on my committee.

I would also like to thank Dr. Keith Good, Mr. Leland Traylor, and Mr. Robert Fredell, for their previous work in the embrittlement of nickel alloys.

The School of Mechanical Engineering is gratefully acknowledged for funding a portion of my research and providing a teaching assistantship.

Finally, I would like to thank my wife, Rebecca, without whose support and encouragement graduate study would not have been possible.

TABLE OF CONTENTS

LIST OF TABLES

LIST OF FIGURES

CHAPTER I

INTRODUCTION

The purpose of this investigation is to explore the plastic deformation characteristics of sample nickel base alloys that might relate to their susceptibility to embrittlement by hydrogen. This investigation builds upon previous studies in the same laboratory by co-authors Price and Good [1, 2], by Traylor [3, 4], and by Fredell [5]. Nickel is an essential ingredient of all superalloys and indeed most superalloys are based upon nickel. The superalloys are the metallic alloys used in the most demanding situations possible for metals. Superalloys are used for rotating components in high temperature turbines, for critical tubing in nuclear reactors, and for down hole tubing in sour gas wells [6]. Hydrogen embrittlement has long been recognized as a problem with high strength ferritic steels and at temperatures of 200 to 250°K austenitic stainless steels are affected also. The superalloys combine good mechanical properties, formability, and weldability with corrosion resistance. They are being used increasingly in the oil industry to combat corrosion, for example, in deep and sour gas wells [7]. With such applications have come an increasing awareness that nickel base alloys can be embrittled by hydrogen also. One pertinent question is whether the embrittlement is a surface or volume process. Liquid metal embrittlement (LME) must be a surface or near surface phenomenon and nickel has alloys which are affected by mercury. LME involves specific couples of solid and liquid

metals. More than 100 examples are known [8]. Usually LME couples have limited mutual solubility. Accordingly, embrittlement by liquid mercury is studied for comparison.

The alloys studied are Nickel 200 (UNS N02200) commercially pure metal, Monel 400 (UNS N04400), Inconel 600 (UNS N06600), and Incoloy 800 (UNS N08800). The latter are representative of major alloy groups. Monel 400 (UNS N04400) is chosen as the most embrittled alloy [1, 3, 5] while Inconel 600 and Incoloy 800 exhibited interested properties in the preliminary study by Price and Good [1, 2]. Each of the alloys studied is chemically the simplest of each alloy group, thereby allowing analysis of these solid solution alloys to be more straightforward.

The embrittlement of these alloys relates at least in part to the chemistry of the alloys, but surely relates also to the mechanical properties such as strain hardening capability, slip character, strain rate sensitivity, yield strength, and cold work. Thus, as previously mentioned, in steels it is the high strength alloys that are affected, meaning that the same steel can be heat treated to different strength levels but only be embrittled when harder than about 22 R_c [10].

This thesis describes a comparison of the tensile test characteristics of the four alloys tested in air, hydrogen, and mercury. In the first part, tensile tests were carried out in air with careful documentation to obtain, for example, complete engineering stress versus engineering strain curves and strain hardening exponents. In the second place, interrupted tests were carried out in hydrogen and mercury to observe the plastic deformation sequence (slip character, rumpling, etc.) and especially crack initiation and propagation. A third test sequence involved

chosen fatigue tests in the environments, again with interruptions for observations in some instances. The relevant aspect of fatigue tests is that cracks are initiated at stress levels low compared to the tensile strength. As a consequence of matters arising from the foregoing, related additional tests were done on cold worked metal and on alloy specimens of different grain sizes.

The findings of Price and Good [1, 2], Traylor [3, 4], and Fredell [5] are expanded in this study to give a more detailed understanding of alloys in general and simple nickel-based superalloys in particular. Occasionally, their test data are used directly, though their results were confirmed by reproducing some representative tests. The goal of this study is to obtain a clearer understanding of the hydrogen embrittlement (HE) of commercial superalloys.

CHAPTER II

REVIEW OF LITERATURE

Introduction

This study is a direct result of work done by Traylor [3] and Fredell [5]; therefore, their reviews of the literature are directly applicable. Consequently, general background material and detailed explanation of leading theories will not be included. A short review of the pertinent theories and a review of the work by Price and Good [1, 2], Traylor [6], and Fredell [5] are included.

Embrittlement by Liquid Metals

Liquid metal embrittlement (LME) is well documented yet not clearly understood. Numerous mechanisms have been proposed to explain LME. Some of the significant work is reviewed here.

Reduction in Cohesion Model

A leading theory of LME advanced by Westwood and Kamdar [10, 11] and Stoloff and Johnston [12] suggests that the liquid metal causes an adsorption-induced reduction in the cohesive strength between the base metal atoms at the crack tip (Figure 1). As the sample is stressed, the liquid metal atom B is spontaneously adsorbed at the crack tip, reducing the strength of the bond $A\text{-}A_o$. When the stress reaches a new, lower critical

Figure 1. Schematic Representation of the Displacement of Atoms at the Tip of a Crack

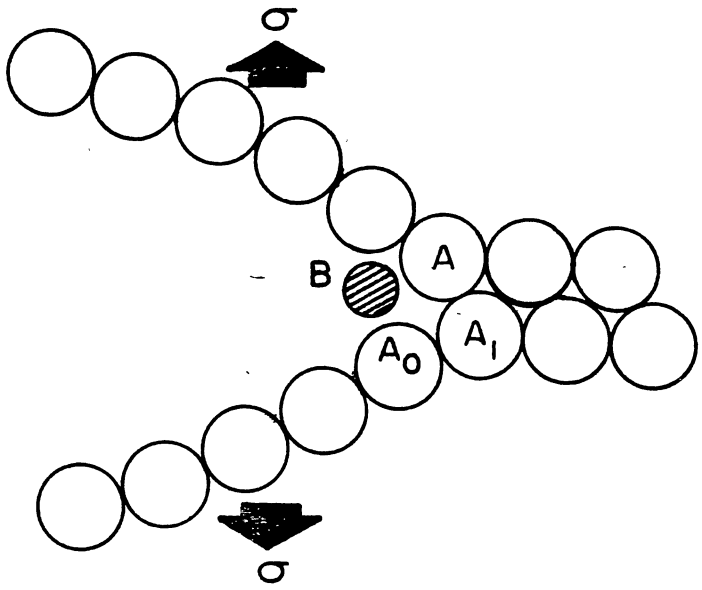
σ
B
A
A_0
A_1
σ

stress, the bond breaks and the crack advances to bond $A\text{-}A_1$, where the sequence repeats. Therefore, Kamdar [11] proposed that LME is a special case of brittle fracture, and that the metallurgical and mechanical effects on LME can be attributed to the principles of brittle fracture.

The general criterion for predicting the ductile or brittle behavior of solids is discussed by Kamdar [11] who references Gilman [13] and Kelly et al. [14]. The argument presented is as follows: An equilibrium crack in a solid subjected to an increasing force will propagate in a fully brittle manner if the ratio of the largest tensile stress, σ, in the vicinity of the crack tip to the largest shear stress, τ, on the most favorably-oriented slip plane near the crack tip is greater than the ratio of the ideal cleavage stress, σ_{max}, to the ideal shear stress, τ_{max}. If the converse is the case, crack propagation will be accompanied by some plastic flow. As a rough approximation for metals, if $\sigma_{max}/\tau_{max} \leq 10$, failure will be predominately by cleavage; if $\sigma_{max}/\tau_{max} > 10$, failure will be predominately by shear. The ratio σ_{max}/τ_{max} is determined by type of bonding in the solid (i.e., ionic, metallic, etc.), by crystal structure, and by Poisson's ratio.

For the reduction in cohesion model to be considered valid, the following effects should be observed for LME:

1. Strain rate effects. Kamdar [11] predicted that an increase in strain rate should increase embrittlement because of an increase in the ductile-to-brittle transition temperature.

2. Grain size effects. In view of the brittle fracture idea, the fracture stress should vary linearly with $d^{-\frac{1}{2}}$, where d is the material grain size [11]. This means that refinement of grain size decreases embrittlement by decreasing the lengths of dislocation pile-ups.

Stress-Aided Diffusion Penetration Model

Originally proposed by Krishtal [15], this mechanism for LME involves stress-aided diffusion of embrittler atoms along the grain boundaries of the base metal. In tests using Indium as an embrittler on 4140 steel, Gordon and An [16] developed the Krishtal idea into a two-step process, whereby (1) the adsorbed embrittler atoms change to the dissolved state, and (2) the dissolved embrittler atoms diffuse along grain boundaries. The embrittler atoms lower crack resistance and decrease slip in the penetrated zones. Crack nucleation occurs when embrittler atoms have penetrated in sufficient quantity to a critical depth. The embrittlement process would be thermally activated and stress dependent. With the stress-aided diffusion penetration model, the following effects should be expected:

1. Delayed failure should occur above some critical stress after the penetration zones have developed.

2. Strain rate effects. According to Gordon and An [16, p. 458], increasing strain rates require higher temperatures for embrittlement to occur. This is to allow "sufficient volume diffusion to dissipate grain boundary penetration zones." Consequently, at constant temperature, increasing strain rate should decrease LME in a normally strain rate insensitive material.

3. Grain size effects. Refining the grain size should decrease LME by reducing the concentrations of embrittler atoms at dislocation pile-ups at grain boundaries due to the increased proportion of grain boundaries to bulk metal.

4. Cold work effects. The extra dislocations from cold work should reduce embrittlement by providing channels to syphon embrittler atoms from the grain boundaries, thereby inhibiting the concentration of embrittler atoms to a critical level.

Adsorption Enhanced Localized Shear

Lynch [17, 18], based largely upon fractographic studies using cadmium, nickel, aluminum alloys, and steels, has suggested that LME, and perhaps HE too, is a consequence of adsorption enhanced localized shear, viz. liquid metal induced lowering of the shear modulus. The role of the embrittler atom is to facilitate dislocation nucleation, thereby concentrating plasticity into narrow zones at the crack tip. LME has been observed to occur in amorphous metals, occurring by intense shear on surfaces inclined at approximately 45° to the stress axis [19]. HE has also been found in amorphous alloys [20, 21]. This model is similar to the reduction in cohesion model by Kamdar [11]. Lynch has recently developed his model further in a comparative study of HE and LME embrittlement in D6ac steel [22].

Embrittlement by Hydrogen

Hydrogen embrittlement in steels is a well documented phenomenon and the subject of extensive research. A recent review is by Thompson and Bernstein [23]. An even more recent study by Vehoff and Rothe [24], studied gaseous hydrogen embrittlement in Iron-Silicon and Nickel single crystals. They concluded that the fracture process occurred within 100 nm of cracktip. Numerous mechanisms have been suggested to account for HE in metals. Some of these depend on diffusion into the metal lattice

[17]. In nickel and its alloys, this volume effect is unlikely because the diffusivity of hydrogen in nickel at 25°C is only ~5×10^{-14} m^2/s. A few of the leading theories of HE are condensed below.

Hydrogen-Assisted Cracking Model

Beachem [25], in tests on steel, found a broad range of fractographic features which were dependent upon the stress intensity at the crack tip. Therefore, he suggested that concentrated hydrogen dissolved in the metal lattice just ahead of the crack tip enhances the deformation process by unlocking dislocations and allowing them to move at lower stress levels. He found a crack progression sequence of intergranular to transgranular tearing and finally to microvoids with increasing stress intensity. His findings were significant because he showed hydrogen-assisted cracking was not identified with one specific type of fracture surface.

Planar Pressure Mechanism

Zapffe [26] and Tetelman and Robertson [27] postulated that high pressure developed within internal hydrogen gas pores of hydrogen-charged materials causes cracking. This theory cannot explain the embrittlement of steel by low pressure hydrogen because high pressures could not develop within the metal [28].

Reduction of Surface Energy Model

Petch and Stables [29] proposed that diffused hydrogen reduces the energy necessary to form free surfaces. Since this would not provide sufficient reduction in energy to propagate a crack, this cannot be a significant effect in HE.

Effect of Grain Boundary Segregation

In tests on nickel-copper alloys ranging from 10 to 67 percent nickel, Costas [30] found that phosphorus content had an effect on the alloys' susceptibility to mercury embrittlement. Segregation of the phosphorus to grain boundaries by furnace cooling improved the alloys' resistance to embrittlement by mercury.

Funkenbusch, Heldt, and Stein [31] confirmed the earlier work by Costas [30] for Monel 400. Specimens were annealed at 900°C and either quenched or furnace cooled. Auger analysis showed phosphorus concentration at grain boundaries in furnace cooled samples to be twice that of quenched samples. Funkenbusch, Heldt, and Stein postulated that the increased phosphorus concentration at grain boundaries decreased the susceptibility to HE and mercury embrittlement due to increased packing efficiency, and hence less adsorption.

Precursory Studies

Tensile Fracture of Nickel-Based Alloys in Mercury

Price and Good [1] performed tensile tests on a range of nickel-based alloys to determine their relative susceptibility to mercury embrittlement at room temperature. Results indicated that all the alloys were embrittled by mercury. The relative susceptibility by category from most to least was Monel, Nickel, Inconel, and Incoloy. Some alloys showed a progression in fractography from intergranular to transgranular to micro-void coalescence across the cross section. Relative embrittlement of the alloys appeared not to correlate with mechanical properties or

stacking fault energies but perhaps with iron content. The alloys with higher iron content were least embrittled.

Fatigue Behavior of Nickel-Based Alloy in Mercury

Price and Good [2] investigated the fatigue behavior of selected nickel-based alloys in liquid mercury at room temperature. For alternating tension ($R = 0$), it was found that the fatigue life was always less in mercury and that a different fracture mode resulted. The alloys, Nickel 200, Inconel 600, Incoloy 800, and Incoloy 825, that failed to show intergranular fracture in slow strain rate tensile tests did so in fatigue testing. In general, crack propagation began intergranular but eventually became transgranular.

Hydrogen Embrittlement of Nickel 200

Traylor [3] used slow strain rate tensile tests and fatigue tests to explore hydrogen embrittlement of Nickel 200 at room temperature. It was found that only dynamic charging with hydrogen led to embrittlement. There was no loss of tensile strength in the embrittled material. A crack progression sequence, beginning at the surface, was identified as intergranular cracking, non-crystallographic transgranular cracking, crystallographic transgranular cracking, and thence microvoid coalescence. This behavior closely paralleled the behavior of Inconel 600 in mercury observed by Price and Good [1, 2]. It was deduced that HE must be substantially a surface phenomenon. Interestingly, hydrogen was found to be a slightly more potent embrittling agent than mercury.

Hydrogen and Mercury Embrittlement of Monel Alloys

Traylor [3] performed slow strain rate tensile tests and alternating tension fatigue tests on Monel 400, Monel 405, and Monel K500 alloys at room temperature in air, in mercury, and in hydrogen. While mercury was found to be a more severe environment than hydrogen, fractures were initially intergranular for all alloys in both embrittling environments for annealed and cold worked samples. In light of similar fractography and allowing that mercury embrittlement must be a surface phenomenon, hydrogen embrittlement must also be a surface phenomenon.

Some Factors Affecting Hydrogen and Mercury Embrittlement of Monel 400

Fredell [5] used tensile tests and alternating tension fatigue tests to study the effects of strain rate, grain size, and cold work on hydrogen and mercury embrittlement of Monel 400 at room temperature. Significant observations were:

1. There is a loss in tensile strength.
2. A crack propagation sequence occurred of intergranular to transgranular and sometimes to microvoid coalescence.
3. Mercury is a more potent embrittling agent than hydrogen.
4. Secondary (longitudinal) cracking is common.
5. Embrittlement occurs in dynamic loading, as distinct from static, only.
6. In mercury, though perhaps not in hydrogen, large grain size inhibits embrittlement.

7. In mercury, slower strain rates enhanced embrittlement.

8. Cold work decreased embrittlement.

CHAPTER III

EXPERIMENTAL PROCEDURE

The Materials

The materials chosen are representative of various categories of nickel-based alloys of varying complexity. The alloys chosen are Nickel 200 (UNS N02200), Monel 400 (UNS N04400), Inconel 600 (UNS N06600), and Incoloy 800 (UNS N08800).

Nickel 200 (UNS N02200) is commercially pure wrought nickel of at least 99.0 percent purity. It has good mechanical properties and excellent corrosion resistance. Typical applications are food processing equipment and caustic handling equipment and piping.

Monel 200 (UNS N04400) is a nickel-copper alloy. It is characterized by high strength, weldability, excellent corrosion resistance, and toughness over a wide temperature range. Typical applications are valves and pumps, process vessels and piping, and boiler feedwater heaters and other heat exchangers.

Inconel 600 (UNS N06600) is a standard engineering material for use in severely corrosive environments at elevated temperatures. With a combination of high strength and workability, and oxidation resistance to 2150°F, typical applications are carburizing baskets, jet engine combustion liners, and nuclear reactors.

The last alloy chosen, Incoloy 800 (UNS N08800), is a nickel-iron-chromium alloy. The alloy is characterized by high strength and resistance to oxidation and carburization at elevated temperatures. Typical applications are heat exchangers, carburizing fixtures, and electric range heating element sheathing.

Typical mechanical properties for all four alloys may be found in Tables I through IV [6]. The chemical analysis of the alloys tested may be found in Table V, and the as-received mechanical properties may be found in Table VI.

All specimens were machined from one-half inch diameter rod. The five-inch long specimens were of two geometries. For tensile tests, the samples had a one-quarter inch diameter constant cross section and a gage length of either one inch or one-half inch. The short gage length was used to minimize the size of the environmental chambers. Tests in air were repeated with smaller and larger diameter specimens to explore possible variation of results with diameter. Tests in air were also repeated with varying degrees of anneal to explore variation of results due to annealing cycle. For fatigue tests, the central region was gradually decreased to one-quarter inch in diameter at the center. Figure 2 illustrates the specimen geometry. This geometry is commonly used in stress corrosion cracking studies [32]. The principle behind the geometry was to localize the fracture zone while avoiding a significant stress concentration. Nickel 200 and Monel 400 samples received a 600 grit finish and then were chemically polished [33]. Inconel 600 and Incoloy 800 received a 600 grit finish and then were mechanically polished to a finish adequate for surface observations in an optical microscope.

TABLE I

ROOM TEMPERATURE MECHANICAL PROPERTIES OF NICKEL 200

Temper	Tensile Strength (kpsi)	Yield Strength (0.2% Offset, kpsi)	Elongation in 2 In., %	Hardness (Brinell)
Hot-Finished	50-60	10-25	60-40	75-100
Cold-Drawn	60-100	35-90	35-10	125-200
Annealed	50-60	10-25	60-40	75-100

TABLE II

ROOM TEMPERATURE MECHANICAL PROPERTIES OF MONEL 400

Temper	Tensile Strength (kpsi)	Yield Strength (0.2% Offset, kpsi)	Elongation in 2 In., %	Hardness (Brinell)
Hot-Finished	80-100	40-100	60-30	140-241
Cold-Drawn, Stress Relieved	84-120	55-100	40-22	160-225
Annealed	70-90	25-50	60-35	110-149

TABLE III

ROOM TEMPERATURE MECHANICAL PROPERTIES OF INCONEL 600

Temper	Tensile Strength (kpsi)	Yield Strength (0.2% Offset, kpsi)	Elongation in 2 In., %	Hardness (Brinell)
Hot-Finished	85-120	35-90	50-25	140-217
Cold-Drawn	105-150	80-125	30-10	180-300
Annealed	80-100	30-50	55-35	120-170

TABLE IV

ROOM TEMPERATURE MECHANICAL PROPERTIES OF INCOLOY 800

Temper	Tensile Strength (kpsi)	Yield Strength (0.2% Offset, kpsi)	Elongation in 2 In., %	Hardness (Brinell)
Hot-Finished	80-120	35-90	50-25	140-217
Cold-Drawn	100-150	75-125	30-10	180-300
Annealed	75-100	30-60	60-30	120-184

TABLE V

CHEMICAL COMPOSITION OF THE ALLOYS TESTED

Alloy	Heat No.	Ni	C	Mn	Fe	S	Si	Cu	Ce	AL	Ti
Nickel 200 (UNS N02200)	N72J5A	99.64	0.07	0.25	0.01	0.001	0.02	0.01	---	---	---
Monel 400 (UNS N04400)	M9631B	65.71	0.16	1.13	1.60	0.009	0.23	31.15	---	0.013	---
Inconel 600 (UNS N06600)	NX2830	73.75	0.09	0.51	9.13	0.003	0.19	0.36	15.97	---	---
Incoloy 800 (UNS N08800)	HH0054A	32.28	0.07	0.94	43.85	0.001	0.35	0.34	21.23	0.46	0.38

TABLE VI

AS-RECEIVED MECHANICAL PROPERTIES OF ALLOYS TESTED

Alloy	Heat No.	Hardness	Yield Strength (0.2% Offset, kpsi)	Tensile Strength (kpsi)	Percent Elongation	Percent Reduction of Area
Nickel 200 (UNS N02200)	N72J5A	$98R_B$	105.7	105.8	17	74
Monel 400 (UNS N04400)	M9631B	$99R_B$	97.5	117.7	25	64
Inconel 600 (UNS N06600)	NX2830	$29R_C$	154.9	158.6	11	46
Incoloy 800 (UNS N08800)	HH0054A*					

*Properties not supplied.

Figure 2. Specimen Geometry for Embrittlement Testing in Fatigue

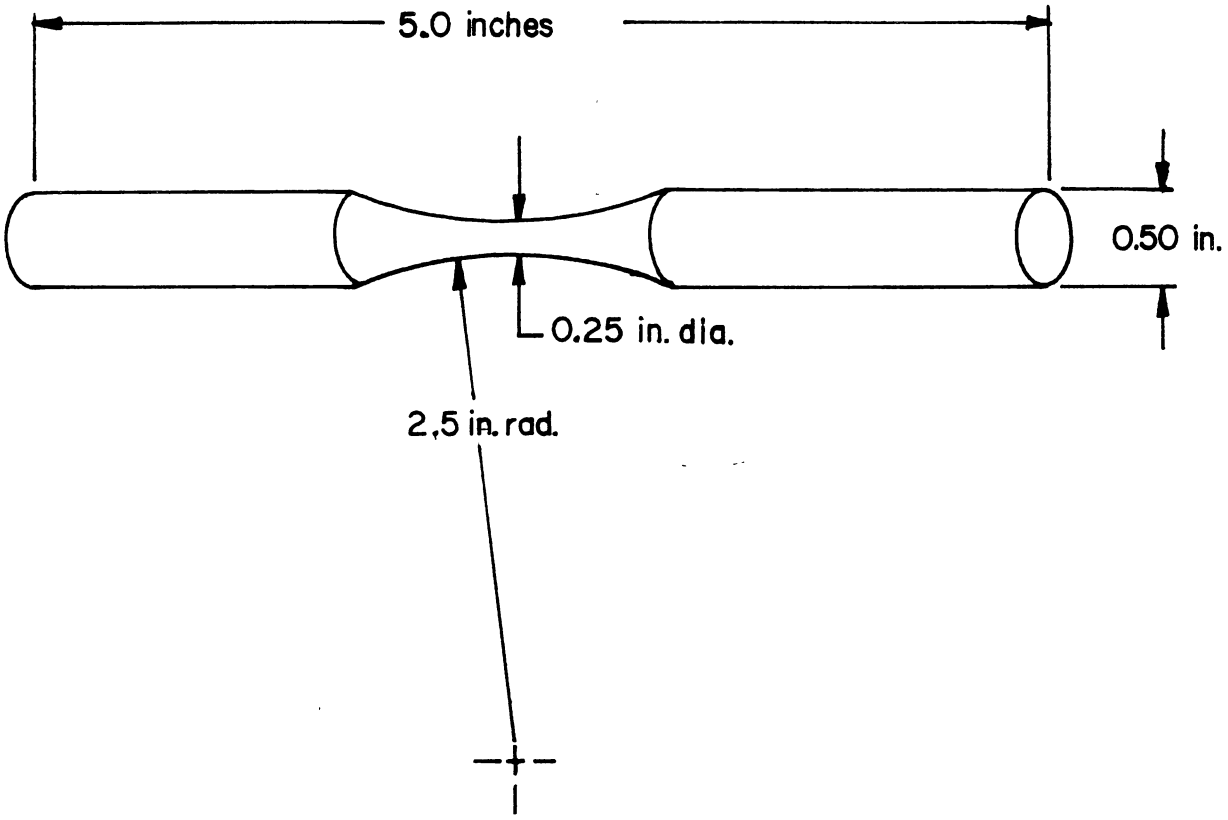
5.0 inches
0.50 in.
0.25 in. dia.
2.5 in. rad.

Grain size was controlled by annealing at temperatures ranging from 750°C to 1100°C, depending on the alloy. Specimens were furnace cooled to minimize specimen-to-specimen variation in microconstituent segregation.

Testing

All tests were performed at room temperature on an MTS machine. Tensile tests were done under displacement control with a ramp input to give a ram velocity of 6×10^{-5} in.-s^{-1}. The strain rate of the waisted geometry was measured experimentally by mounting a one millimeter long, foil-type, variable resistance strain gage at the center of the specimen. Circuitry included a Vishay/Ellis 20 Digital Strain Indicator, with temperature compensation. With the MTS ram velocity at 6×10^{-5} in.-s^{-1}, this arrangement gave a strain rate of 1.6×10^{-5} s^{-1}. Fatigue tests were performed in load control in fluctuating tension (R = 0) at 30 to 35 Hz, with a sinusoidal loading pattern.

Testing was done in air, mercury, and hydrogen. For the mercury tests, the samples were cleaned in HCl to ensure proper wetting of the specimen, then fitted into a small cup to hold the mercury at the gage length. For the hydrogen tests, the samples were ultrasonically cleaned in trichloro-ethylene, a degreasing solvent, to remove oils and polishing compounds. The samples formed the cathode of an electrolytic cell and were dynamically charged at a rate of 200 A-m^{-2} [3, 5]. Two platinum wires formed the noble metal anode. The electrolyte was sulfuric acid at a pH of 3.2, to which 0.25 gm/ℓ of sodium arsenite was added to inhibit recombination [3, 5]. Charging was accomplished using a Princeton

Applied Research Model 173 Potentiostat/Galvanostat. Figure 3 illustrates the environmental cell used for hydrogen testing.

Data Recording and Reduction

After surface preparation and recording of initial diameter and hardness, the samples were mounted for testing in the MTS machine. During tensile tests in air, engineering stress versus engineering strain curves were obtained by plotting load versus strain curve on a Hewlett-Packard Model 7045 X-Y Plotter, then rescaling the vertical axis. Strain was measured directly using an MTS electronic clip gage extensometer and MTS signal conditioning equipment. Log true stress versus log true strain curves of the plastic regime were plotted using discrete points from the original engineering stress versus engineering strain curves. A detailed development of this conversion of data can be found in Appendix A. The strain hardening exponent was determined by drawing the best line through the data and finding the resultant slope.

An analysis in the text by Hertzburg [28] shows that the amount of uniform strain is related to the magnitude of the strain hardening exponent. The plastic true strain at the tensile strength is numerically equal to the strain hardening exponent. The validity of this analysis with respect to the alloys studied was investigated. For more detailed development, refer to Appendix B.

Microscopic Observations

In preparation for microscopic examination, each sample was cleaned ultrasonically. Some tests were interrupted periodically to document the surface damage as the test progressed. Surface damage was photographed

Figure 3. Environmental Cell Used for Hydrogen Testing

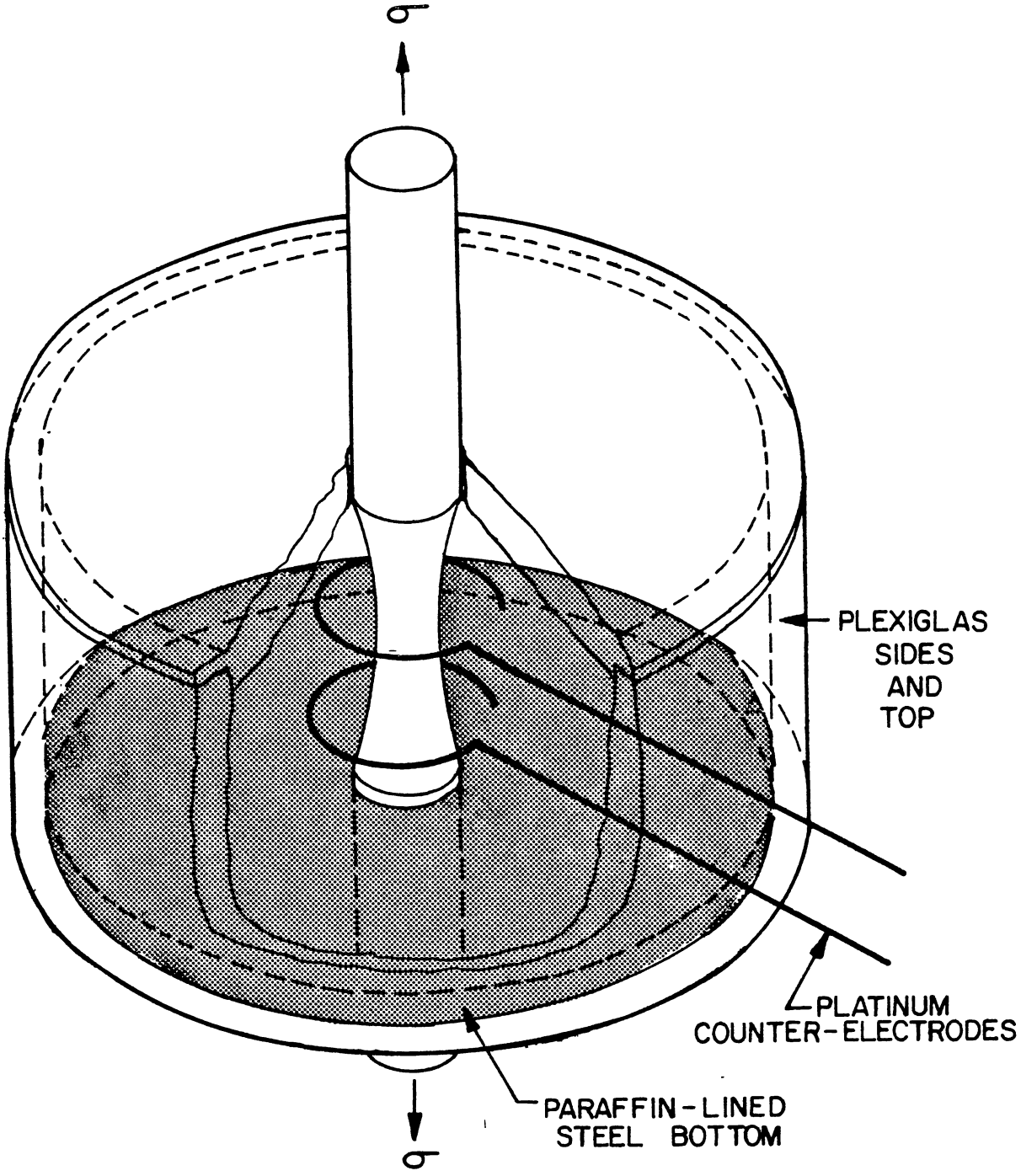
PLEXIGLAS
SIDES
AND
TOP
PLATINUM
COUNTER-ELECTRODES
PARAFFIN-LINED
STEEL BOTTOM

on black and white 35 millimeter film through a Reichert optical microscope. Though not used in the photographs, the Reichert microscope was outfitted with Nomarski interference contrast equipment. This gave outstanding views of very small height differences. This is especially useful when observing the slip character early in the tests. After fracture, the samples were first ultrasonically cleaned, then viewed in a Bausch and Lomb 10-70X Stereoscopic Zoom Microscope (SZM) and later examined and photographed in a Joel Model 35 Scanning Electron Microscope (SEM).

CHAPTER IV

EXPERIMENTAL RESULTS

Introduction

In the present investigation, tests were conducted in three series. The results of experimentation are presented by series for clarity. Discussion of results appears in the final section of this chapter.

Mechanical Properties Tests

This series of tests was intended to form the data base for further tests. Additionally, Traylor [3] suggested that in nickel-based alloys, at least, the strain hardening exponent of each alloy appears to correlate with the susceptibility to embrittlement by hydrogen and mercury. Consequently, the alloys Nickel 200 (UNS N02200), Monel 400 (UNS N04400), Inconel 600 (UNS N06600), and Incoloy 800 (UNS N08800) were tested as closely as possible to American Society for Testing and Materials standards [34]. To facilitate calculation of the strain hardening exponent, samples were fully annealed for two hours in a mild vacuum (~23 P_a), then furnace cooled [35]. The various annealing temperatures, hardness values, and grain sizes are listed in Table VII. Henceforth, standard annealing temperatures are 750°C for Nickel 200 and Monel 400, 1100°C for Inconel 600, and 1050°C for Incoloy 800.

The tensile tests performed on the annealed samples generated a large amount of data. The mechanical properties which were extracted

TABLE VII

ANNEALING TEMPERATURE FOR NICKEL 200, MONEL
INCONEL 600, AND INCOLOY 800

Material	2hr Annealing Temperature, ^{o}C	Grain Size, 10^{-6} m	Hardness R_B	Hardness, R_B
Nickel 200	750	35	37	28-54
Monel 400	750	32	66	62-80
Inconel 600	1000	7	83	67-86
	1050	13	82	
	1100	70	77	
Incoloy 800	1000	12	80	67-89
	1050	60	66	
	1100	--	64	

from the data appear in Table VIII. As stated in Chapter III, Experimental Procedure, a graph of log true stress versus log true strain was generated to find the strain hardening exponent. Those graphs are presented as Figures 4 through 8. Three different diameters were tested to explore possible surface zone effects on the value of the strain hardening exponent. The lack of effect of varying diameters is particularly well illustrated by Figure 4 for Nickel 200. The effect of the two-hour annealing temperature was explored. Figure 8 for Incoloy 800 is especially illustrative. In general, the value of the strain hardening exponent increased with increasing temperature. It seems that numbers approach some limiting value. The best value of the strain hardening exponent is found in Table IX.

Tensile Damage Tests

Surface Damage and Fracture

The fracture surface characteristics of the four alloys in the environments considered have been adequately documented in the precursory studies, especially for Nickel 200 and Monel 400, yet the nature of damage leading to fracture is not known. This series of tests was intended to answer several questions:

1. When do cracks initiate in the respective environments?

2. Does failure follow crack initiation promptly in the environments?

3. Since tests on Inconel 600 and Incoloy 800 are very limited in preceding studies, is there any loss in tensile strength in mercury and hydrogen?

TABLE VIII

MECHANICAL PROPERTIES OF ALLOYS TESTED

Material	Annealing Temperature (^{o}C)	Initial Diameter	Elastic Modulos (10^6 psi)	Tensile Strength (kpsi)	Yield Strength (kpsi)	True Strain at Neck	Reduction in Area (%)	Hardness (R_B)
Nickel 200	750	.250	34.9	73	17	.213	84	45
	750	.375	—	81	16	.267	84	37
	750	.126	34.0	79	22	.239	90	36
Monel 400	750	.250	29.9	92	37	.213	77	66
Inconel 600	1000	.250	35.0	122	62	.182	63	83
	1050	.250	26.0	122	46	.210	67	82
	1100	.125	—	106	33	.252	66	63
	1100	.250	33.8	119	36	.235	64	77
	1100	.365	36.0	112	33	.269	60	64
Incoloy 800	1000	.250	29.8	107	37	—	64	80
	1050	.250	—	94	35	.265	65	66
	1050	.365	36.0	94	30	.286	67	66
	1100	.250	34.0	92	29	.290	66	64

Figure 4. Log True Stress Versus Log True Strain for Nickel 200

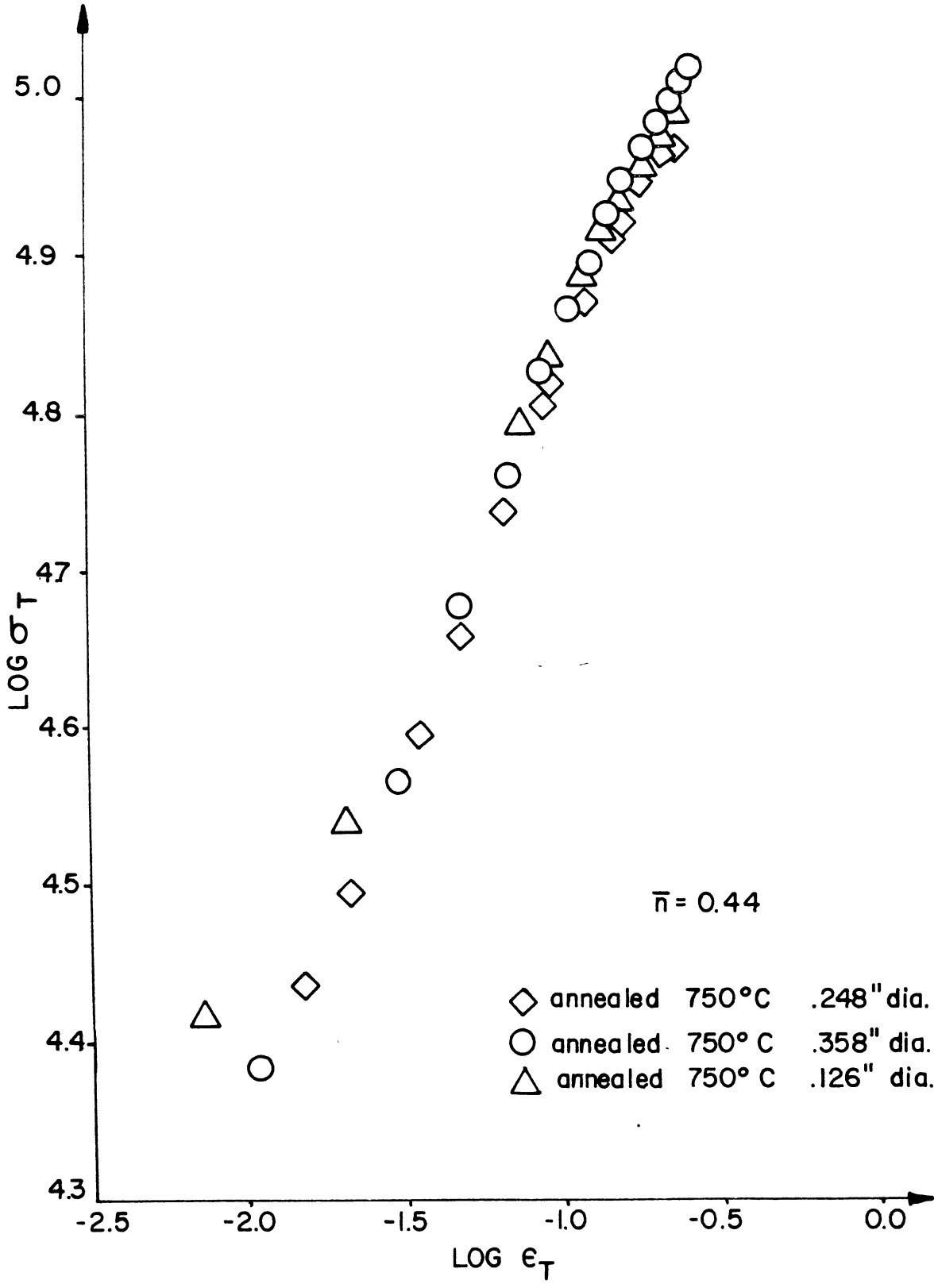
5.0
4.9
4.8
4.7
4.6
4.5
4.4
4.3
LOG σ_T
-2.5
-2.0
-1.5
-1.0
-0.5
0.0
LOG ϵ_T
$\bar{n}$ = 0.44
annealed 750°C .248" dia.
annealed 750° C .358" dia.
annealed 750° C .126" dia.

Figure 5. Log True Stress Versus Log True Strain for Monel 400

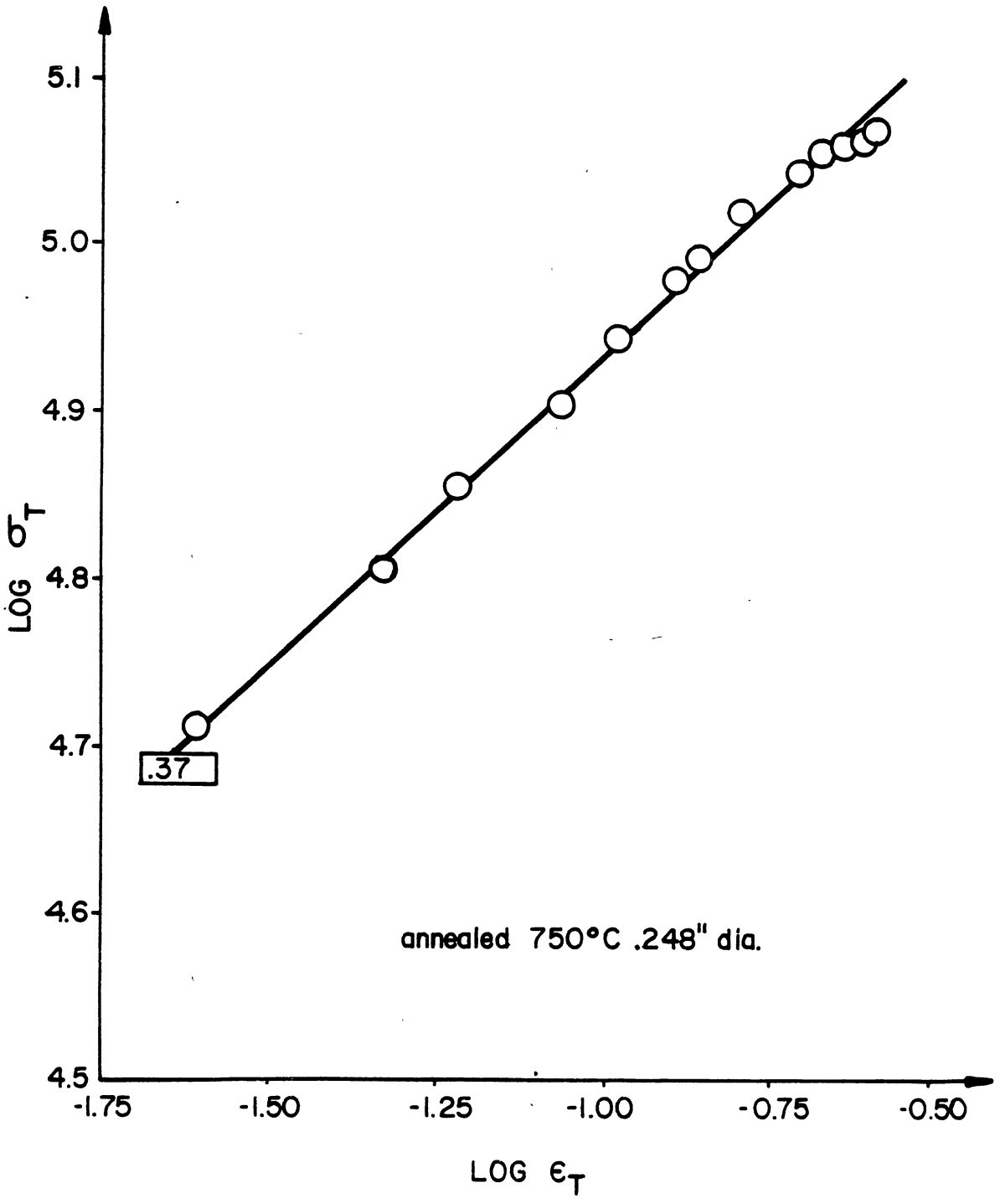
5.1
5.0
4.9
4.8
4.7
4.6
4.5
LOG σ_T
.37
annealed 750°C .248" dia.
-1.75
-1.50
-1.25
-1.00
-0.75
-0.50
LOG ϵ_T

Figure 6. Log True Stress Versus Log True Strain for Inconel 600 for Various Annealing Temperatures

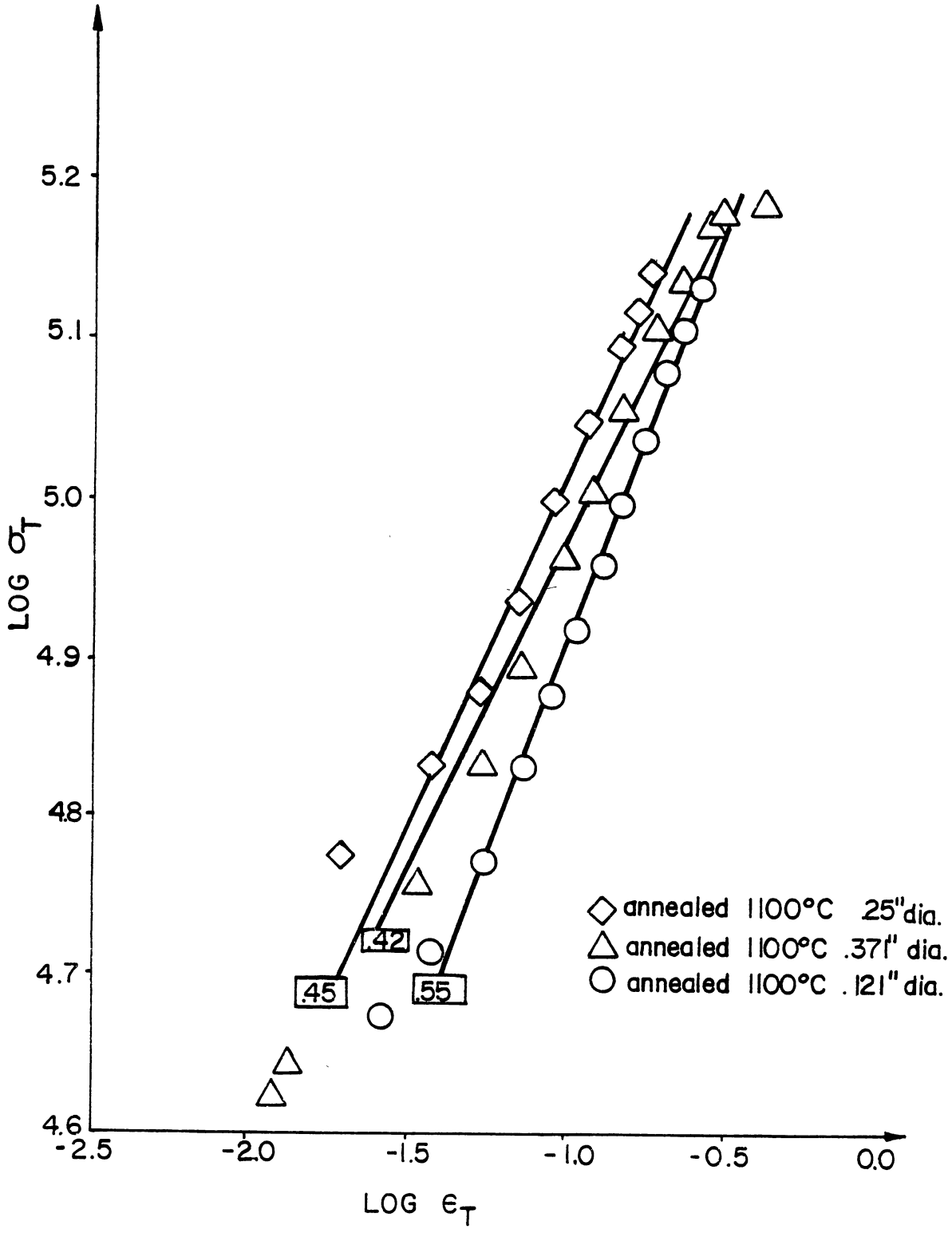
5.2
5.1
5.0
4.9
4.8
4.7
4.6
LOG σ_T
-2.5
-2.0
-1.5
-1.0
-0.5
0.0
LOG ϵ_T
.42
.45
.55
annealed 1100°C .25" dia.
annealed 1100°C .371" dia.
annealed 1100°C .121" dia.

Figure 7. Log True Stress Versus Log True Strain for Inconel 600 for Various Specimen Diameters

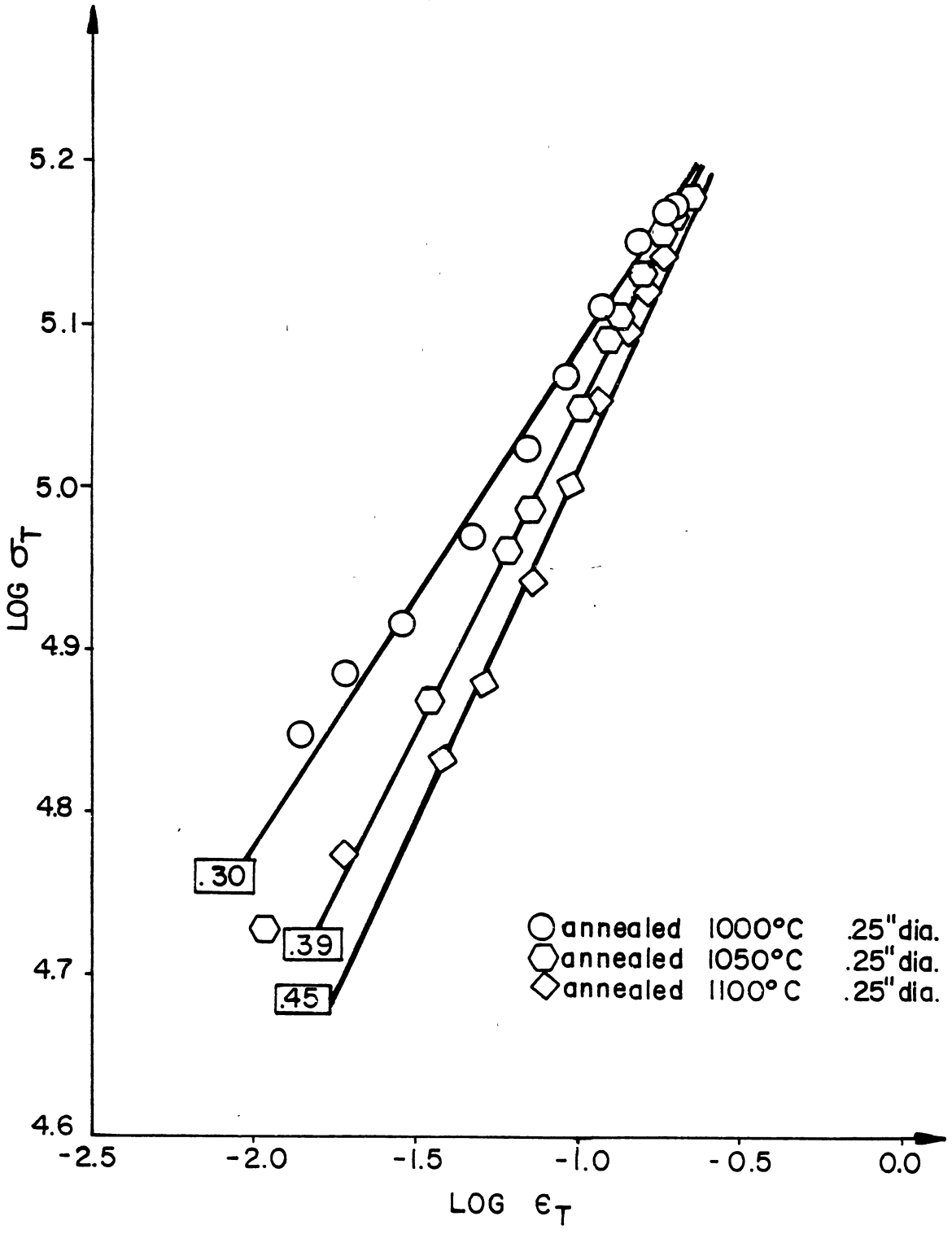
5.2
5.1
5.0
4.9
4.8
4.7
4.6
LOG σ_T
-2.5
-2.0
-1.5
-1.0
-0.5
0.0
LOG ϵ_T
.30
.39
.45
annealed 1000°C .25" dia.
annealed 1050°C .25" dia.
annealed 1100° C .25" dia.

Figure 8. Log True Stress Versus Log True Strain for Incoloy 800

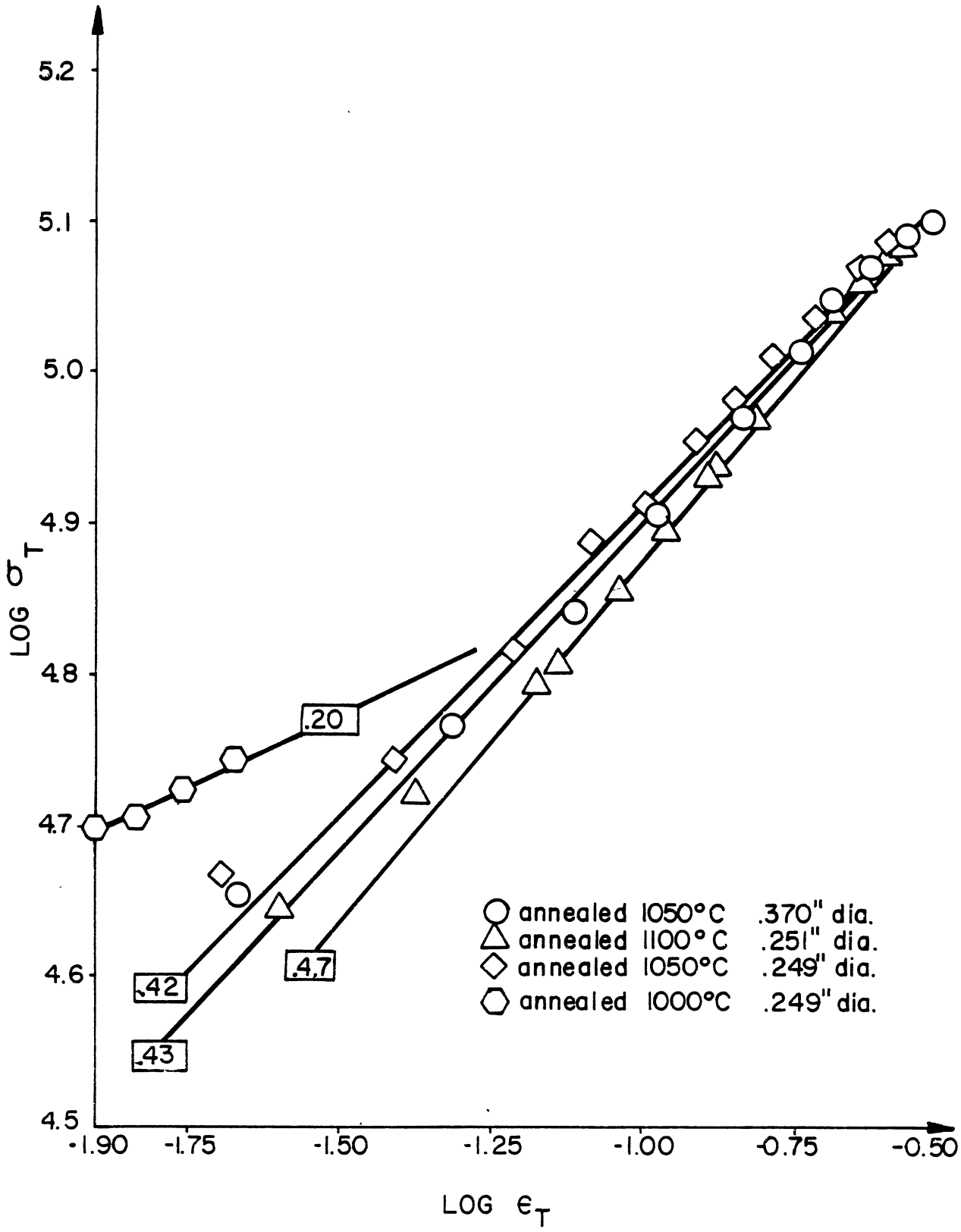
5.2
5.1
5.0
4.9
4.8
4.7
4.6
4.5
LOG σ_T
-1.90
-1.75
-1.50
-1.25
-1.00
-0.75
-0.50
LOG ϵ_T
.20
.42
.43
.47
annealed 1050°C .370" dia.
annealed 1100°C .251" dia.
annealed 1050°C .249" dia.
annealed 1000°C .249" dia.

TABLE IX

STRAIN HARDENING EXPONENT VALUES

Alloy	Exponent
Nickel 200	0.44
Monel 400	0.37
Inconel 600	0.42
Incoloy 800	0.45

4. Recognizing that the four alloys have relatively similar strain hardening exponents but apparently different stacking fault energies, how do the slip characters compare, at crack initiation, at necking, and at fracture?

Slow strain rate tensile tests were performed on each of the four alloys in air, mercury, and hydrogen. The tests were interrupted periodically to examine the surface damage under the optical microscope, then manually reloaded to just below the previous stress, and then the test was resumed. The results of alloys are described below, each in turn.

Alloy Nickel 200. Nickel 200 showed no loss in tensile strength in either mercury or hydrogen. There was some loss in ductility as reflected in the reduction in area. Hydrogen was the more severe environment. Reduction in area declined from 83 percent in air to 62 percent in mercury to 40 percent in hydrogen. In mercury, cracking initiated at about 90 percent of the tensile strength in air after the onset of necking. In hydrogen, cracking initiated at the tensile strength. In both environments, failure was preceded by a large amount of plastic deformation.

As a base line, the sample tested in air was examined in the SEM for side cracking and slip. As shown in Figure 9, rumpling and plastic flow are the dominant features. No cracks are visible at this magnification but in the enlargement, Figure 10, side cracking is visible. In this view in the necked region, cracking is predominantly longitudinal but cracks at 45° to the tensile axis are not uncommon. Farther from the neck, Figure 11, cracking is roughly transverse to the tensile axis.

Figure 12 is an optical micrograph of the surface of a fine grained, 35 μm, Nickel 200 sample which has been loaded in hydrogen to 30 percent of the tensile strength. The tensile axis in this figure and all side

Figure 9. Surface Damage of Nickel 200 Broken in Air at Side of Neck (100X)

Figure 10. Enlargement of Figure 9 Near Fracture (1000X)

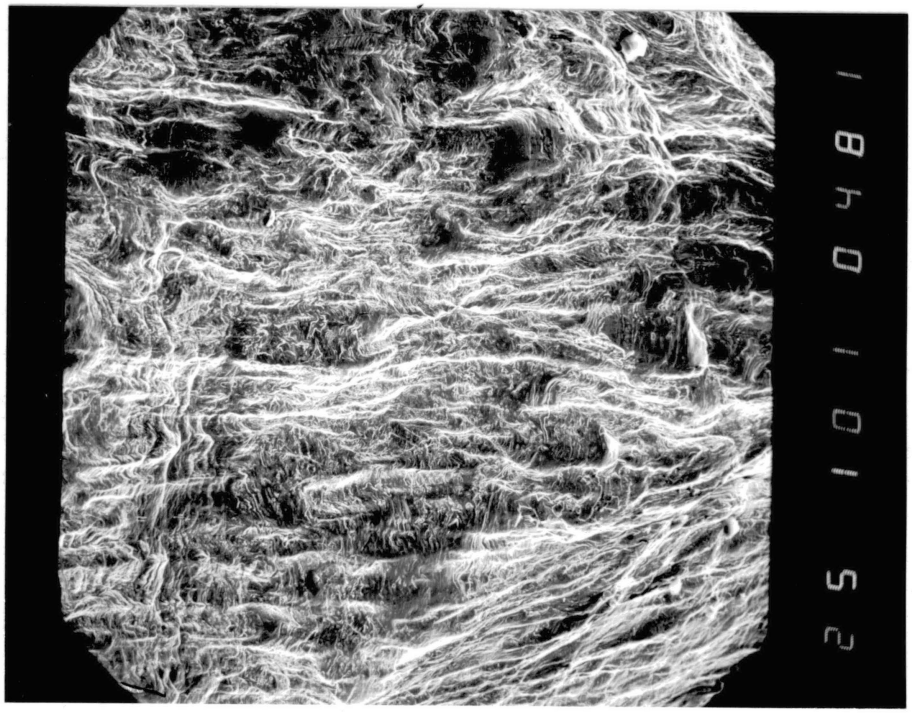
25 101 04h 18

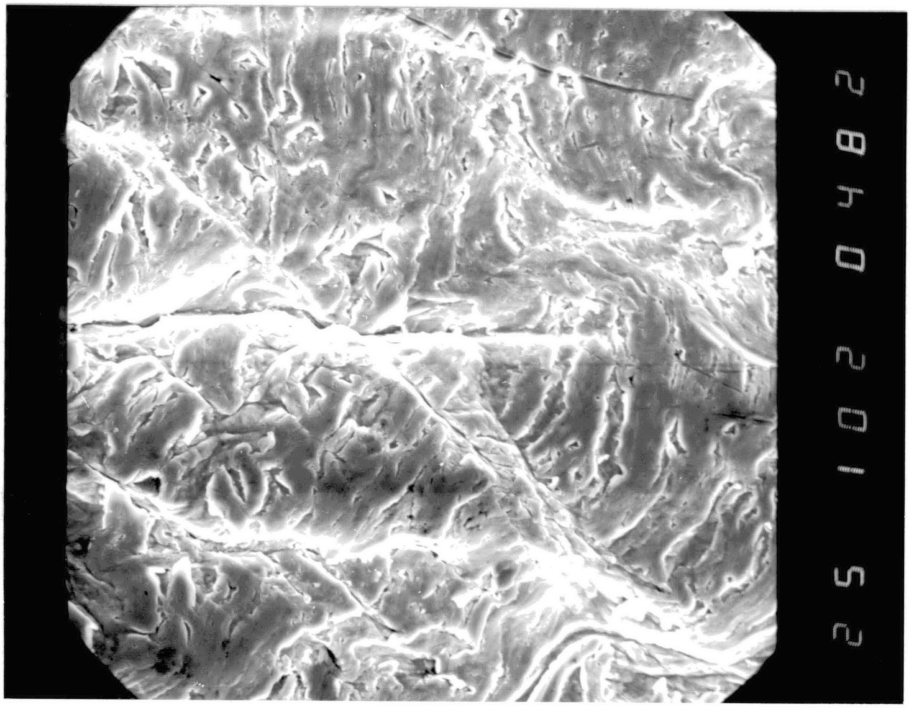
25 102 04h 28

Figure 11. Enlargement of Figure 9 Away from Fracture (1000X)

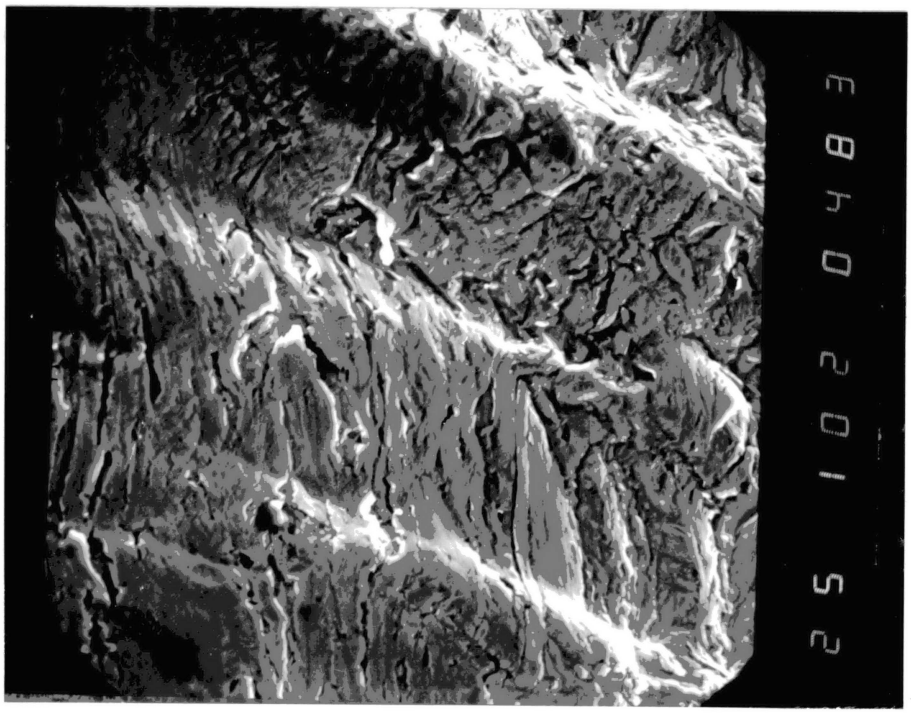
25 JUL 2001 08h 03

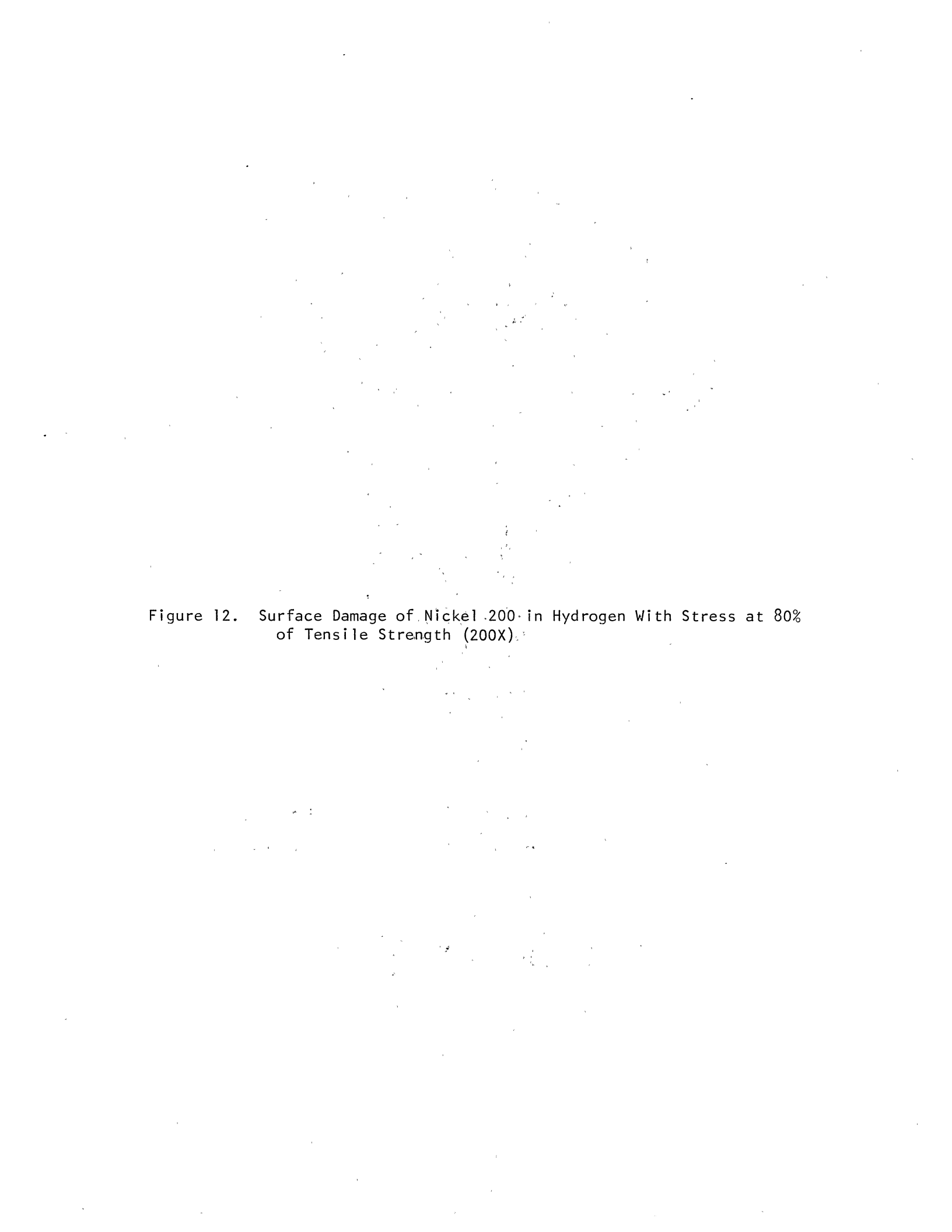

Figure 12. Surface Damage of Nickel 200 in Hydrogen With Stress at 80% of Tensile Strength (200X)

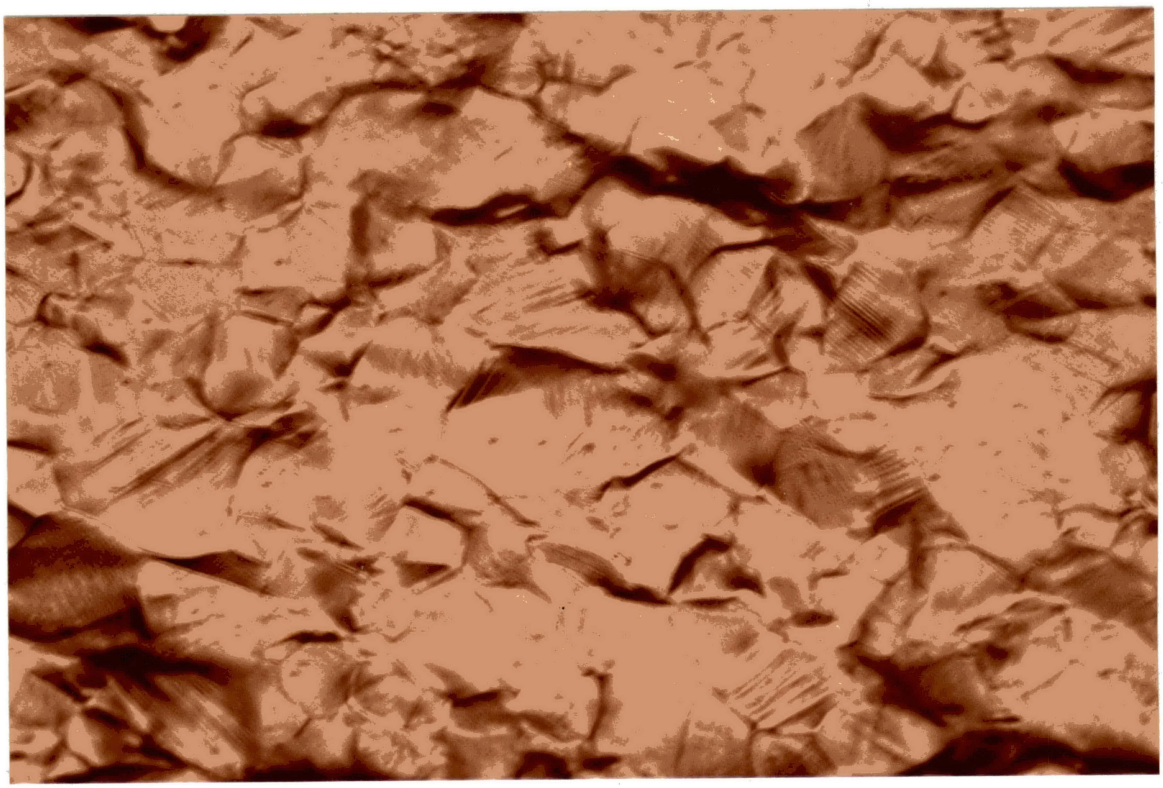

views in this thesis is horizontal. The surface of the sample is rumpled and some slip is visible. Cracking initiated at the tensile strength; this is shown in Figure 13. The cracks are initially short, wide, and transverse to the tensile axis. Rumpling and plastic flow are extensive. After fracture, the side cracking was examined in the SEM. In Figure 14, side cracking is widespread and tends to be linked at 45° to the tensile axis. Rumpling is about the same as at crack initiation. Figure 15 is an enlargement of the previous figure to examine the slip character. Slip has occurred on at least two systems and is somewhat wavy.

After fracture in mercury, the side cracking is less widespread than in hydrogen but the cracking is deep and at 45° to the tensile axis (Figure 16). Plastic flow is more visible than in hydrogen. The enlargement, Figure 17, reveals extensive wavy slip.

A large grained Nickel 200 sample was tensile tested in hydrogen for comparison. Figure 18 is a view at 80 percent of the tensile strength. Slip is prominent and relatively straight. Once again, cracking initiated at the tensile strength (Figure 19). Rumpling is severe and wavy slip is very visible.

A similar test in mercury shows almost identical slip character at 80 percent of the tensile strength (Figure 20). The slip is perhaps a little heavier. At the tensile strength (Figure 21), cracking has not yet initiated. Cracking did not begin until just after the onset of necking. At the tensile strength, rumpling and slip are like that in hydrogen.

Alloy Monel 400. The base line test in air was examined. The necked region of the cup-cone fracture, Figure 22, has a conspicuous plastic

Figure 13. Surface Damage of Nickel 200 in Hydrogen With Stress at Tensile Strength (200X)

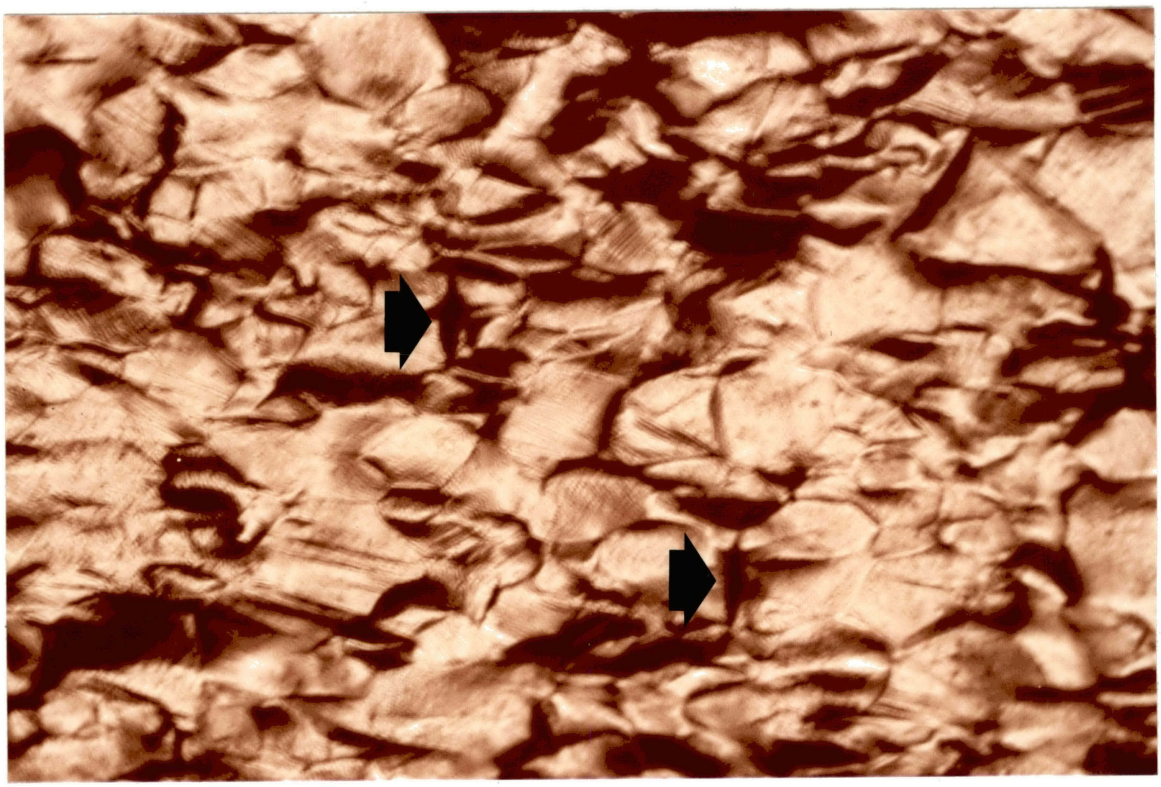

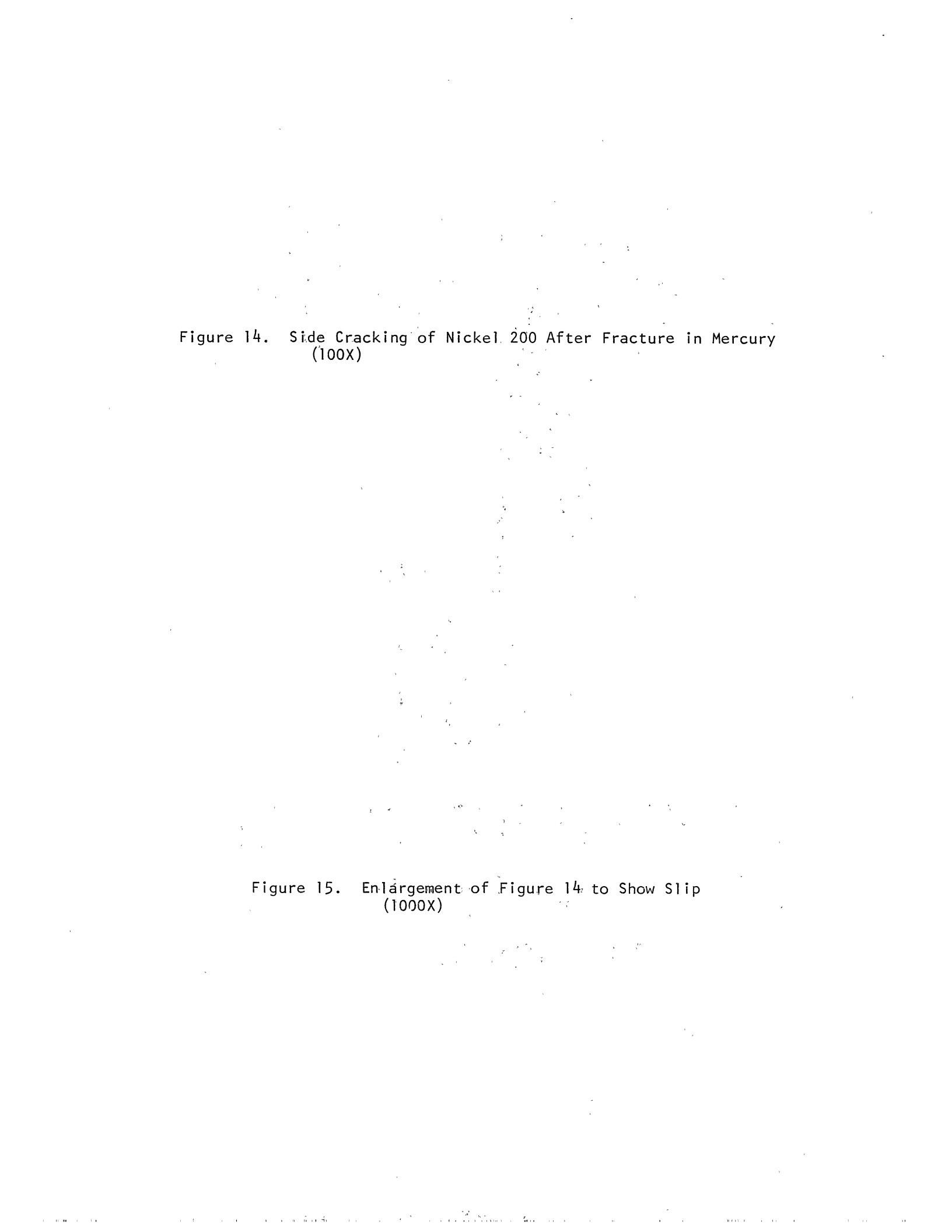

Figure 14. Side Cracking of Nickel 200 After Fracture in Mercury (100X)

Figure 15. Enlargement of Figure 14 to Show Slip (1000X)

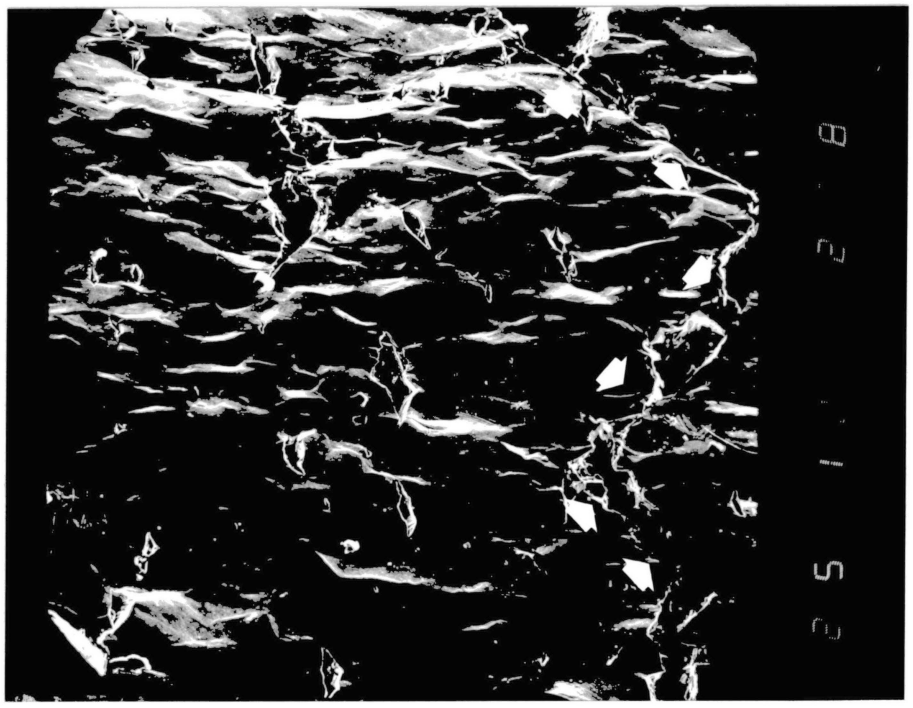

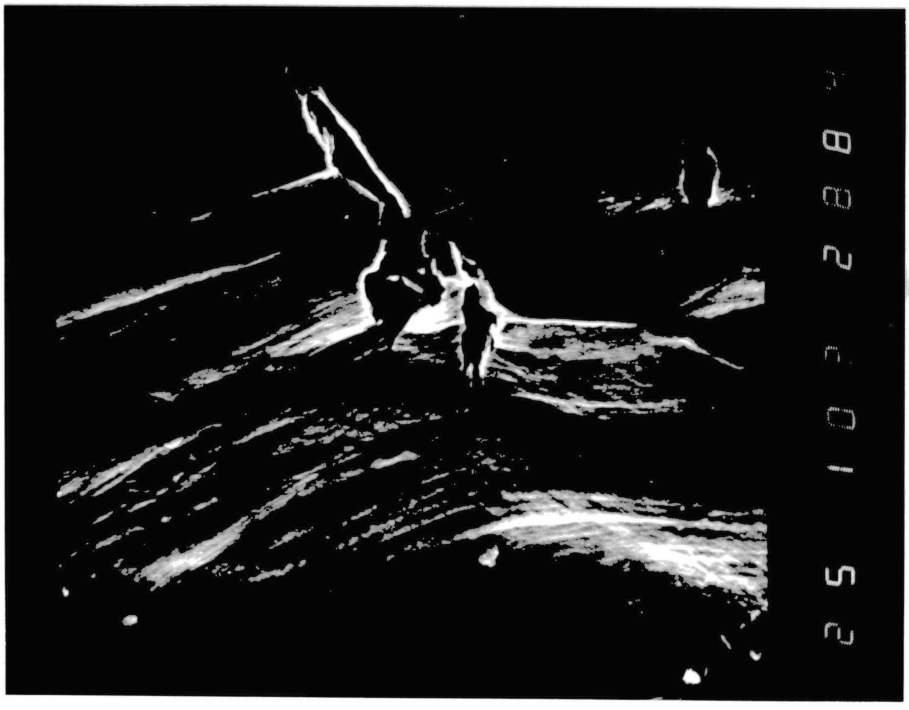

Figure 16. Side Cracking of Nickel 200 After Fracture in Mercury (100X)

Figure 17. Enlargement of Figure 16 to Show Slip (1000X)

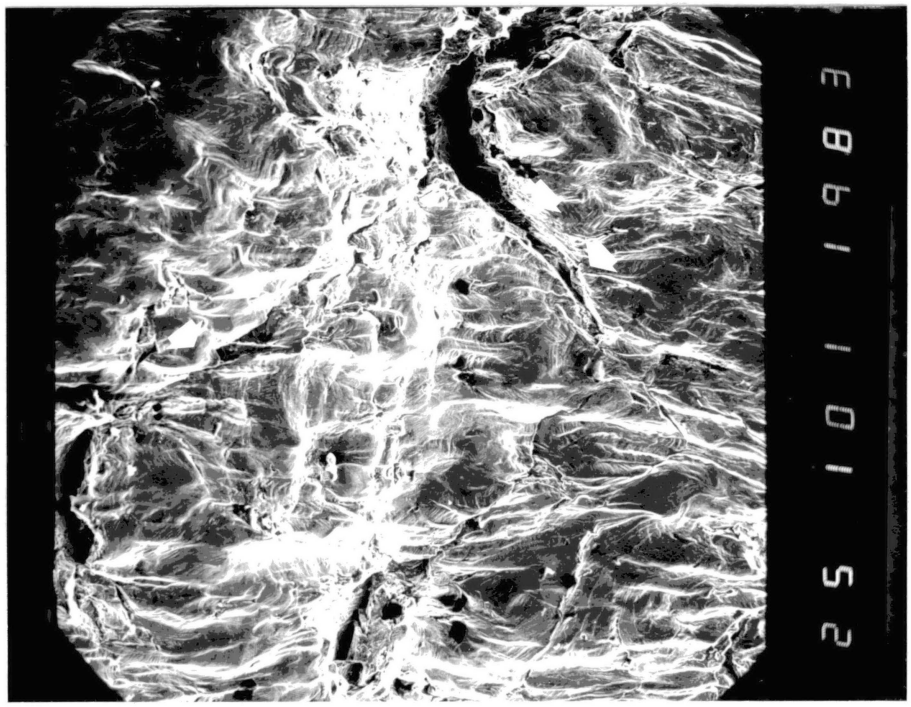
25 101 1983

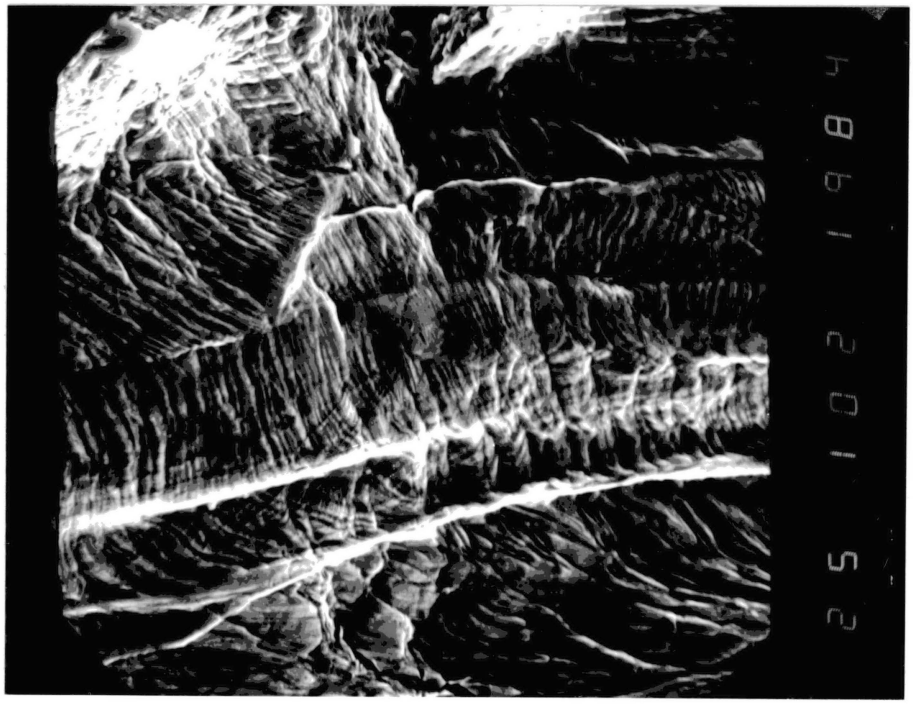
25 102 1984

Figure 18. Surface Damage of Large Grain (120 μm) Nickel 200 in Hydrogen at 80% of Tensile Strength (200X)

Figure 19. Surface Damage of Large Grain Nickel 200 in Hydrogen at Tensile Strength (200X)

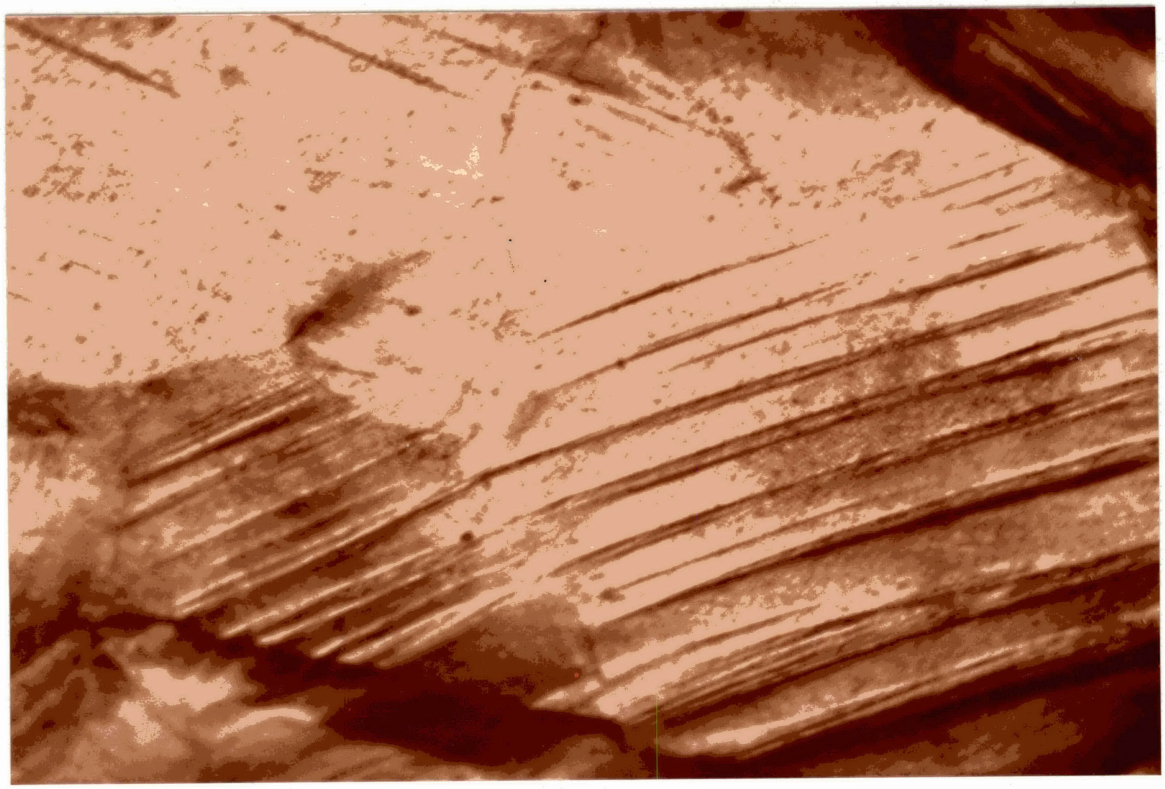

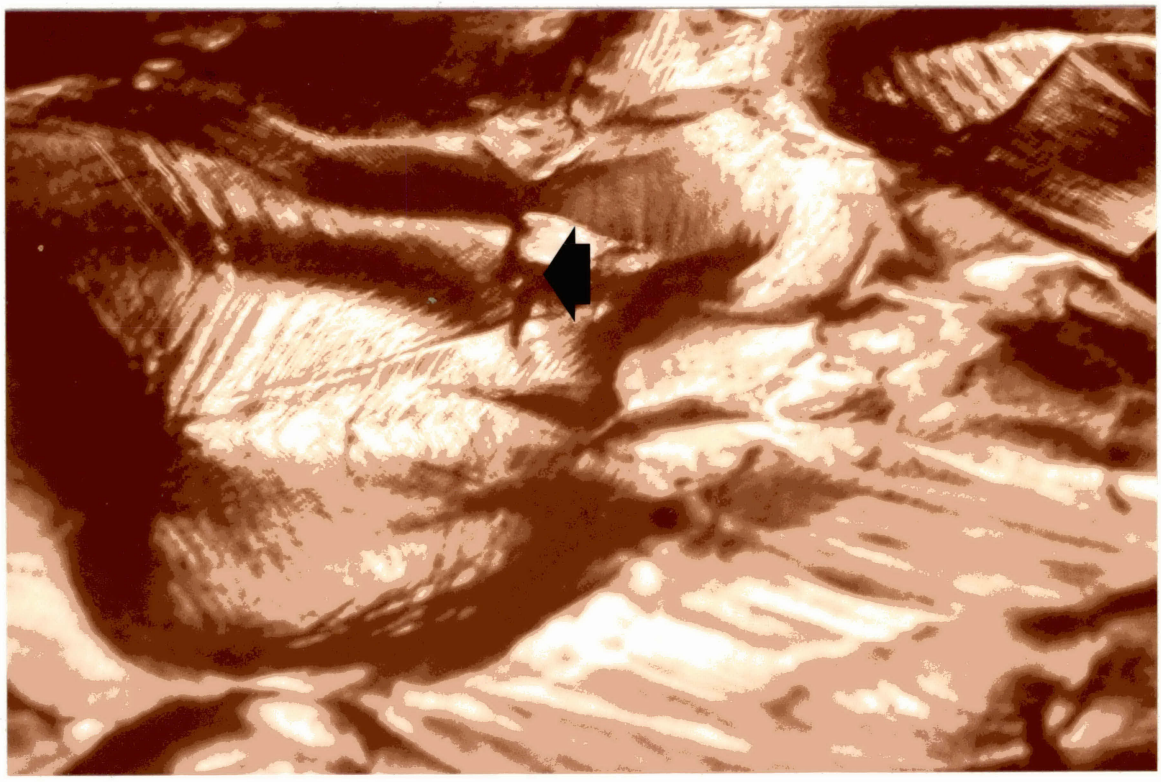

Figure 20. Surface Damage of Large Grain (120 μm) Nickel 200 in Mercury at 80% of Tensile Strength (200X)

Figure 21. Surface Damage of Large Grain Nickel 200 in Mercury at Tensile Strength (200X)

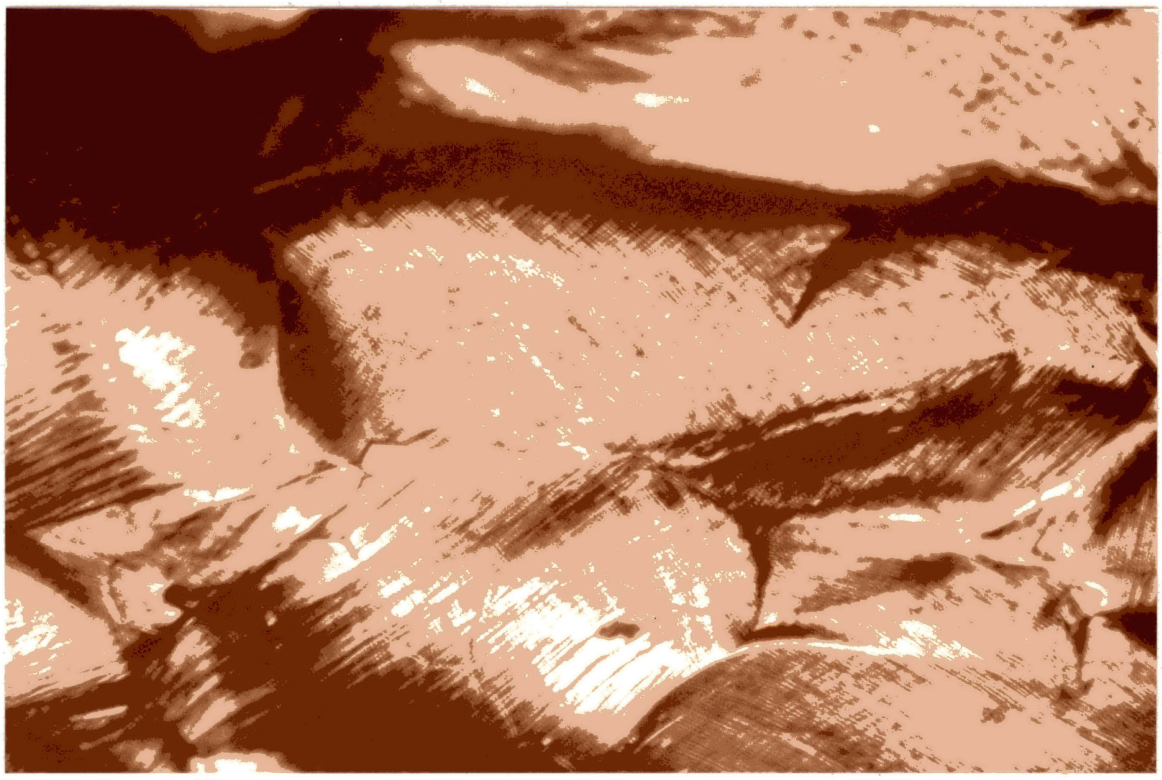

Figure 22. Side Cracking of Monel 400 in Air After Fracture (100X)

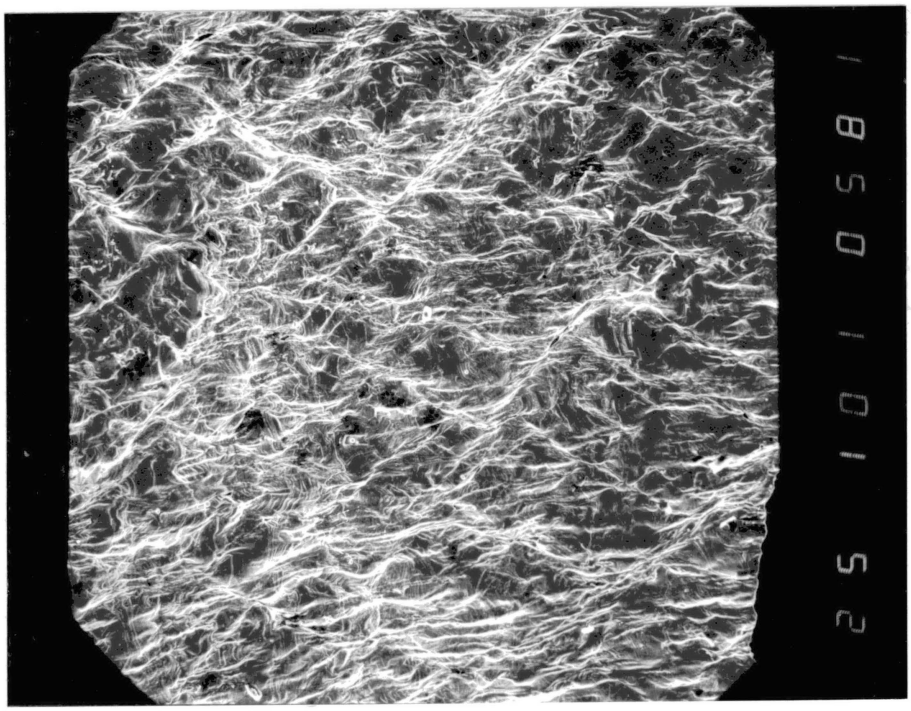
25 10 1850 1

flow pattern at 45° to the tensile axis. The enlargement, Figure 23, reveals cracking as well as plastic flow along 45° planes. This is interesting because side cracking in air was not entirely expected.

Monel 400 loaded in hydrogen to 80 percent of the tensile strength (Figure 24) is fine grained (30 μm) and extensively rumpled. The diagonal marks are remnants of polishing. Fracture occurred without necking at 95 percent of the tensile strength. The side cracking after fracture (Figure 25) is a network of fine intergranular cracks. There is no visible plastic flow. The enlargement, Figure 26, confirms the intergranular nature of the side cracks and reveals almost no slip markings. Apparently rumpling is due to slip of one grain with respect to another rather than slip within each grain.

In mercury at 80 percent of the tensile strength, the side surface is the same as that in hydrogen (Figure 27). Rumpling is the dominant surface feature. Fracture occurred at 84 percent of the tensile strength without evidence of necking. The side cracking after fracture, Figure 28, is sparse. Rumpling is notable and a few small cracks are visible. The enlargement, near one of the cracks (Figure 29), shows small deep cracks and light slip; both tend to be transverse to the tensile axis. Seemingly, the first crack in either mercury or hydrogen propagated rapidly to failure.

Alloy Inconel 600. Again, a sample tested in air was examined for side damage. As shown in Figure 30, plastic flow and rumpling are prominent. Like Monel 400 in air (Figures 22 and 23), cracking and plastic flow are at 45° to the tensile axis. Cracks are wider but not as numerous. As shown in Figure 31, plastic flow is extensive enough to obscure the slip character, though some faint slip lines are discernible.

Figure 23. Enlargement of Figure 22 Showing 45^{o} Cracking (1000X)

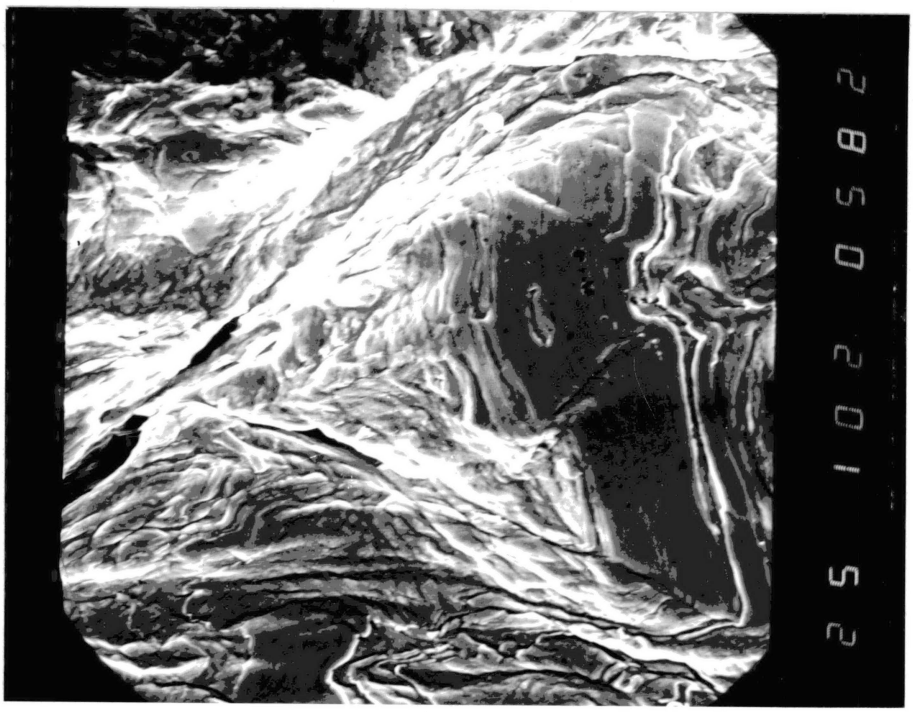
25 102 0582

Figure 24. Surface Damage on Side of Monel 400 in Hydrogen at 80% of Tensile Strength (200X)

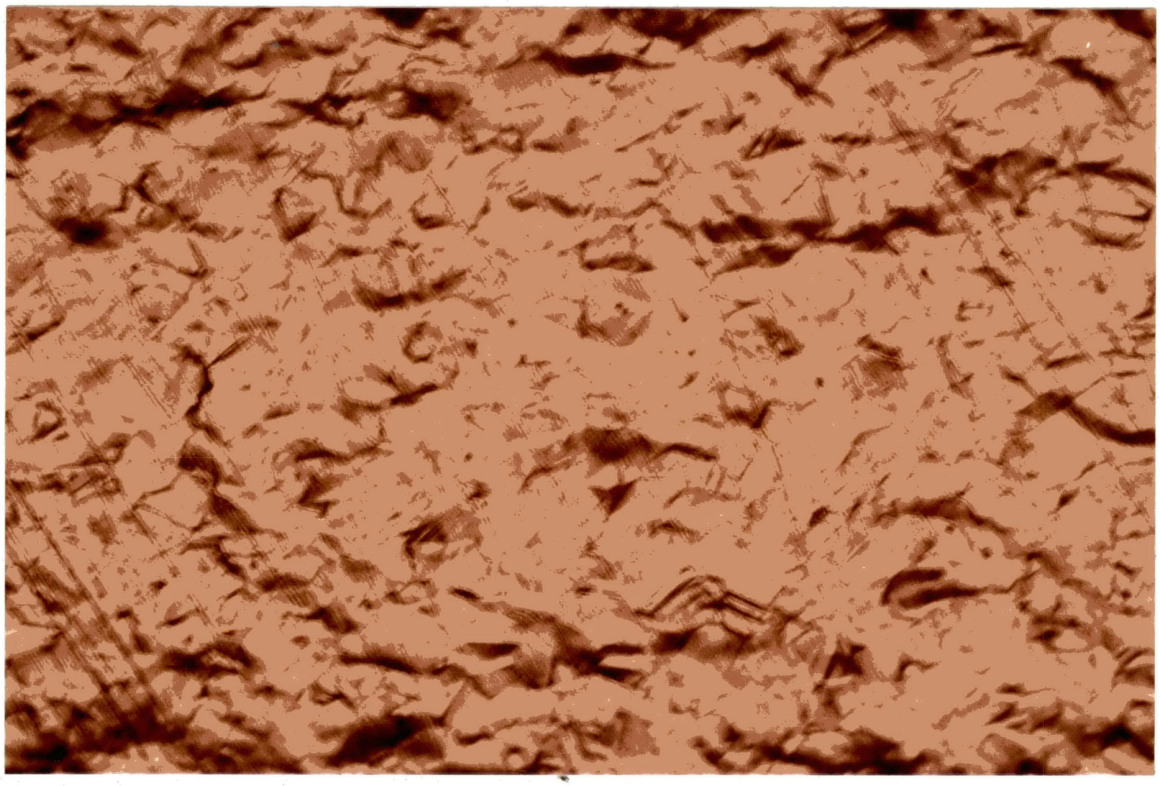

Figure 25. Side Cracking of Monel 400 in Hydrogen After Fracture (100X)

Figure 26. Enlargement of Figure 25 Showing Intergranular Cracking (1000X)

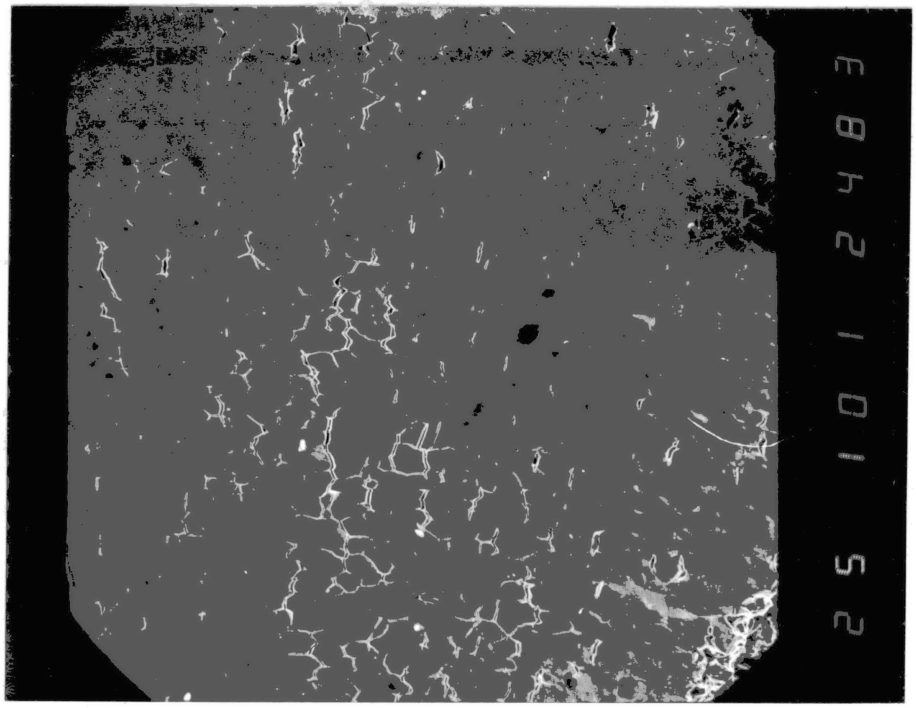
E8h2 I0I 52

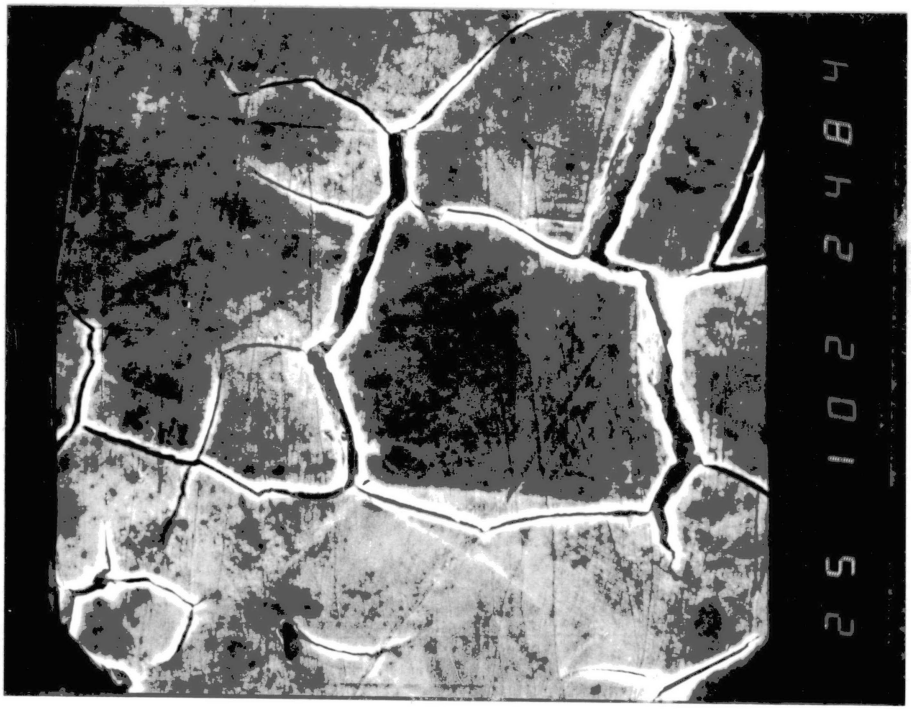
52 I02 48h

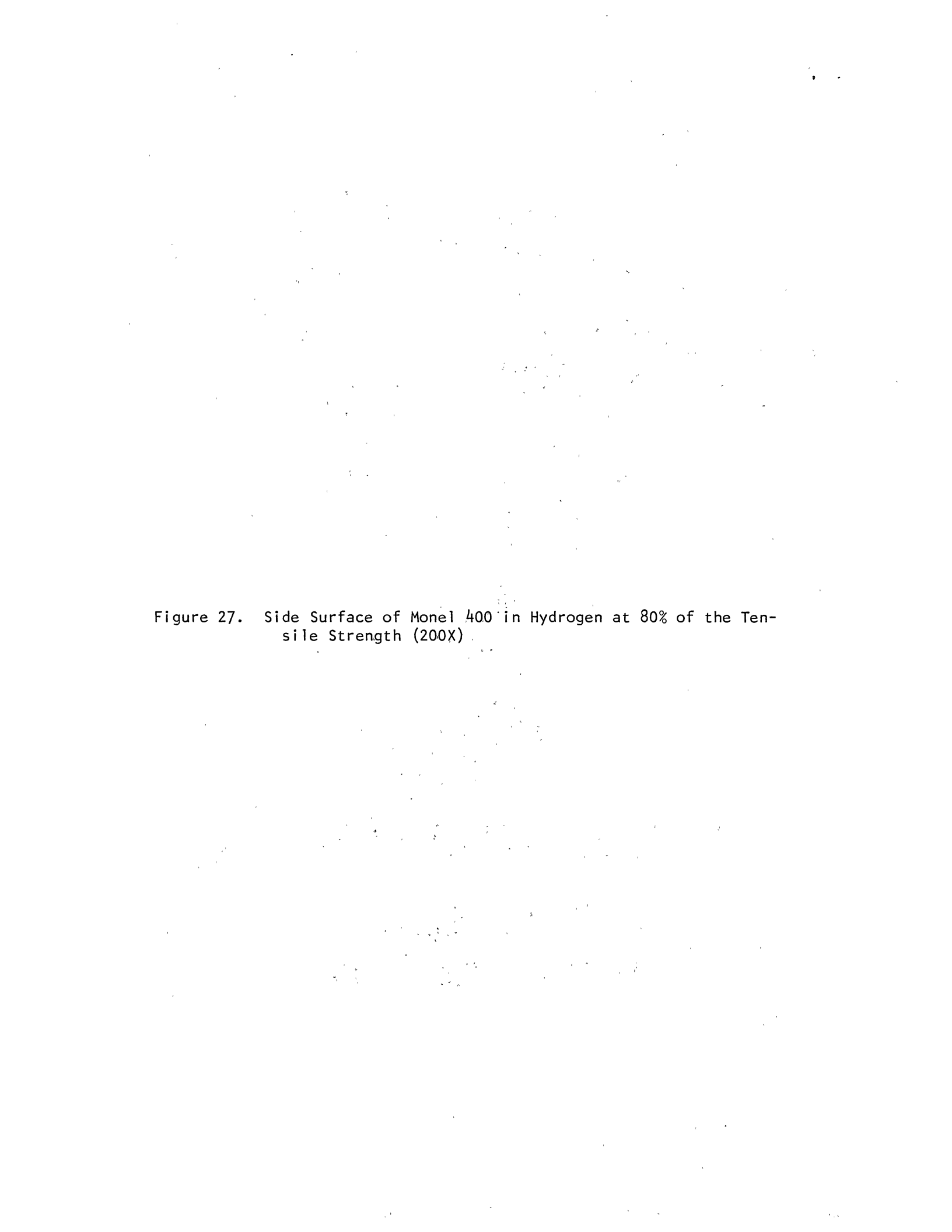

Figure 27. Side Surface of Monel 400 in Hydrogen at 80% of the Tensile Strength (200X)

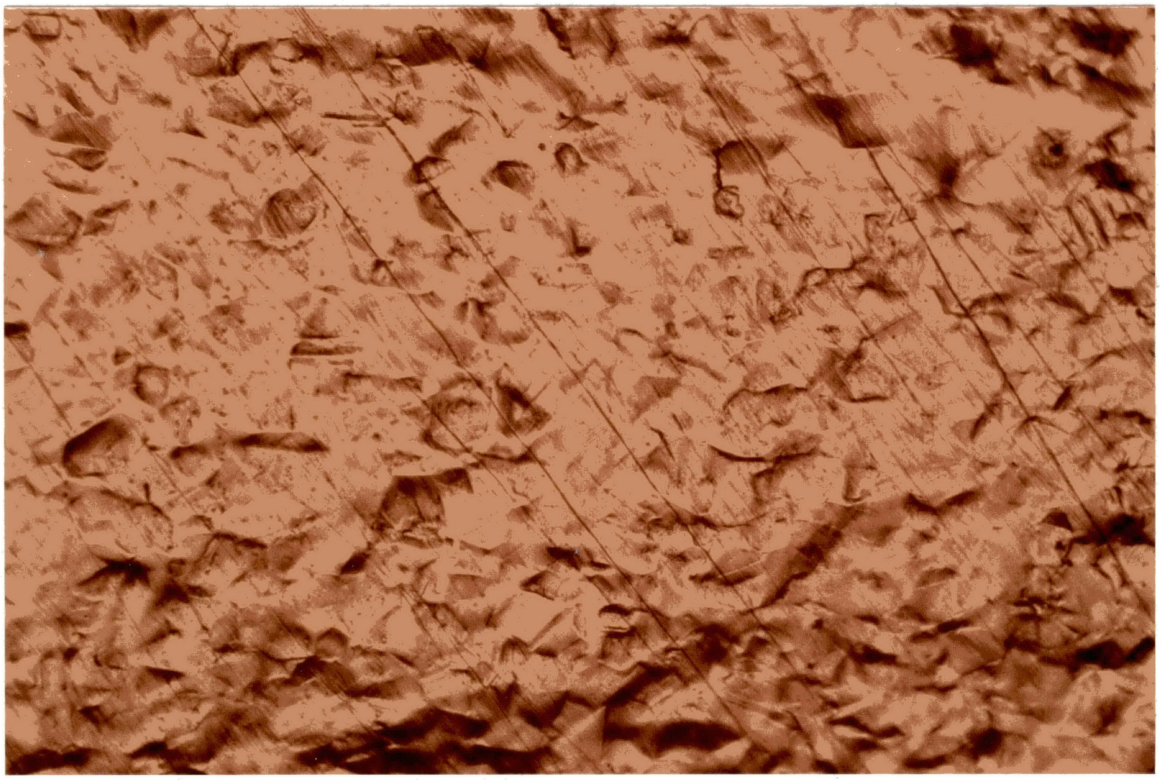

Figure 28. Side Cracking of Monel 400 in Mercury After Fracture (100X)

Figure 29. Enlargement of Figure 28 Showing Slip (1000X)

E8E2 101 52

52 102 2E8h

Figure 30. Side Cracking of Inconel 600 Tested in Air (100X)

Figure 31. Enlargement of Figure 30 Showing Slip (1000X)

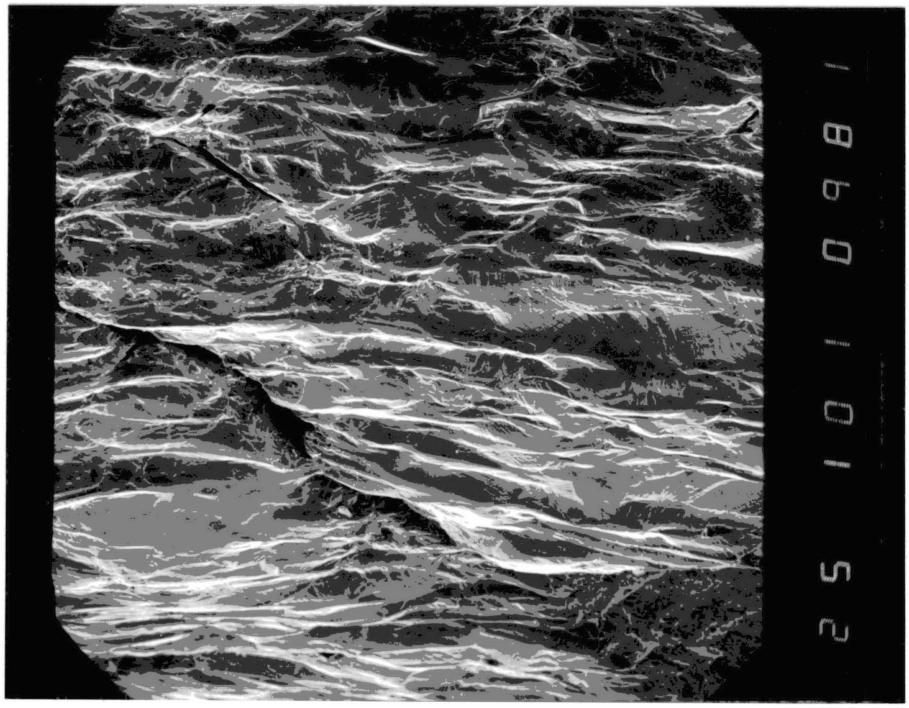
25 10 1 0 8 8 1

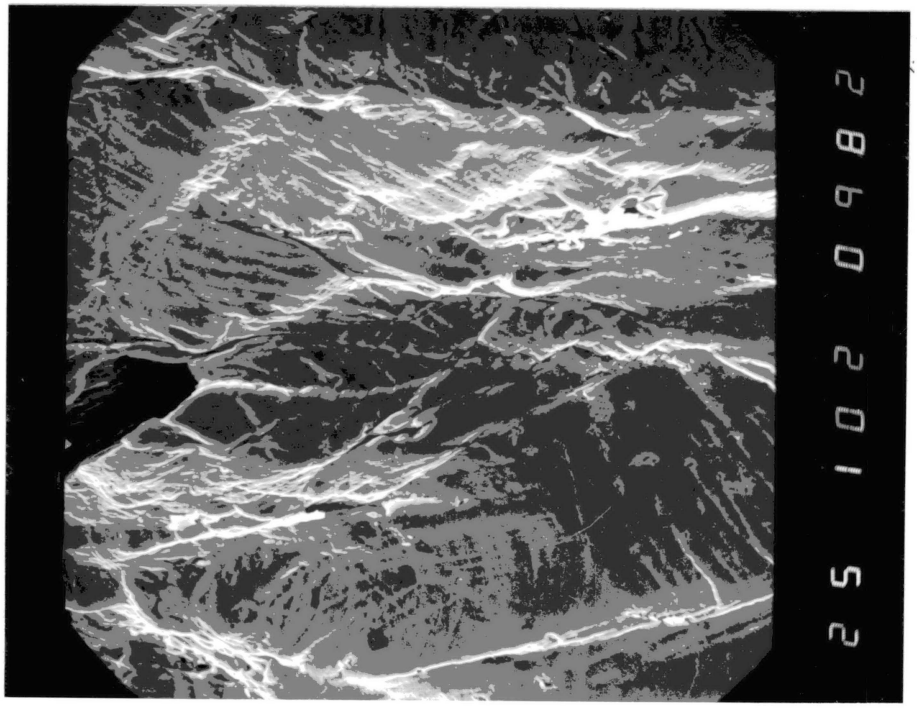
25 10 2 0 8 8 2

Inconel 600 tested in hydrogen had a striking behavior. At 80 percent of the tensile strength, the sample had extensive intergranular cracks (Figure 32). Cracks transverse to the tensile axis are slightly wider. At the peak stress, transverse cracks are extensive and wide; all cracks are intergranular (Figure 33). Fracture occurred at 96 percent of the tensile strength. As shown in Figure 34, side cracking is a network of intergranular cracks with a few large transverse separations. In the enlarged view (Figure 35), the separation of each grain is clear and slip markings are conspicuously absent.

Figure 36 is a sample stressed to 80 percent of the tensile strength in mercury. Instead of intergranular cracks, rumpling and slip marks are the notable features. At the tensile strength, rumpling is extensive and slip marks are prominent (Figure 37). As might be expected, fracture occurred after necking. The side cracking, as shown in Figure 38, is at 45° to the tensile axis. This is clarified by Figure 39, a tracing of the previous view. Rumpling of the surface is notable but not severe. The enlarged view (Figure 40) shows extensive slip which is slightly wavy, though not nearly as wavy as Nickel 200 in mercury.

Alloy Incoloy 800. The baseline specimen shown in Figure 41 resembles the Monel 400 tested in air (Figures 22 and 23) more than the Inconel 600 tested in air (Figures 30 and 31). A pattern of heavy plastic flow and some cracks are visible at 45° to the tensile axis, though not as distinctly as in the Monel 400 sample. Figure 42, an enlargement of the previous view, details the 45° cracking and heavy plastic flow which is extensive enough to obscure the slip character.

Figure 32. Side Cracking of Inconel 600 in Hydrogen at 80% of Tensile Strength (200X)

Figure 33. Side Cracking of Inconel 600 in Hydrogen at Tensile Strength (200X)

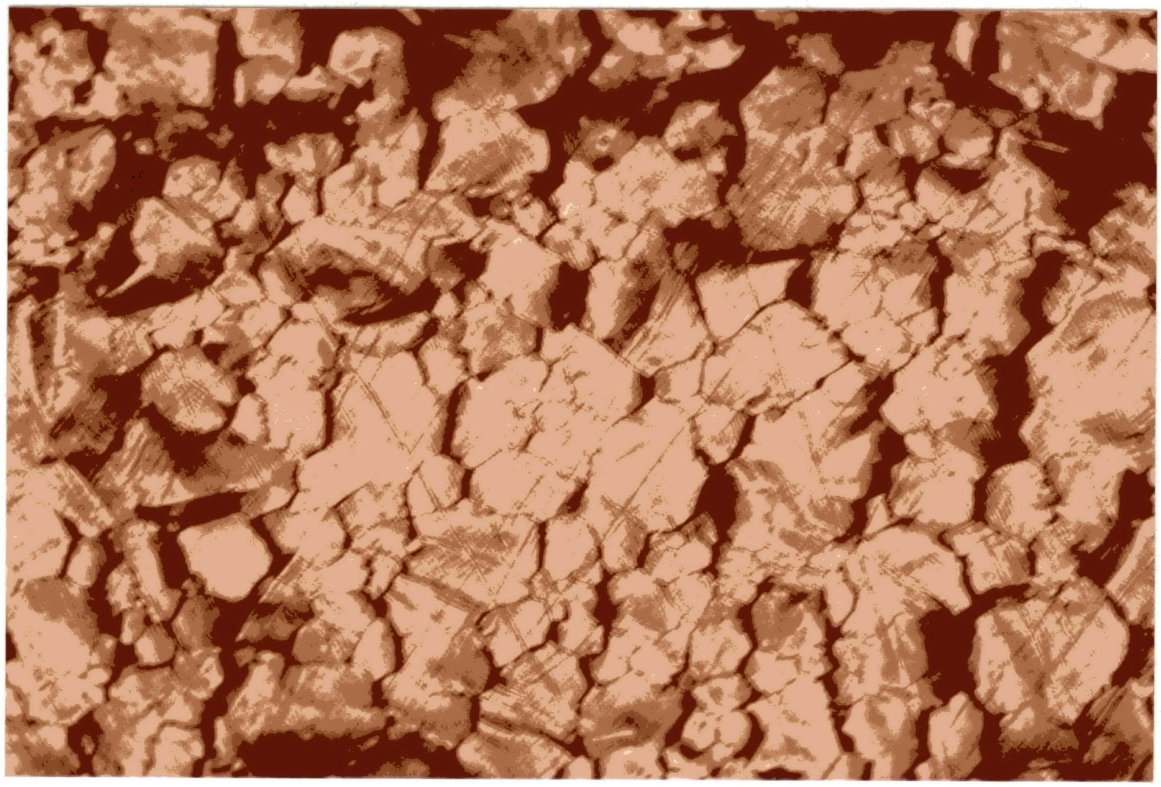

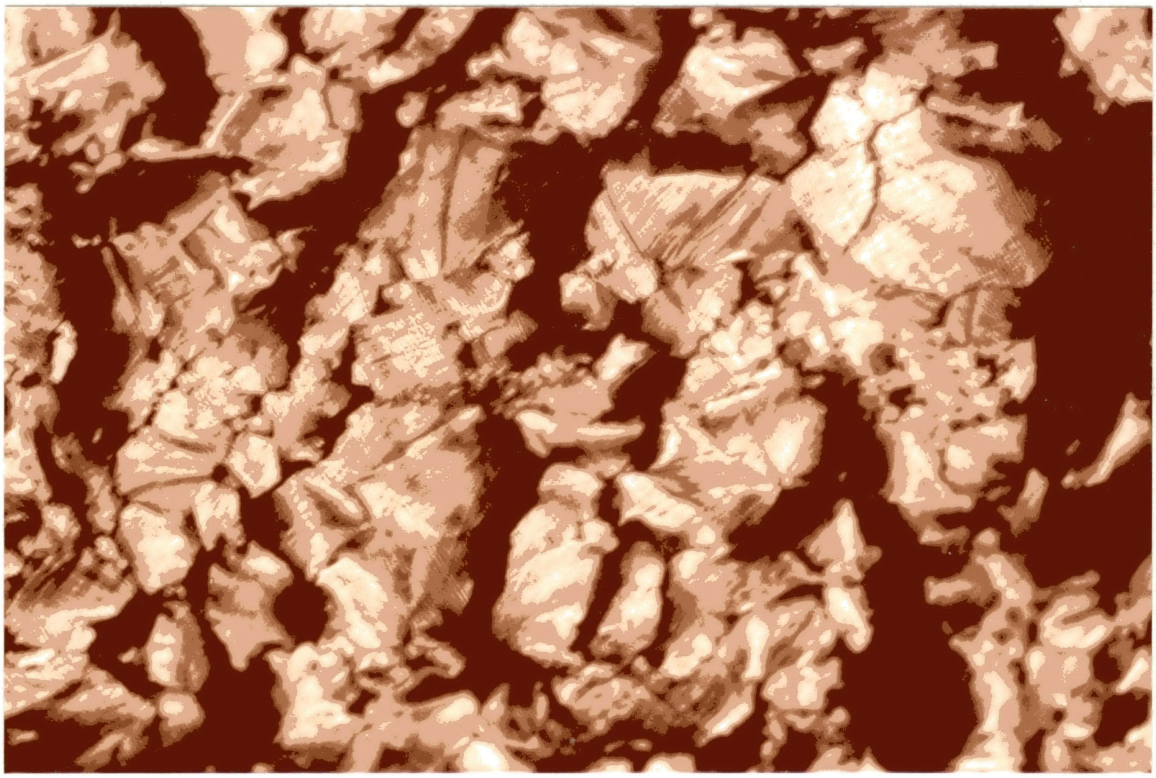

Figure 34. Side Cracking of Inconel 600 After Fracture in Hydrogen (100X)

Figure 35. Enlargement of Figure 34 to Show Slip (1000X)

25 101 2583

25 102 2584

Figure 36. Surface Damage of Inconel 600 in Mercury at 80% of Tensile Strength (200X)

Figure 37. Surface Damage of Inconel 600 in Mercury at Tensile Strength (200X)

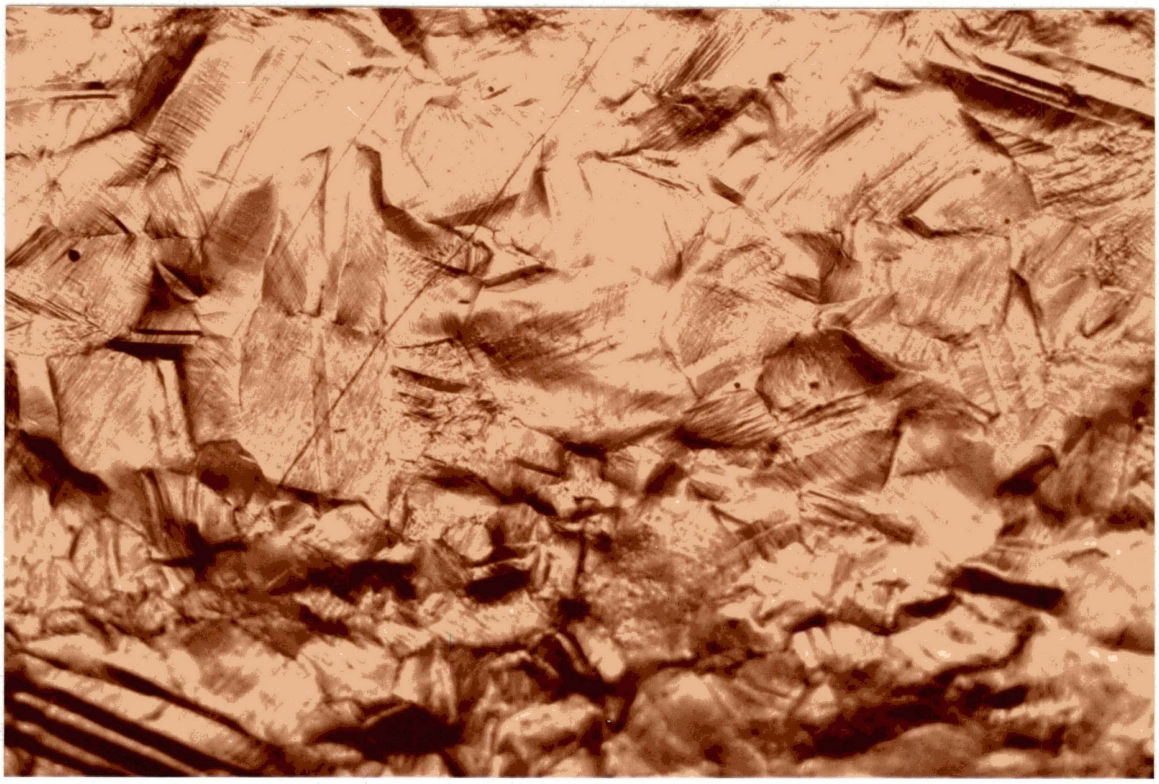

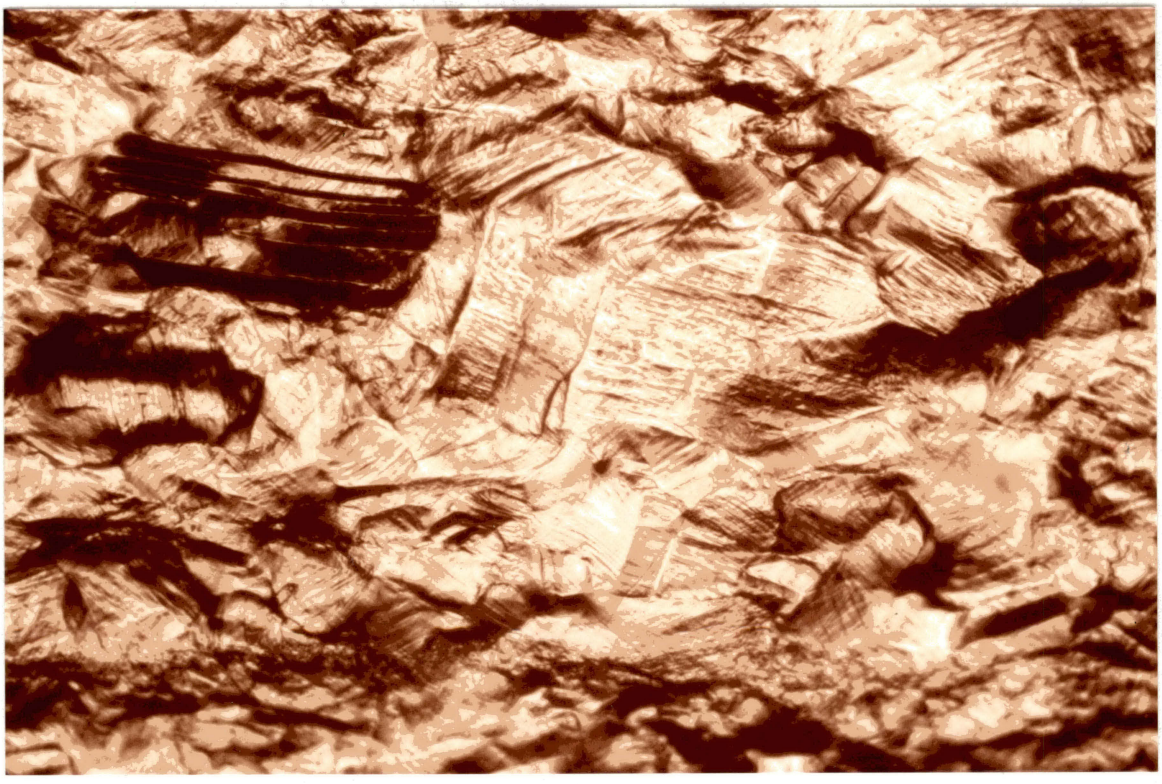

Figure-38. Side Cracking of Inconel 600 After Fracture in Mercury (100X)

Figure 39. Detail of Figure 38 Illustrating 45° Cracking

25 10 1 2183

25 10 1 2183

Figure 40. Enlargement of Figure 38 Showing Slip (1000X)

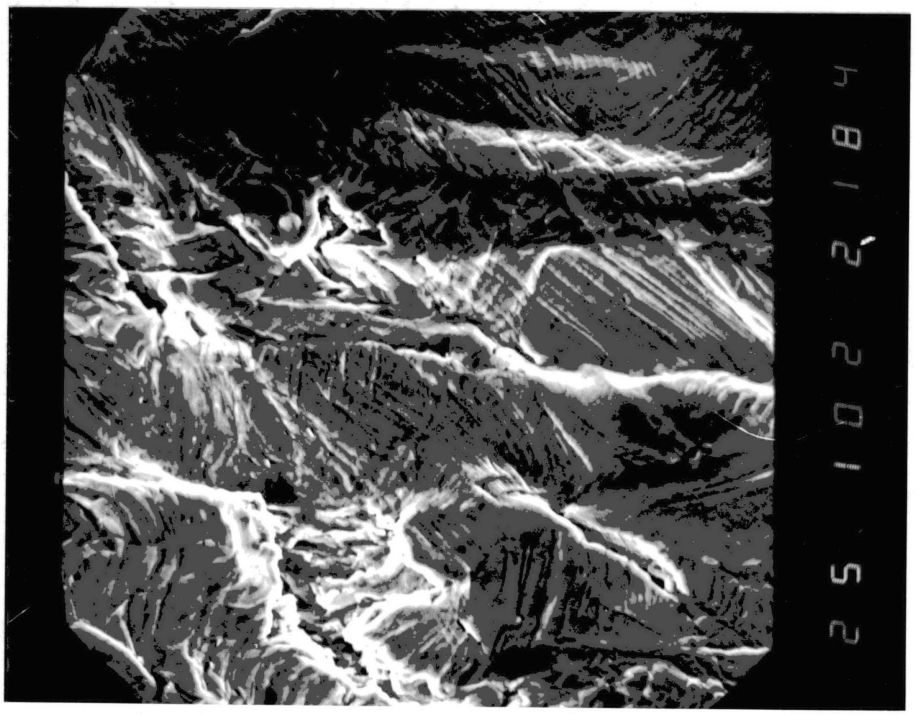
25 10 2018

Figure 41. Side Cracking of Incoloy 800 After Fracture in Air (100X)

Figure 42. Enlargement of Figure 40 Showing Slip and 45° Cracking (1000X)

25 10 1 0681

25 10 2 0682

Incoloy 800 loaded in hydrogen to 80 percent of the tensile strength had very little surface slip but rumpling was notable (Figure 43). Cracking initiated at the tensile strength, transverse to the tensile axis. As shown in Figure 44, rumpling of the surface is extreme and the beginnings of plastic flow can be seen. Fracture occurred with virtually no loss in tensile strength. The side view after fracture (Figure 45) reveals heavy rumpling and numerous cracks at 45° to the horizontal tensile axis. A tracing of the previous figure (Figure 46) illustrates the extent and nature of the major cracks. An enlargement of the side (Figure 47) shows the waviness of the slip and the tendency of cracks to follow slip marks. Slip is wavy, perhaps slightly more than Nickel 200 in hydrogen (Figure 15) and definitely less wavy than Nickel 200 in mercury (Figure 17).

In mercury at 80 percent of the tensile strength, for Incoloy 800, rumpling and slip are notable but no cracks had appeared (Figure 48). At the tensile strength, plastic flow and rumpling obscured slip marks and still no cracks had appeared (Figure 49). Fracture actually occurred after considerable necking and resulted as with all tensile tests of Incoloy 800 in cup and cone fractures. The side cracking after fracture (Figure 50) is minimal and at 45° to the tensile axis. Plastic flow and surface rumpling are prominent features. A tracing of the previous figure (Figure 51) illustrates the nature and extent of the side cracking. An enlarged view of the side (Figure 52) shows heavy, wavy slip which is about the same as Nickel 200 in mercury (Figure 15).

Summary. A compilation of tensile strength, reduction in area, and stress to initiate cracking in air, mercury, and hydrogen for each alloy

Figure 43. Surface Damage of Incoloy 800 in Hydrogen at 80% of Tensile Strength (200X)

Figure 44. Surface Damage of Incoloy 800 in Hydrogen at Tensile Strength (200X)

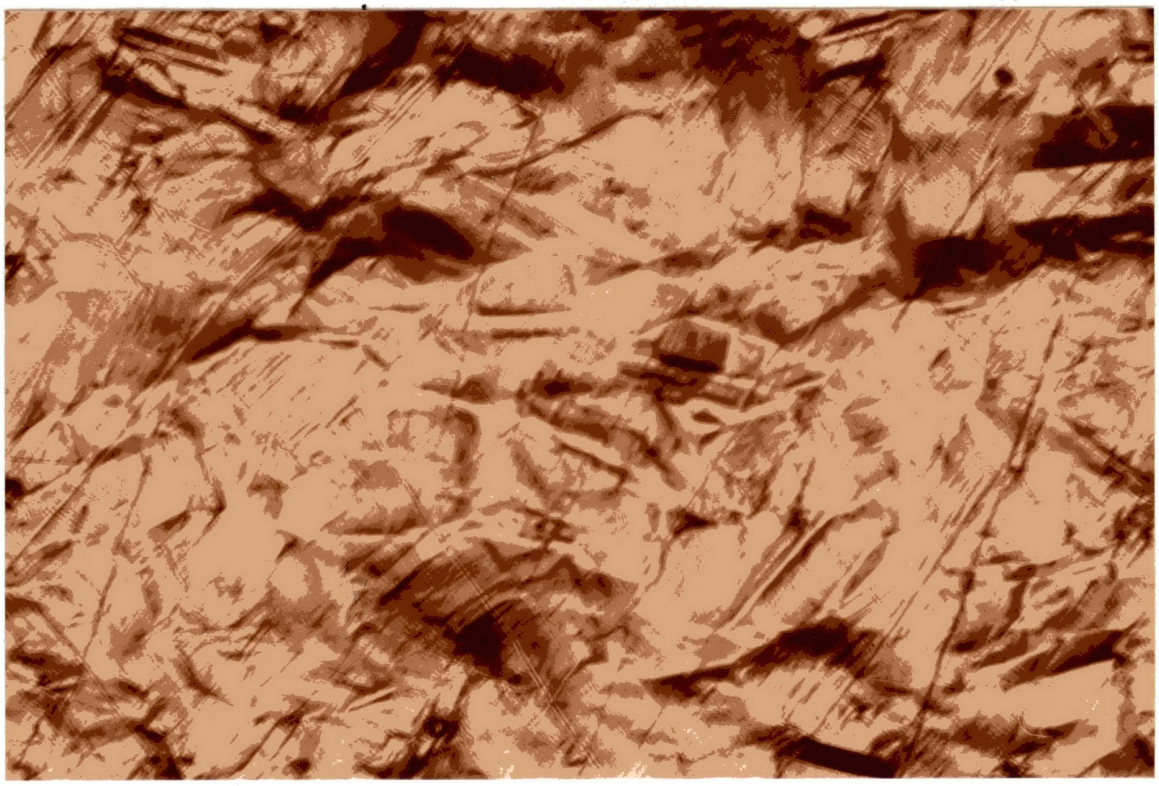

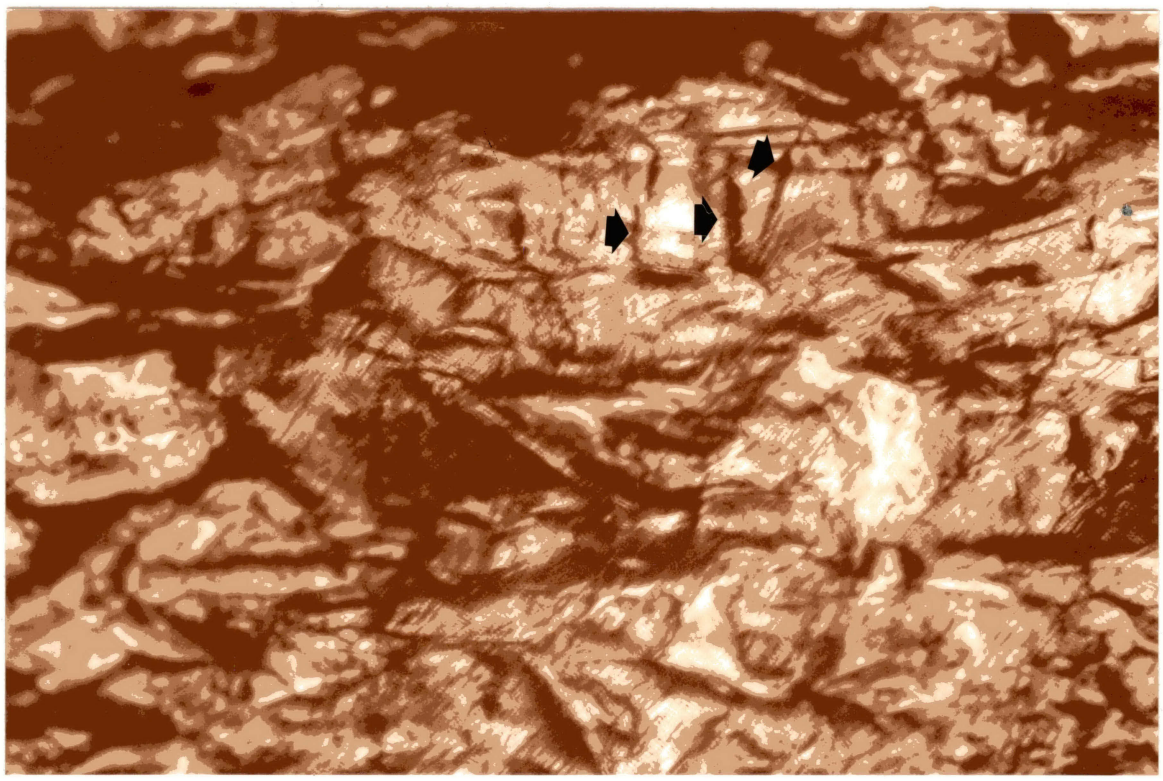

Figure 45. Side Cracking of Incoloy 800 After Fracture in Hydrogen (100X)

Figure 46. Detail of Figure 44 Illustrating 45° Cracking

25 10 1 2 4 8 E

25 10 1 2 4 8 E

Figure 47. Enlargement of Figure 38 Showing Wavy Slip (1000X)


25 IUJ 2688

Figure 48. Surface Damage of Incoloy 800 in Mercury at 80% of Tensile Strength (200X)

Figure 49. Surface Damage of Incoloy 800 in Merucry at Tensile Strength (200X)

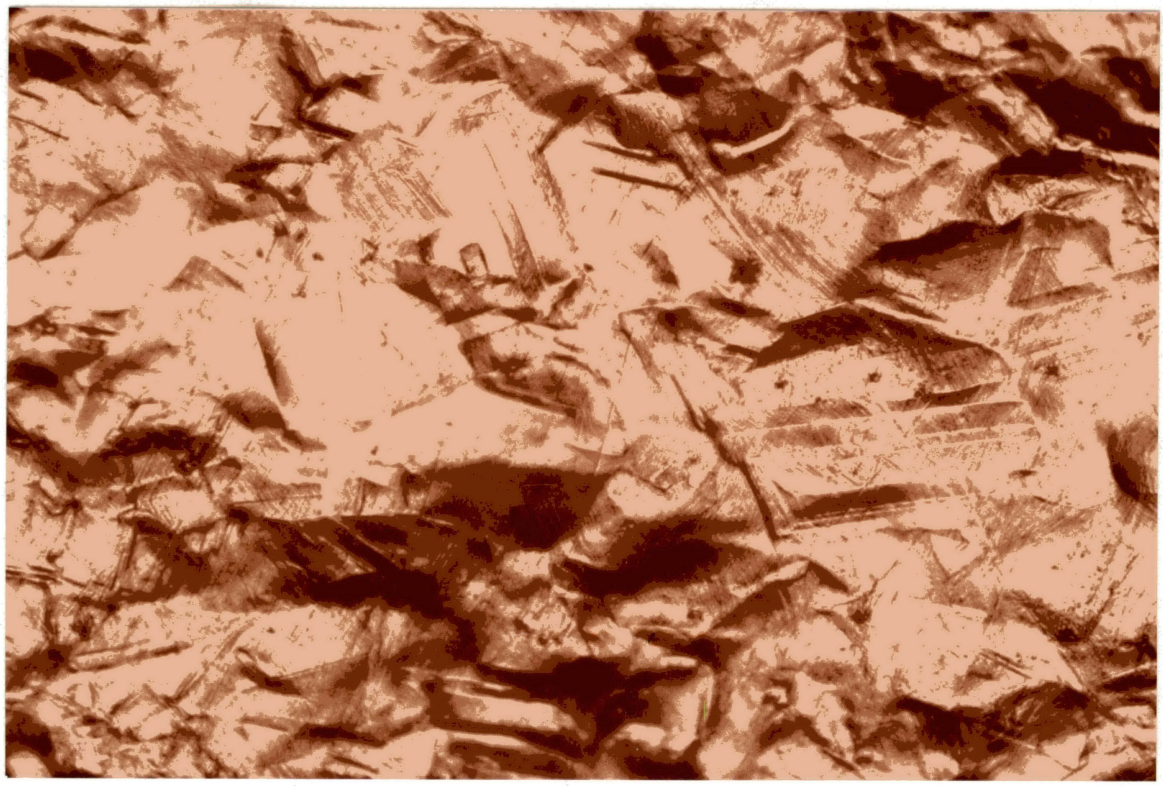

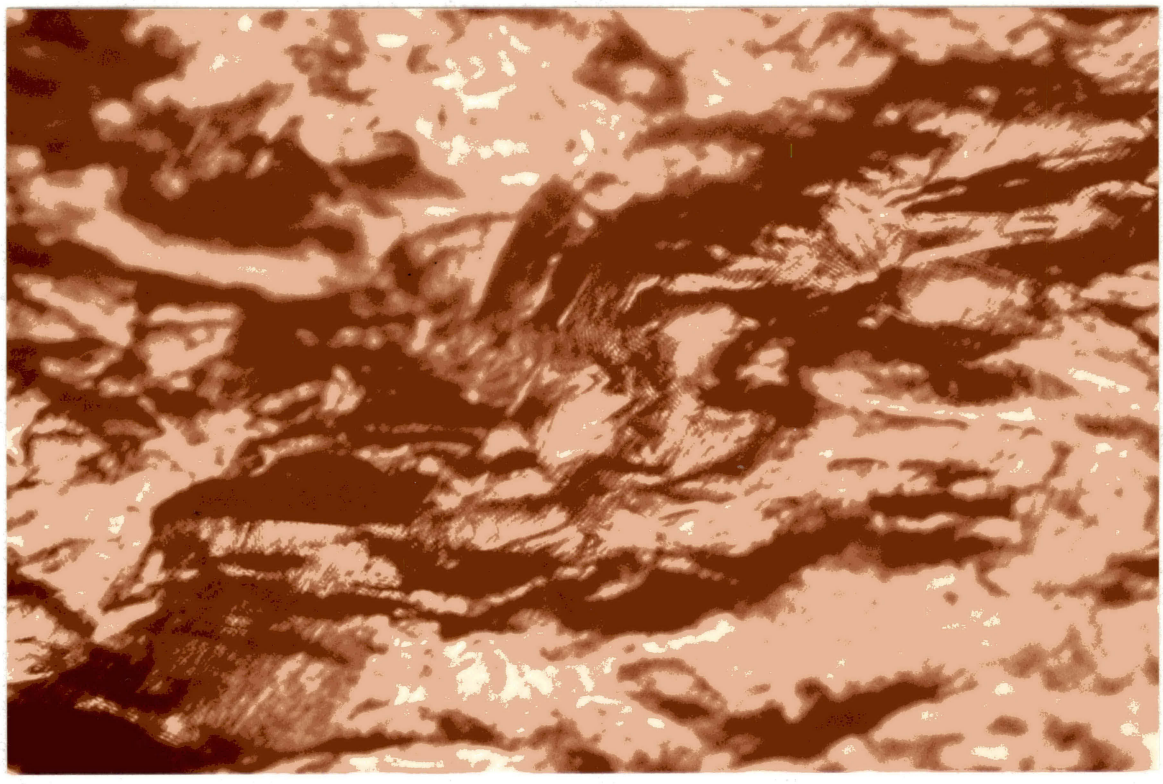

Figure 50. Side Cracking of Incoloy 800 After Fracture in Mercury (100X)

Figure 51. Detail of Figure 50 Illustrating 45° Side Cracking

25 10 1 2283

25 101 2283

Figure 52. Enlargement of Figure 50 Showing Wavy Slip (1000X)

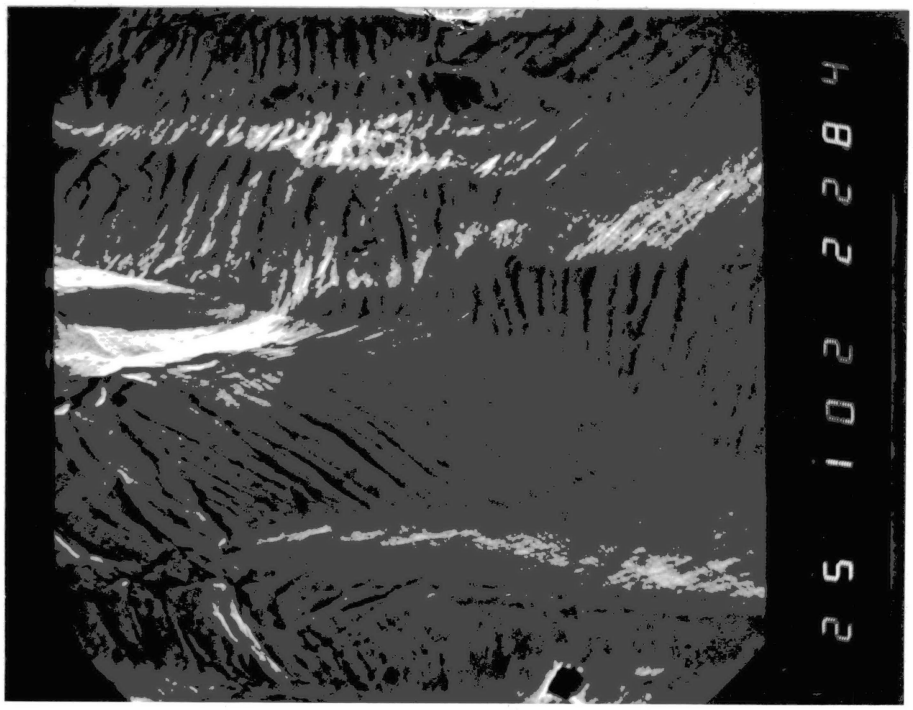
25 10 2201 4822

appears in Table X. A careful examination of this table reveals much about the relative propensity for embrittlement of each alloy.

The fracture surface details of each alloy in each environment have been documented and photographed reasonably well in previous studies and therefore do not merit repetitive analysis and description here. The fracture surface characteristics of each specimen are still of interest; therefore, each surface is catagorized in Table XI. This compact description simplifies analysis of qualitative data.

Mechanical Property Degradation

Introduction. In the performance of tensile tests to observe physical damage, a great deal of mechanical property data for air, mercury, and hydrogen environments was generated for all four alloys.

Engineering stress versus engineering strain curves were generated for annealed samples of all four alloys and appear as Figures 53 through 56. These standard graphs are useful for comparing one alloy to another in air. Accurate representation of specimen behavior in environment was not feasible due to environmental limitations of the extensometer.

In this and precursory studies, several different annealing cycles were used. The material behavior in environment with respect to properties in air shows trends in alloy susceptibility to embrittlement. Embrittlement is considered as loss of strength and/or ductility; this is usually reflected in the tensile strength or reduction in area or both. Those two properties were among those monitored during tensile tests. Using data taken from preceding studies with data from this study, tables were generated for each alloy to show the trends in embrittlement.

TABLE X

EMBRITTLEMENT AND CRACKING STRESS FOR NICKEL 200, MONEL 600, INCONEL 600, AND INCOLOY 800

Alloy	Air		Mercury			Hydrogen		
	Tensile Strength (kpsi)	Reduction in Area (%)	Tensile Strength (kpsi)	Reduction in Area, (%)	Stress at Cracking, (kpsi)	Tensile Strength (kpsi)	Reduction in Area, (%)	Stress at Cracking, (kpsi)
Nickel 200	77	83	77	62	68*	77	40	76
Monel 400	92	77	76	12	76	88	15	85
Inconel 600	119	64	119	59	94*	114	41	<91
Incoloy 800	95	65	94	62	75*	94	65	93

* After onset of necking

TABLE XI

FRACTURE SURFACE CLASSIFICATION OF THE ALLOYS TESTED IN AIR, MERCURY, AND HYDROGEN

Alloy	Air	Mercury	Hydrogen
Nickel 200 (UNS No. 2200)	M	T	T - i
Monel 400 (UNS No. 4400)	M	I	I - t
Inconel 600 (UNS No. 6600)	M	M - t	I - T
Incoloy 800 (UNS No. 8800)	M	M - i	M - i

M,m - microvoid coalescence

T,t - trangranular fracture

I,i - intergranular fracture

Upper Case - major feature

Lower Case - minor feature

Figure 53. Engineering Stress Versus Engineering Strain for Annealed Nickel 200

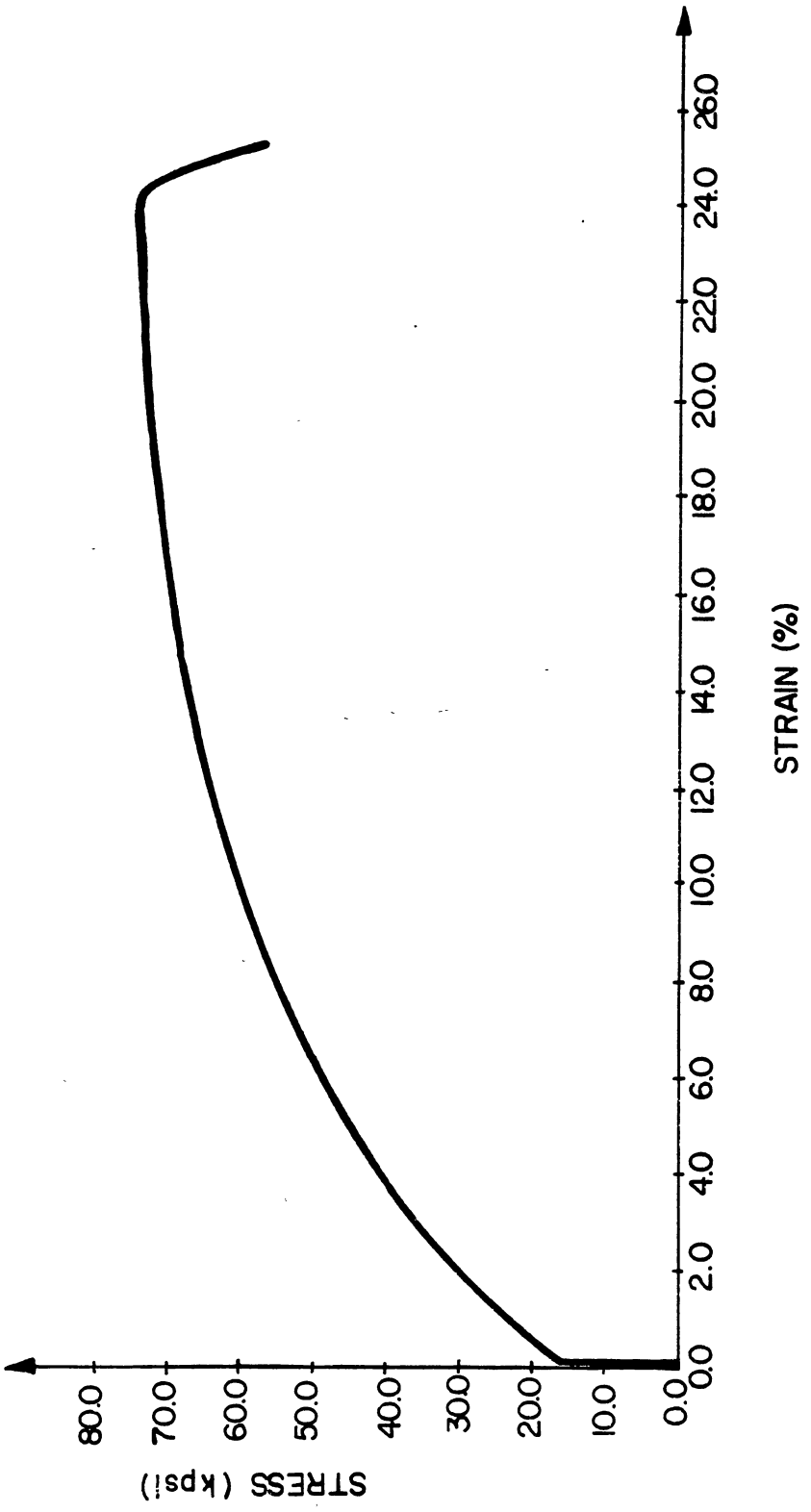
STRESS (kpsi)
80.0
70.0
60.0
50.0
40.0
30.0
20.0
10.0
0.0
0.0
2.0
4.0
6.0
8.0
10.0
12.0
14.0
16.0
18.0
20.0
22.0
24.0
26.0
STRAIN (%)

Figure 54. Engineering Stress Versus Engineering Strain for Monel 400

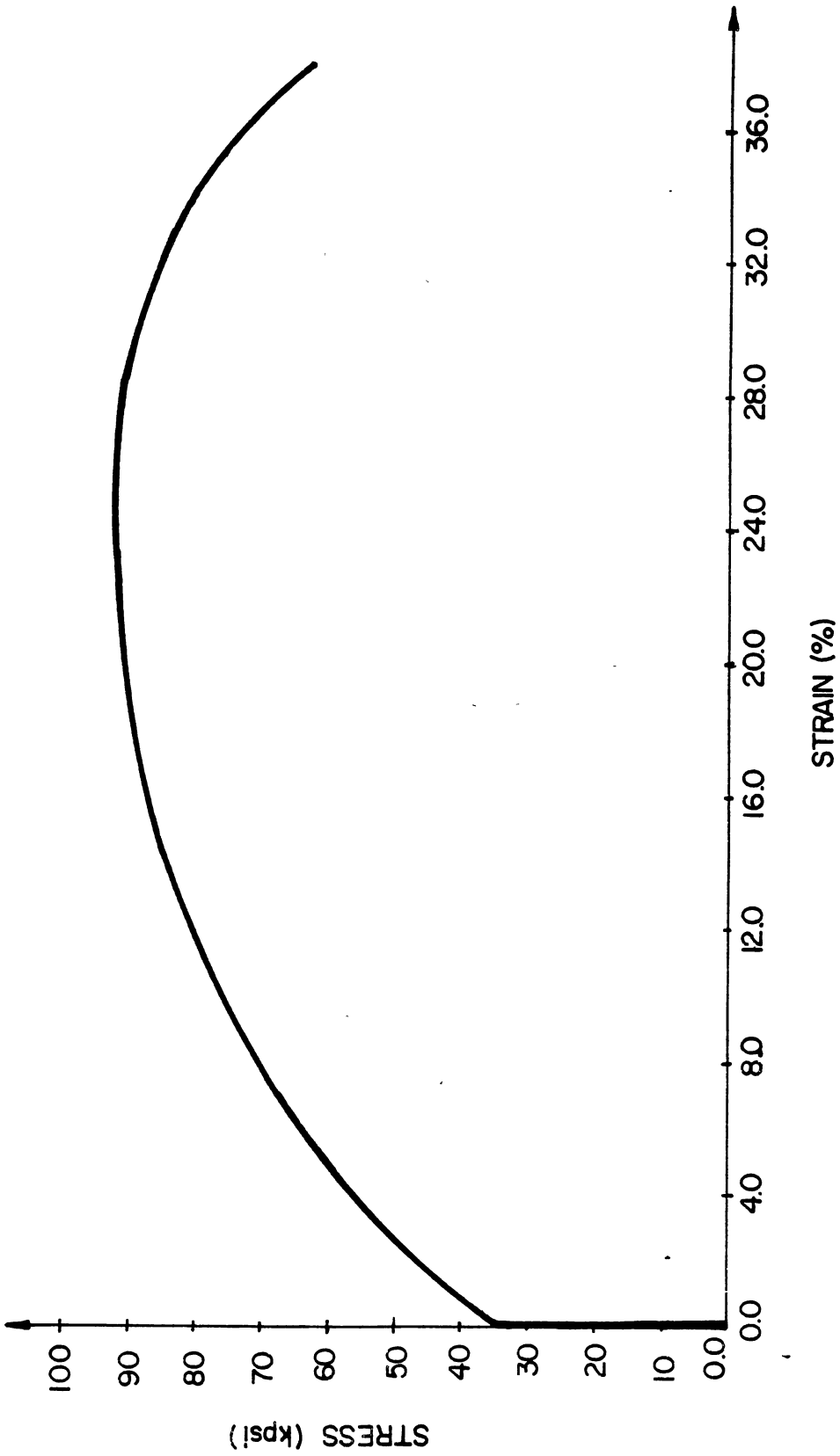
STRESS (kpsi)
0.0
10
20
30
40
50
60
70
80
90
100
0.0
4.0
8.0
12.0
16.0
20.0
24.0
28.0
32.0
36.0
STRAIN (%)

Figure 55. Engineering Stress Versus Engineering Strain for Inconel 600

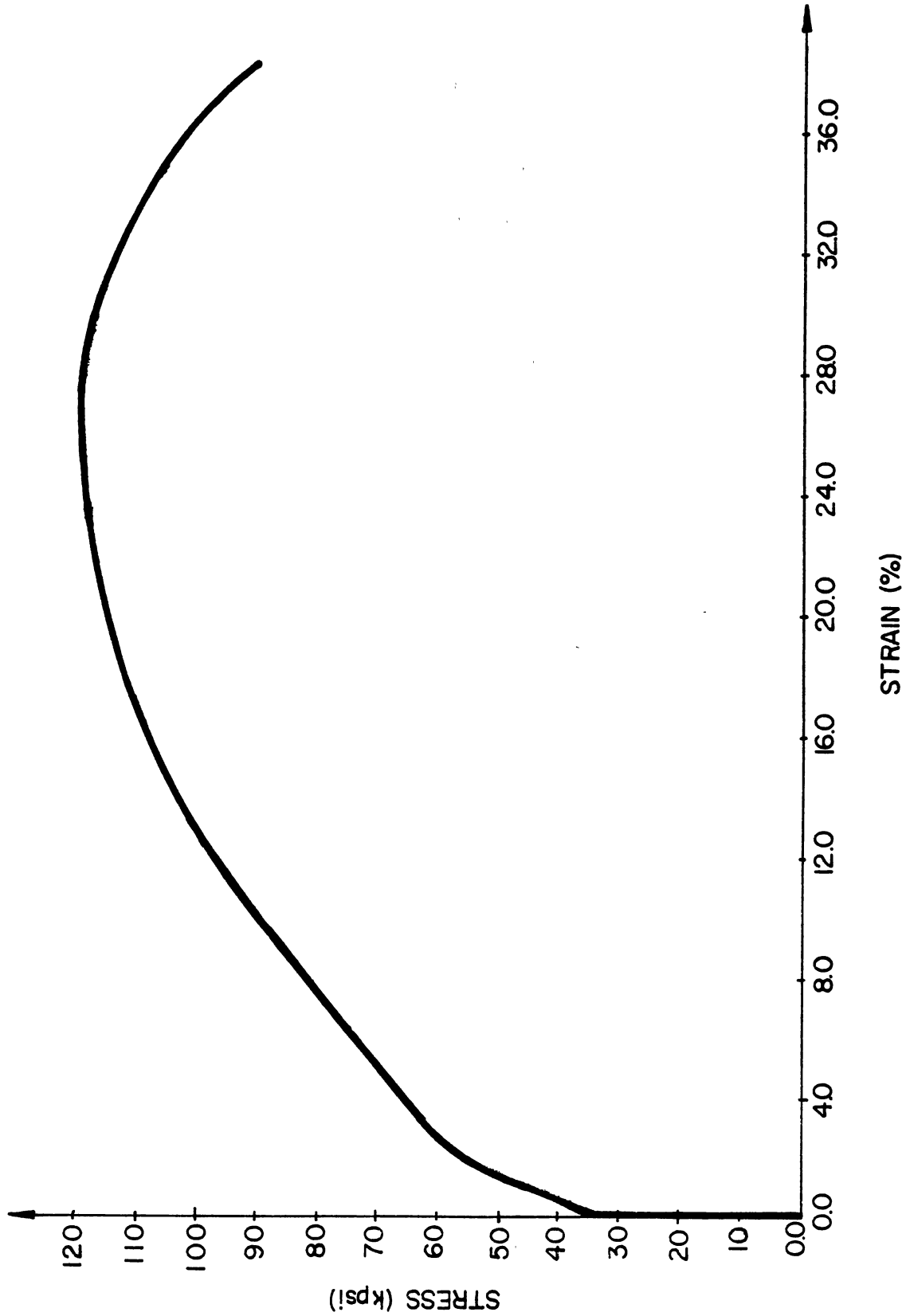
STRESS (kpsi)
0.0
10
20
30
40
50
60
70
80
90
100
110
120
0.0
4.0
8.0
12.0
16.0
20.0
24.0
28.0
32.0
36.0
STRAIN (%)

Figure 56. Engineering Stress Versus Engineering Strain for Incoloy 800

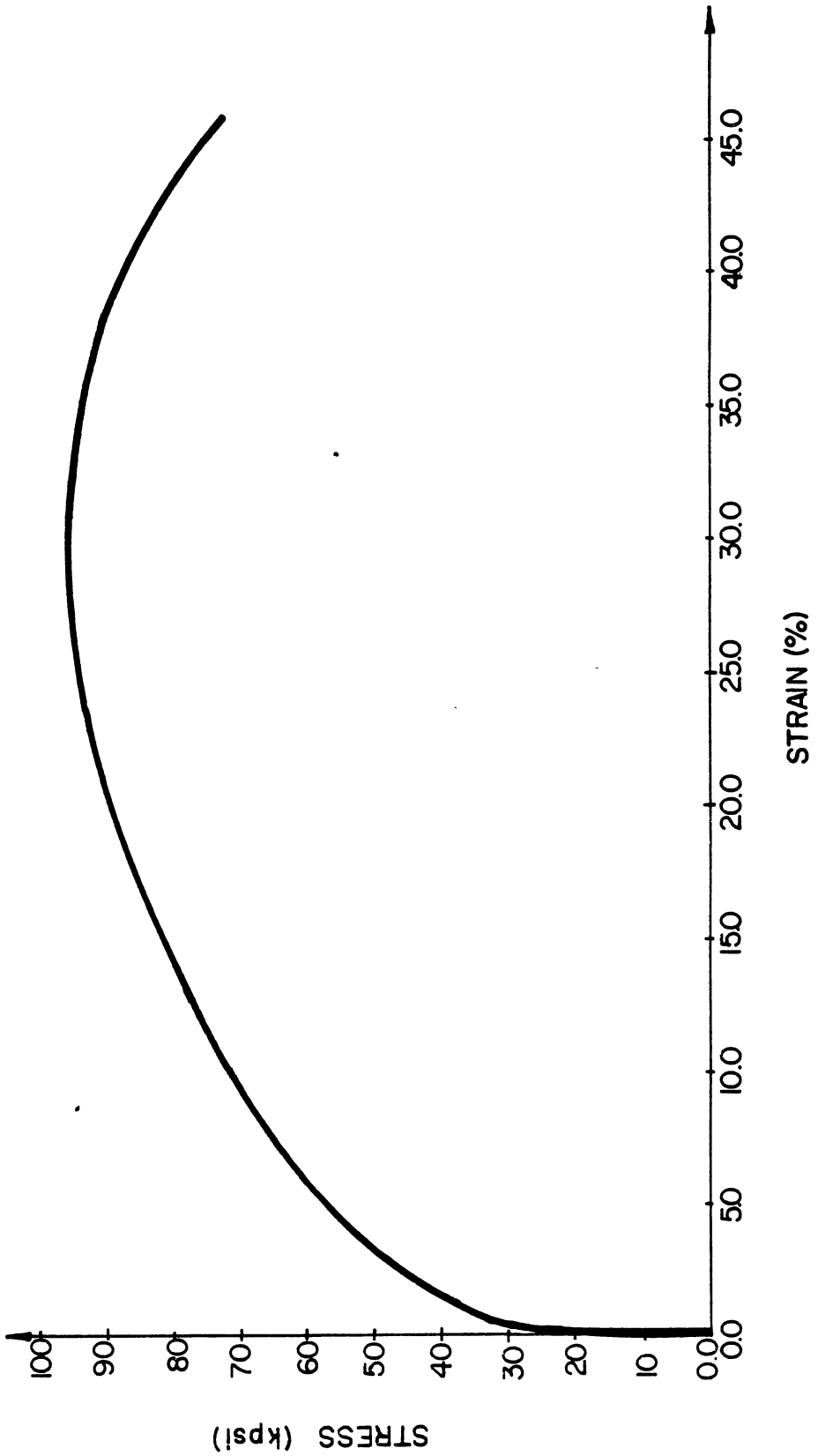
STRESS (kpsi)
0.0
10
20
30
40
50
60
70
80
90
100
0.0
5.0
10.0
15.0
20.0
25.0
30.0
35.0
40.0
45.0
STRAIN (%)

Alloy Nickel 200. For Nickel 200, the data for a two-hour anneal at 750°C were consistent with the results by Traylor [3]. There was no loss in tensile strength in either mercury or hydrogen, while reduction in area dropped from 83 percent in air to 62 percent in mercury to 40 percent in hydrogen. Available data are compiled into Table XII, which shows tensile strength and reduction in area in air, mercury, and hydrogen for several annealing cycles. As the annealing temperature, hence the grain size, increases the susceptibility of Nickel 200 to embrittlement by mercury or hydrogen decreases.

Alloy Monel 400. Tensile test data for Monel 400 were checked in air, mercury, and hydrogen. Consistent with Fredell [5], about 5 percent loss in tensile strength in hydrogen and 15 to 20 percent loss in mercury was noted for 30 to 35 μm grain size. More striking is the loss of ductility as reflected in the reduction in area. Also consistent with Fredell [5], reduction in area declined from 75 percent in air to 15 percent in hydrogen to 12 percent in mercury. Available data are compiled into Table XIII in the same format as the previous table. From the table, increasing annealing temperature, hence grain size, decreases embrittlement in both hydrogen and mercury, though the effect is much more pronounced in hydrogen.

Alloy Inconel 600. Less preliminary data were available for Inconel 600, one of the two commercial superalloys in this study. Consequently, the purpose was to check and extend the previous data by Price and Good [1]. Consistent with Price and Good [1], no loss in tensile strength in either mercury or hydrogen was notable. More significantly, for samples annealed two hours at 1100°C, reduction in area dropped from 64

TABLE XII

NICKEL 200--TENSILE STRENGTH AND REDUCTION IN AREA FOR SEVERAL ANNEALING CYCLES

Temp °C	Time hrs	Air		Mercury		Hydrogen	
		Ten. Str. (kspi)	R.A. (%)	Ten. Str. (kspi)	R.A. (%)	Ten. Str. (kspi)	R.A. (%)
750	2	77	83[1]	77	62[1]	77[1]	40[1]
1000	2	—	—	72	61[2]	71	40[2]
1050	2	73	77[2]	—	—	69	43[3]
1090	2	71	70[2]	70	45[3]	—	—

[1]This study

[2]Traylor [4]

[3]Fredell [5]

TABLE XIII

MONEL 400--TENSILE STRENGTH AND REDUCTION IN AREA FOR SEVERAL ANNEALING CYCLES

Temp °C	Time hrs	Air		Mercury		Hydrogen	
		Ten. Str. (kspi)	R.A. (%)	Ten. Str. (kspi)	R.A. (%)	Ten. Str. (kspi)	R.A. (%)
700	2	92	67[3]	73	12[2]	81	12[c]
750	2	92	77[1]	76	12[1]	88	15[1]
800	2	—	—	73	10[2]	—	—
900	2	—	—	71	12[2]	81	19[2]
1000	2	—	—	63	12[2]	86	43[2]
1075	3	89	70[2]	63	11[2]	83	32[2]

[1]This study

[2]Fredell [5]

[3]Traylor [4]

percent in air to 59 percent in mercury to 41 percent in hydrogen. Available data are compiled into Table XIV in the same format as before. As with Nickel 200 and Monel 400, as the annealing temperature increases--hence the grain size--the susceptibility to embrittlement by mercury decreases. It appears that the susceptibility to hydrogen embrittlement increases with decreasing grain size. The effect is not large and hence may be a result of experimental scatter.

Alloy Incoloy 800. Also of primary interest is Incoloy 800, the other commercial superalloy in this study. Very little tensile test data were available from precursory studies. Consequently, both vertical and horizontal series tests were performed. Specimens from three different annealing cycles were tested in air and specimens from the intermediate cycle were tested in mercury and hydrogen. As expected, tensile strength decreased with increasing annealing temperature. Hydrogen caused no notable decrease in tensile strength or ductility. In mercury, the tensile strength decreased only slightly and reduction in area decreased only 10 percent. The available data are compiled into Table XV. In every test, the failure was cup and cone. Because of cup and cone fractures and lack of notable embrittlement, further tensile tests would probably be unproductive.

Fatigue Tests

Fatigue testing offers a method of introducing cracks at stress levels much below the tensile strength, hence should increase the propensity toward intergranular failures. This might prove especially useful in investigating alloys which are somewhat resistant to embrittlement.

TABLE XIV

INCONEL 600--TENSILE STRENGTH AND REDUCTION IN AREA FOR SEVERAL ANNEALING CYCLES

Temp °C	Time hrs	Air		Mercury		Hydrogen	
		Ten. Str. (kspi)	R.A. (%)	Ten. Str. (kspi)	R.A. (%)	Ten. Str. (kspi)	R.A. (%)
1000	2	122	63[1]	125	51[2]	138	47[2]
1050	2	121	67[1]	124	61[2]	123	45[2]
1100	2	119	64[1]	119	59[1]	114	41[1]

[1] This study

[2] Good [2]

TABLE XV

INCOLOY 800--TENSILE STRENGTH AND REDUCTION IN AREA FOR SEVERAL ANNEALING CYCLES

Temp °C	Time hrs	Air		Mercury		Hydrogen	
		Ten. Str. (kspi)	R.A. (%)	Ten. Str. (kspi)	R.A. (%)	Ten. Str. (kspi)	R.A. (%)
1000	2	107	64	109	41[1]	—	—
1050	2	95	65	94	62	94	65
1100	2	92	66	—	—	—	—

[1] Good [2]

Fatigue testing also provides a second set of test conditions to compare hydrogen and mercury embrittlement, thereby broadening the data base.

Annealed Materials

Alloys Nickel 200 and Monel 400 have been studied by Traylor [3] and Fredell [5], respectively; therefore, attention was concentrated on the commercial superalloys Inconel 600 (UNS N06600) and Incoloy 800 (UNS N08800). For Nickel 200 (UNS N02200), Traylor found that intergranular failures, which were uncommon in tensile testing, occurred in hydrogen and mercury in fatigue. Additionally, fatigue lives were much reduced in mercury and somewhat reduced in hydrogen. For Monel 400 in fatigue, Fredell [5] found that failures were intergranular in both mercury and hydrogen. While fatigue lives in hydrogen were much reduced, the lives in mercury were reduced to less than one percent of the life in air. The background for Inconel 600 came from the limited, preliminary, exploratory work of Price and Good [1]. Their study hinted at relatively little embrittlement in mercury in fatigue. In the same study, Incoloy 800 failed intergranularly when fatigued in mercury, when tensile tests had given cup-cone failures.

In light of the limited data on Inconel 600 and Incoloy 800, tests were performed on both alloys in air, mercury, and hydrogen at a stress equal to 70 percent of the tensile strength in air. The results appear in Table XVI. Seventy percent of the tensile strength in air was selected as being a stress level in the high cycle fatigue regime without giving excessive lives. The results were disconcerting in two respects: (1) in general, failures were transgranular in contrast with intergranular

TABLE XVI

ENVIRONMENTAL FATIGUE LIVES OF INCONEL AND INCOLOY 800 AT 70 PERCENT OF THE TENSILE STRENGTH

Alloy	Stress Kspi	Fatigue Life (x 1000 Cycles)		
		Air	Mercury	Hydrogen
Inconel 600	77.0	204	56	234
Incoloy 800	64.4	142	98	155

failures in limited data by Price and Good [1, 2]; and (2) fatigue lives were enhanced in hydrogen.

The fracture surface of Inconel 600 in air was covered with ridges or tears in the fatigue zone, Figure 57. At the origin, Figure 58, the fracture was slightly faceted but a few grains deeper only tear ridges were visible. The sample fatigued in hydrogen did not have the faceted appearance at the origin but tear ridges were more prominent (Figures 59 and 60). This appears to be consistent with the enhanced life in hydrogen without explaining it. The fracture surface of the sample broken in mercury was not completely transgranular (Figure 61). The fracture originated cleanly intergranular, but at 5 to 7 grains deep changed to transgranular (Figure 62). Scanning the surface some small secondary cracks could be discerned beneath the veil of tear ridges.

The fracture surface of Incoloy 800 (UNS N08800) in air was transgranular and covered with intense tear ridges with a slight faceted appearance at the origin (Figures 63 and 64). Similarly, the fracture surface of the sample fatigued in hydrogen was covered with intense tear ridges but without the faceted appearance at the origin (Figures 65 and 66). The fracture surface of the sample fatigued in mercury was substantially transgranular (Figure 67) but some faceting and clean grain faces were visible at the origin (Figure 68). This is evidence of some intergranular character, though not nearly so clean as the aforementioned Inconel 600 sample fatigued in mercury (Figures 61 and 62).

After completion of the initial series of fatigue tests, the progression of fatigue damage was thence monitored for an Inconel 600 specimen in mercury by removing the sample periodically for observing and

Figure 57. Fracture Surface of Inconel 600 Fatigued in Air at 70% of Tensile Strength (16X)

Figure 58. Origin Zone of Figure 57 (500X)

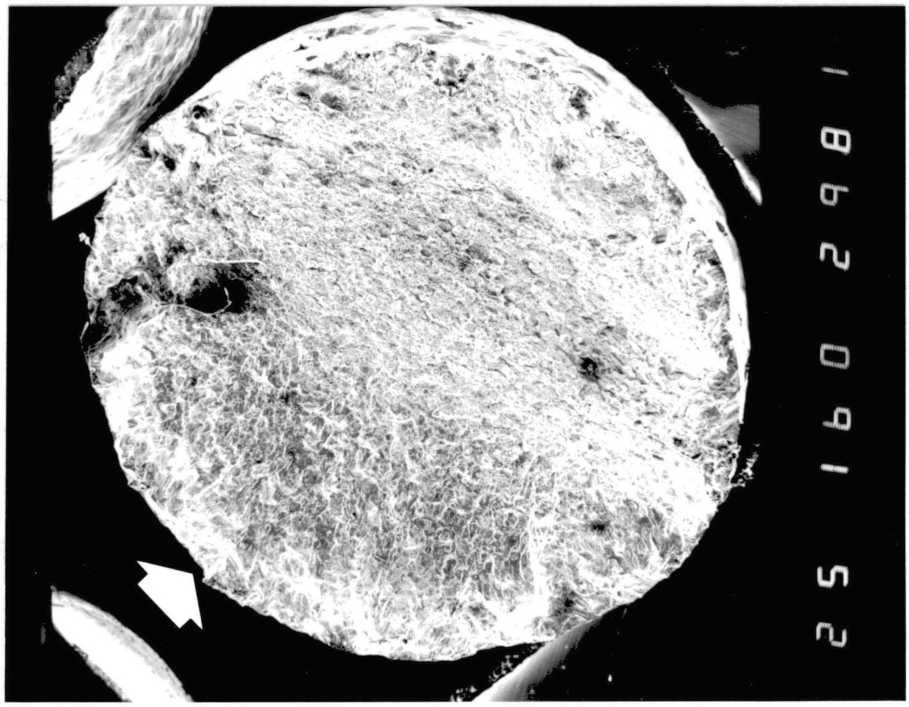
25 160 29801

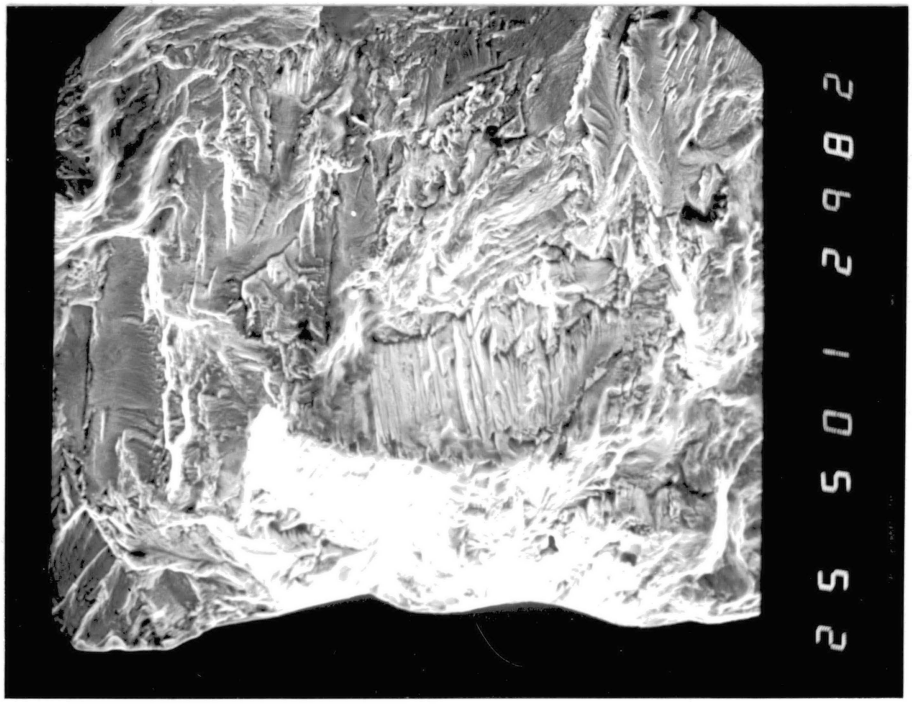
25 501 29802

Figure 59. Fracture Surface of Inconel 600 Fatigued in Hydrogen at 70% of Tensile Strength (16X)

Figure 60. Origin Zone of Figure 59 (500X)

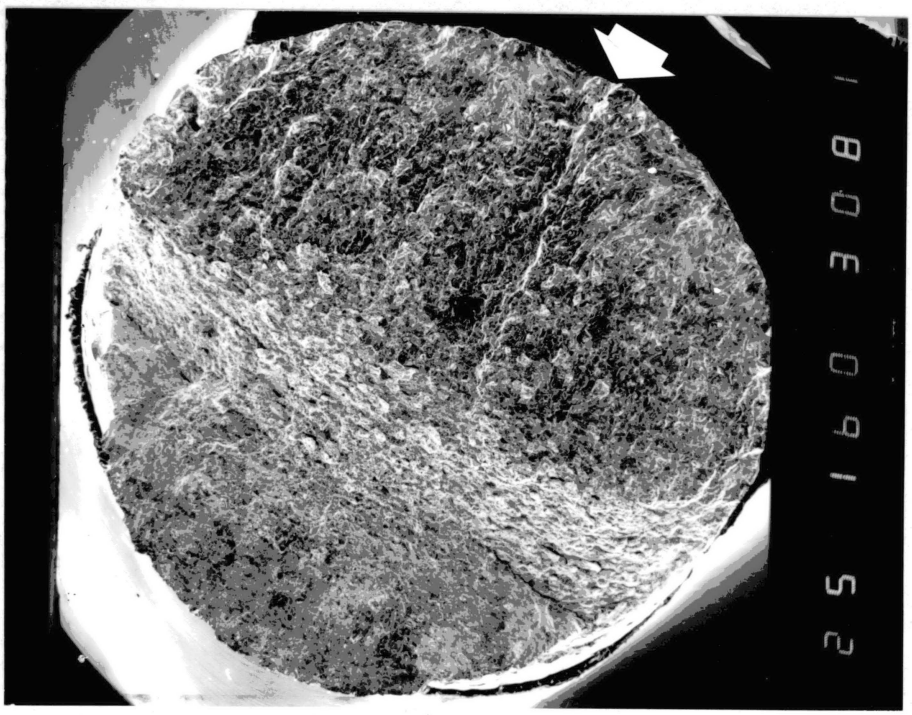
2 S 1 80 E 08 1

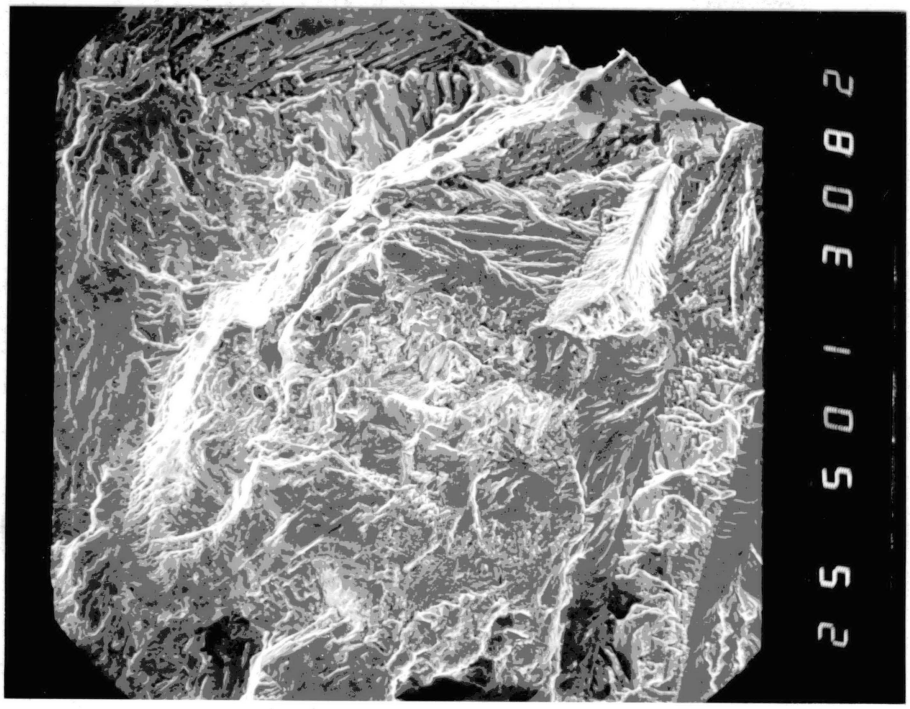
2 S 80 E 08 2

Figure 61. Fracture Surface of Inconel 600 Fatigued in Mercury at 70% of Tensile Strength (16X)

Figure 62. Origin Zone of Figure 61 (100X)

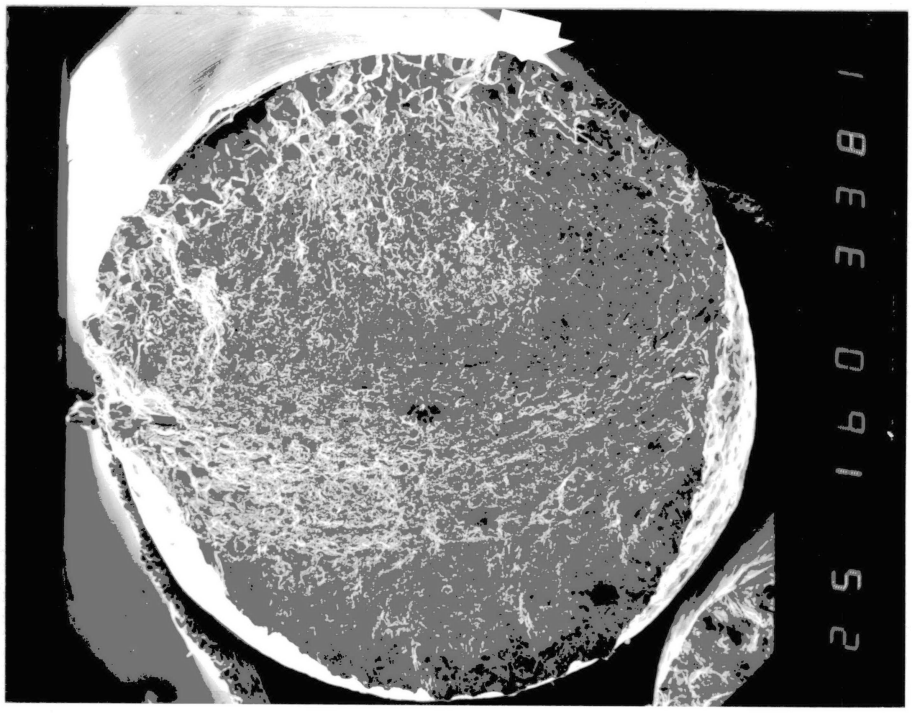
S2 160 EEB 1

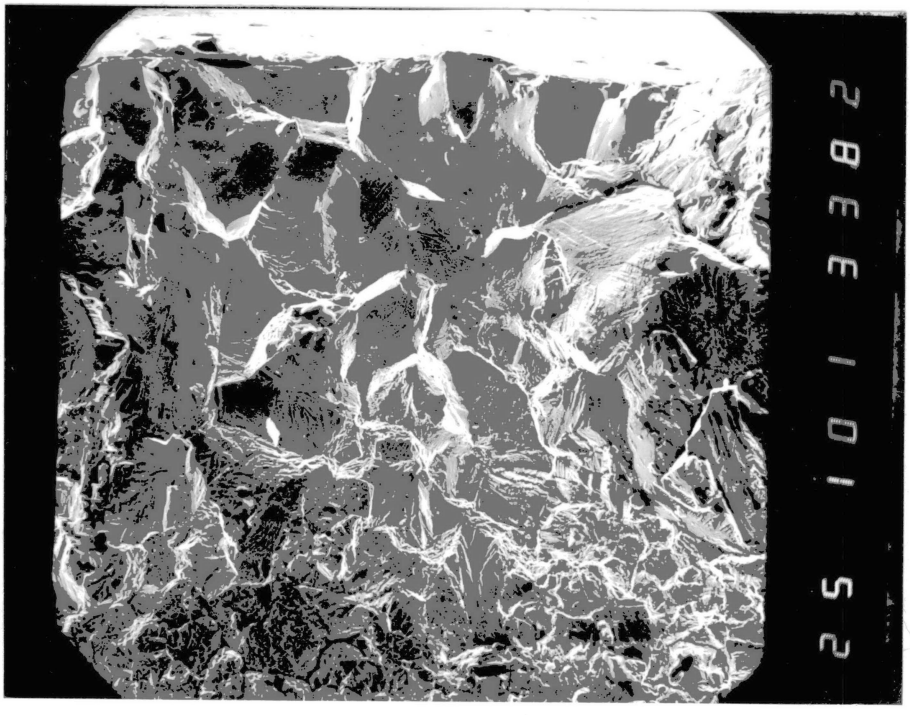
S2 101 EEB 2

Figure 63. Fracture Surface of Incoloy 800 Fatigued in Air at 70% of Tensile Strength (16X)

Figure 64. Origin Zone of Figure 63 (500X)

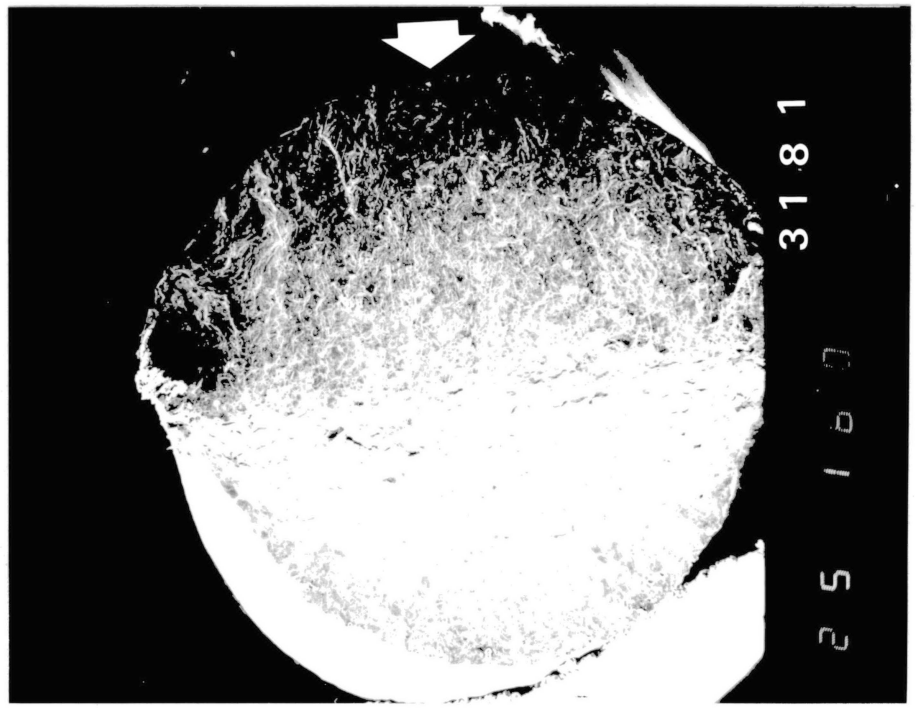
25 JUL 80
3181

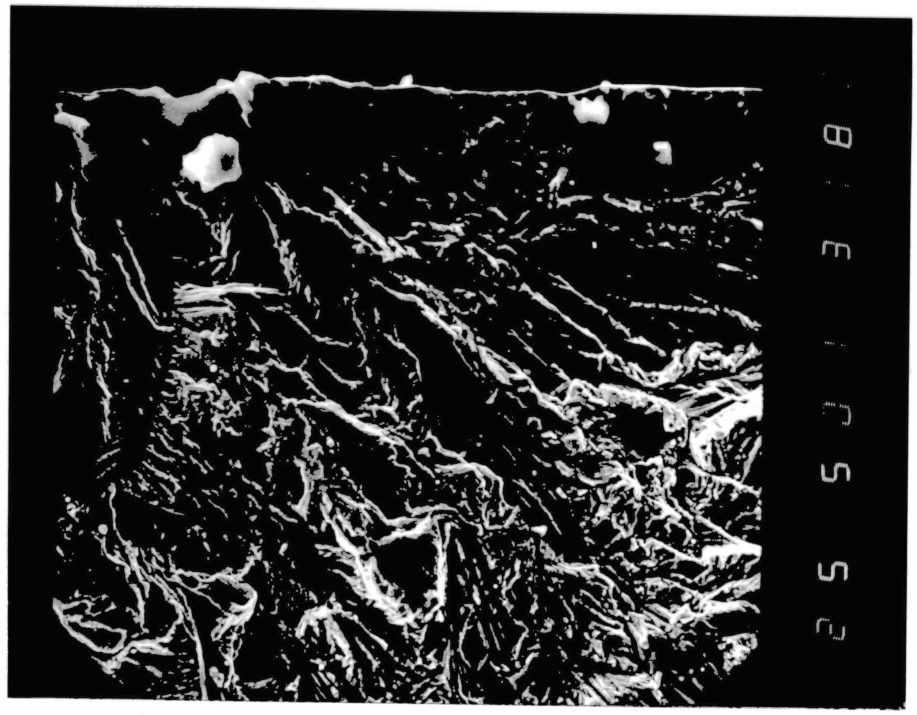
25 JUL 80

Figure 65. Fracture Surface of Incoloy 800 Fatigued in Hydrogen at 70% of Tensile Strength (16X)

Figure 66. Origin Zone of Figure 65 (500X)

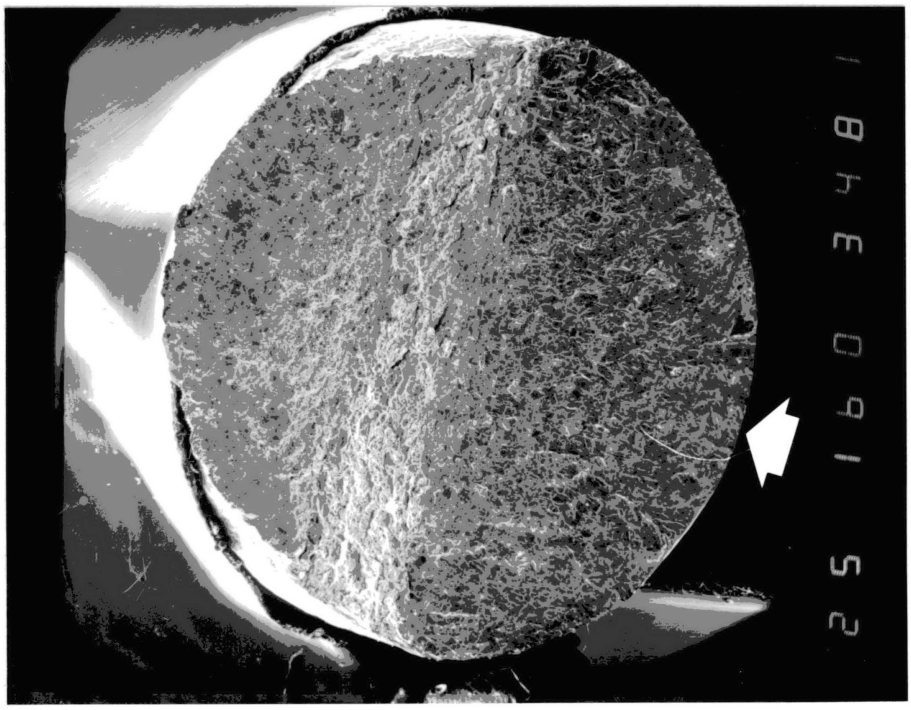
1 THE 091 52

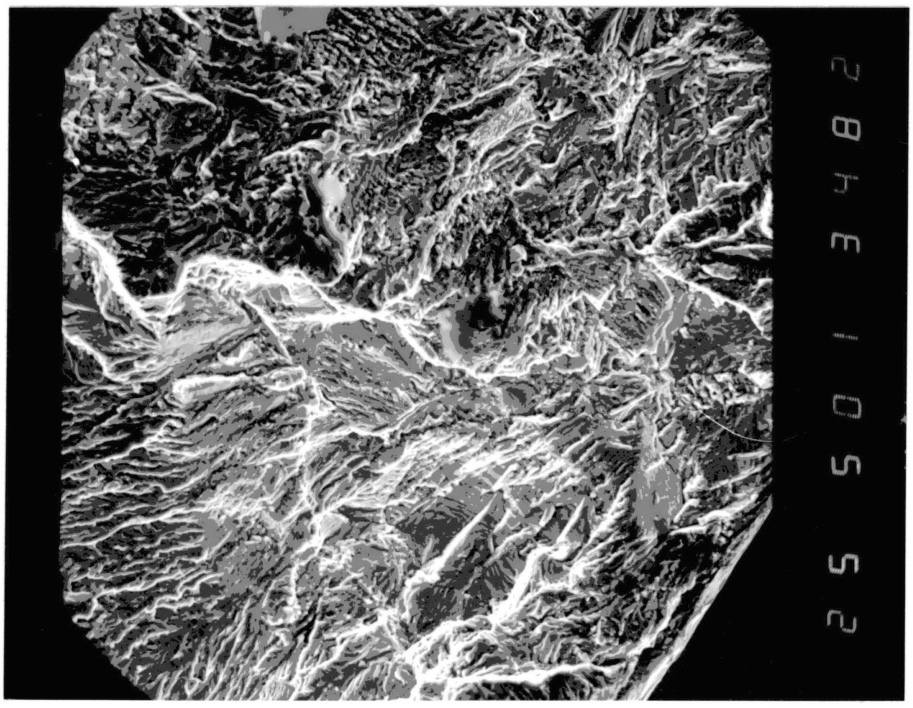
2 THE 105 52

Figure 67. Fracture Surface of Incoloy 800 Fatigued in Mercury at 70% of Tensile Strength (16X)

Figure 68. Origin Zone of Figure 67 (500X)


25 160 E281

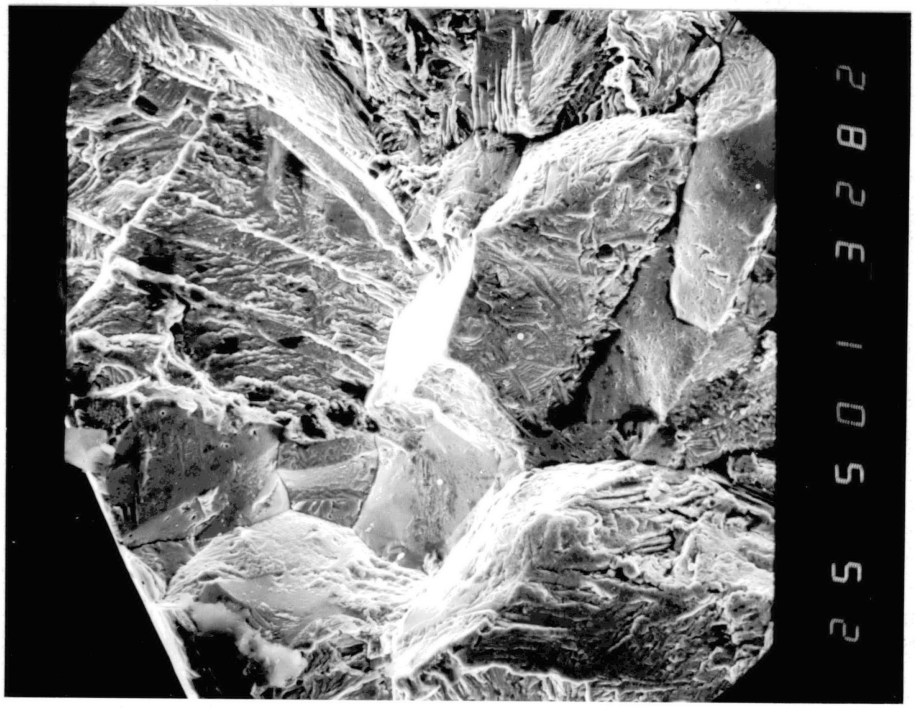
25 SOI E282

photographing in the Reichart optical microscope. The continual intensification of surface damage throughout the fatigue life can be seen in Figures 69 through 71. The fatigue life was 81,600 cycles at 70 percent of the tensile strength in alternating tension. Notice the crack in the initial figure. It may be followed through the series. Surprisingly, though the crack is apparent at 34 percent of the fatigue life, it is not appreciably larger at 83 percent of the life. This was the first crack observed yet failure did not occur there. Because of difficulty in discerning the fine details of the crack initiation stage with the optical microscope approach, it was deemed prohibitive to extend the procedure to other environments, stress levels, or the Incoloy 800 alloy.

Further study concentrated on following up the disconcerting observations of the lack of intergranular fracture and enhanced life in hydrogen. The enhanced life in hydrogen was confirmed by Good [2] for Inconel 600. Scrutiny of the broken samples of Good showed intergranular failures. The only apparent difference between the samples of Good and this study was the finer grain size in the former. This stimulated a recollection from the work of Fredell [5] that given a coarse enough grain size, nonintergranular tensile fractures could even be achieved in extremely embrittlement sensitive Monel 400. Some of his data appear as Table XVII. Consequently, the next stage of the investigation was to put the foregoing matters to immediate investigation for Inconel 600 and Incoloy 800.

Accordingly, fatigue tests were performed on Inconel 600 in air, mercury, and hydrogen at a larger grain size than that used by Good [36]. This study used a grain size of about 70 μm; Good used a grain size of

Figure 69. Surface Damage of Inconel 600 Fatigued in Mercury for 34% of Life (28030 Cycles) (200X)

Figure 70. Surface Damage of Inconel 600 Fatigued in Mercury for 69% of Life (56610 Cycles) (200X)

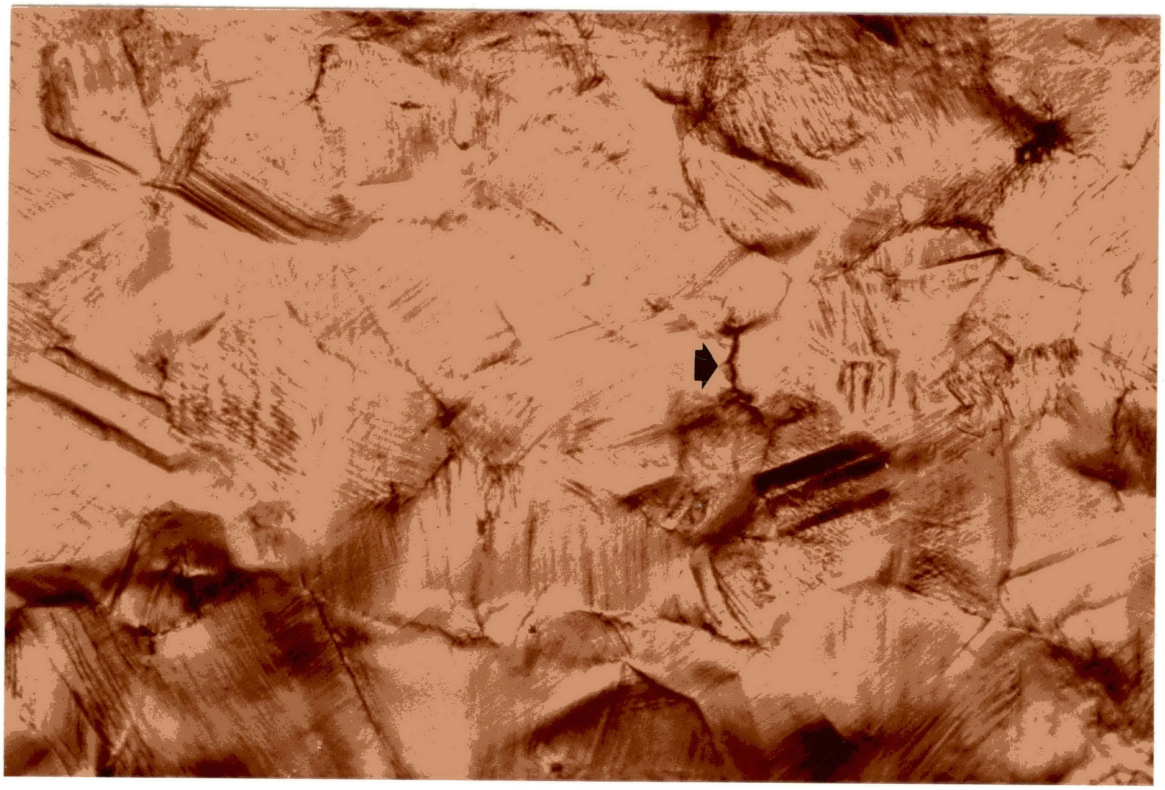

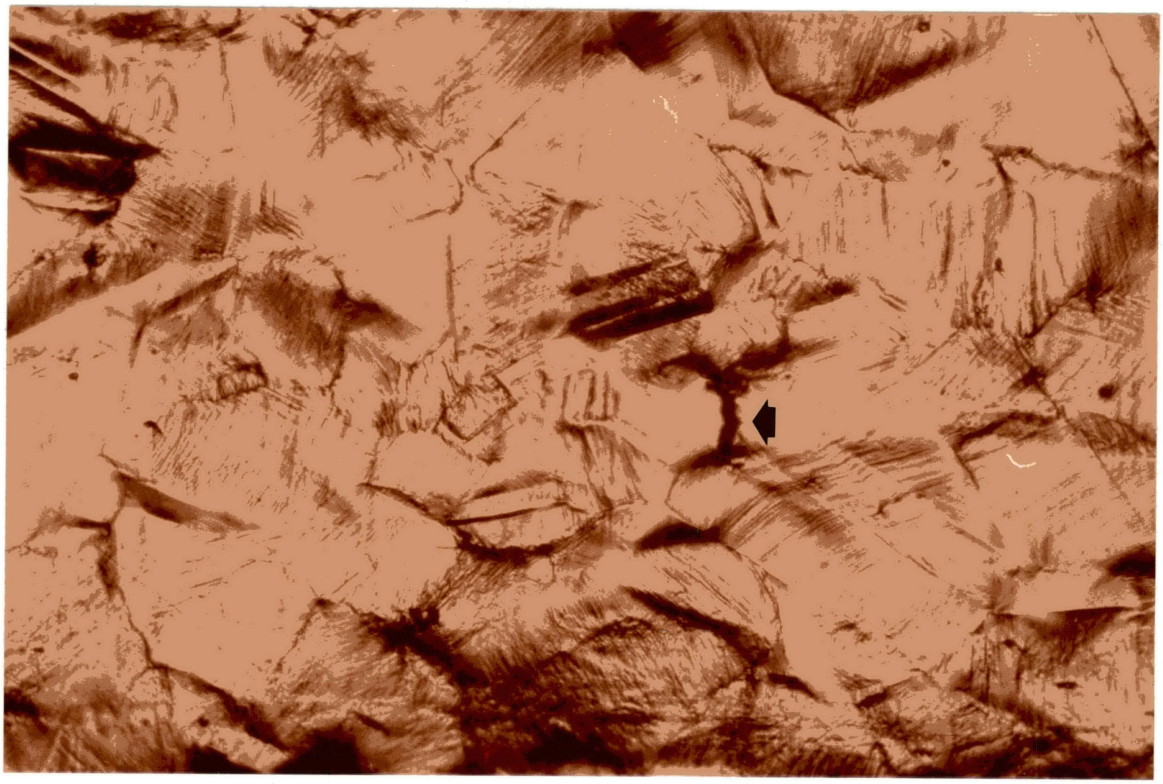

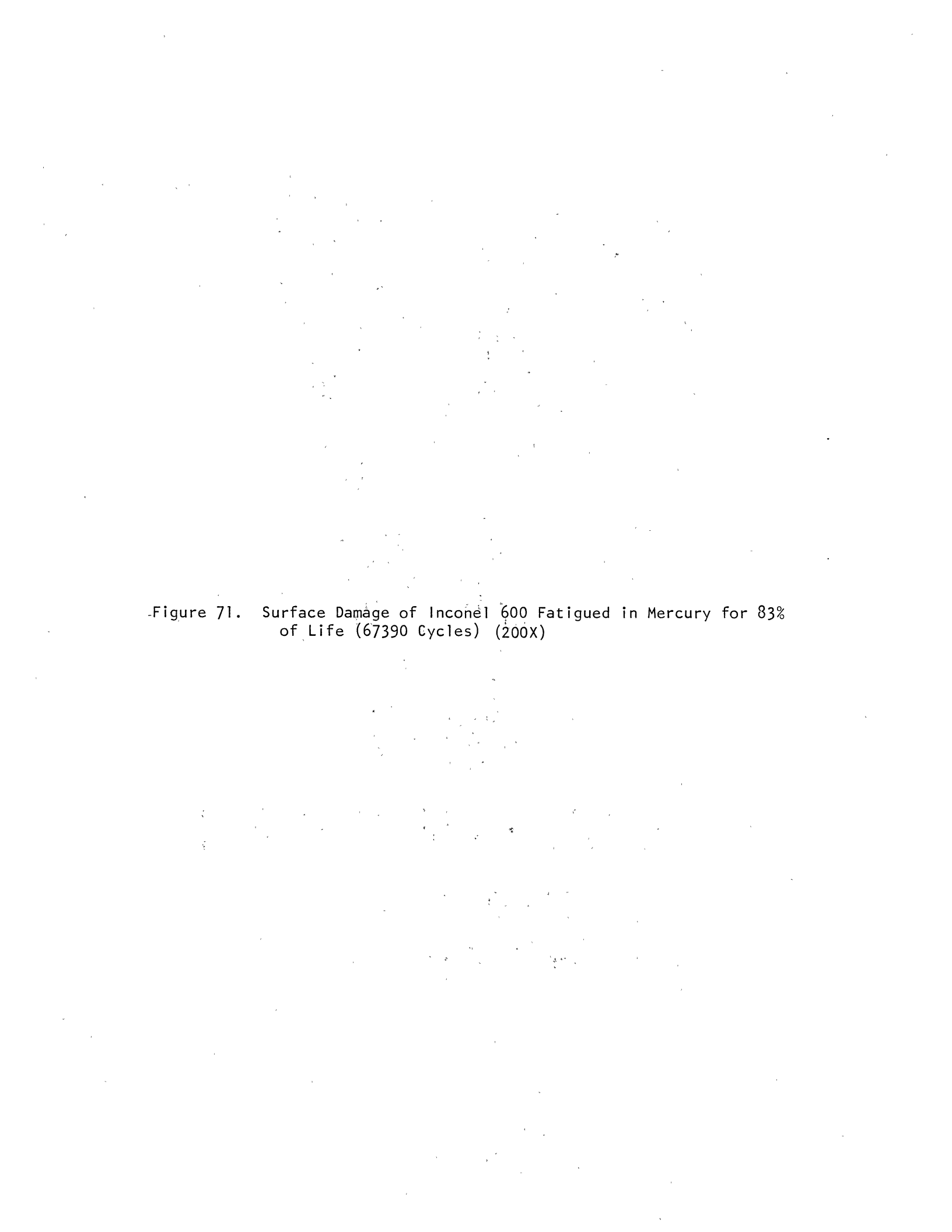

Figure 71. Surface Damage of Inconel 600 Fatigued in Mercury for 83% of Life (67390 Cycles) (200X)

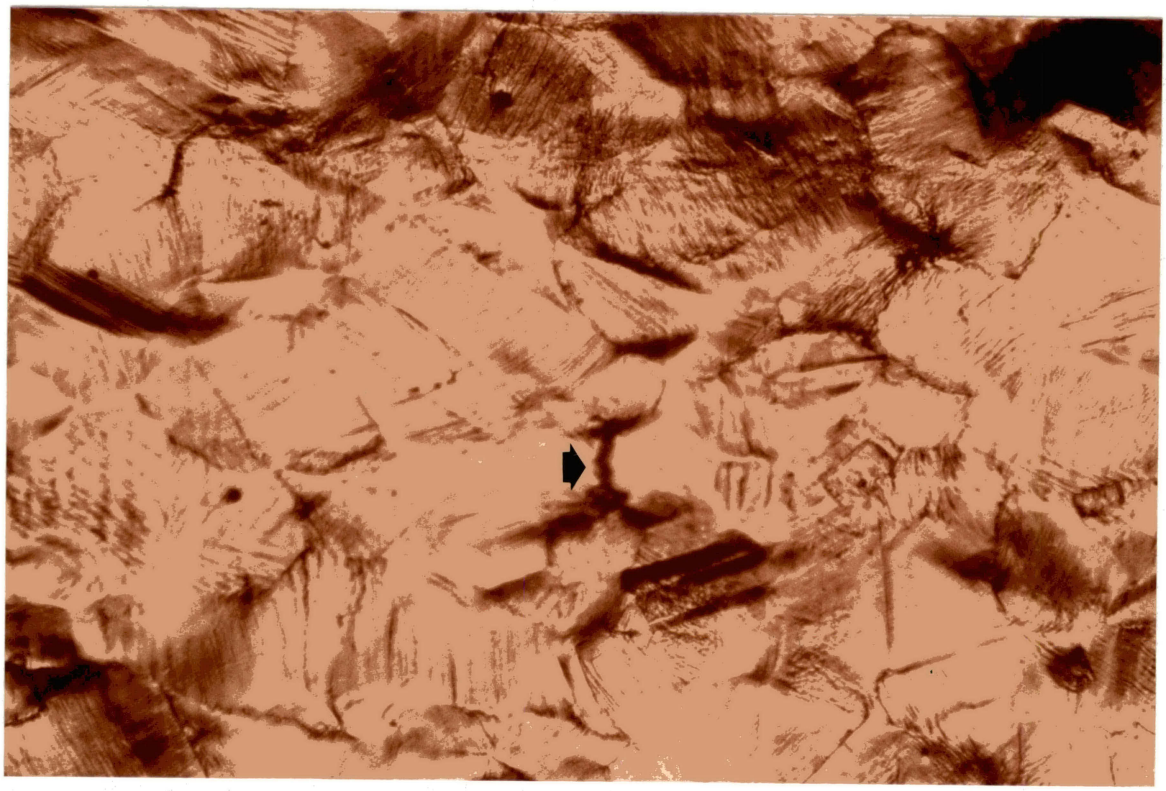

TABLE XVII

ENVIRONMENTAL FATIGUE LIFE OF MONEL 400[1]

Grain Size (10^{-6} m)	Peak Stress (kspi)	Fatigue Life (x 1000 Cycles)		
		Air	Mercury	Hydrogen
35	60	630	3.4	79
250	56	635	—	173
250	40	—	644	—

[1] Fredell [5]

about 7 μm. The results appear in Table XVIII with those of Good for comparison.

Next, fatigue tests were performed on Incoloy 800 in air, mercury, and hydrogen for two different grain sizes, 12 μm and 60 μm, and for different stress levels. As before, environmental tests were performed at a peak stress of 70 percent of the tensile strength in air. The results are found in Table XIX. It is apparent that the large grained material is not as adversely affected by mercury, nor is the life as enhanced in hydrogen. The fracture surface characteristics of the large grain samples were previously described on page and are shown in Figures 63 through 68. In contrast, the small grained samples showed much more intergranular-type failure. The sample tested in mercury illustrates the difference well, because mercury increases the tendency toward intergranular failure. Figures 72 and 73 show that the fracture was intergranular with tear ridges on some grains. The samples tested in hydrogen and air have almost identical fracture surfaces because the sample exposed to hydrogen did not break in the exposed gage length. Recalling the waisted geometry, the fracture occurred at a lower stress level in a protected area rather than at a higher stress in the exposed gage length. Notice that the fatigue life was exceptionally high for this series. Unfortunately, the life in hydrogen is not really known, though fatigue life enhancement is undeniable. The fracture surface of the sample fatigued in hydrogen, Figures 74 and 75, shows a great deal of transgranular tearing and little else. This seems to confirm for Incoloy 800 that increasing grain size decreases the susceptibility to hydrogen and mercury embrittlement in fatigue. One curiosity is that despite the greater propensity for intergranular failure of the fine grain size material,

TABLE XVIII

ENVIRONMENTAL FATIGUE LIFE OF INCONEL 600 AT 70 PERCENT OF THE TENSILE STRENGTH

Grain Size (10^{-6} m)	Hardness R_B	Fatigue Life (x 1000 Cycles)		
		Air	Mercury	Hydrogen
7	81	200[1]	60[1]	223
70	61	204	56	234

[1] Good [2]

TABLE XIX

ENVIRONMENTAL FATIGUE LIFE OF INCOLOY 800 AT
70 PERCENT OF THE TENSILE STRENGTH

Grain Size (10^{-6} m)	Hardness R_B	Fatigue Live (x 1000 Cycles)		
		Air	Mercury	Hydrogen
12	85	361	69	876[1]
60	65	142	98	155

[1] did not break in gage length

Figure 72. Fracture Surface of Small Grain (12 μm) Incoloy 800 Fatigued in Mercury at 70% of Tensile Strength (16X)

Figure 73. Origin Zone of Figure 72 Showing a Dirty Intergranular Fracture (500X)


25 160 548 1

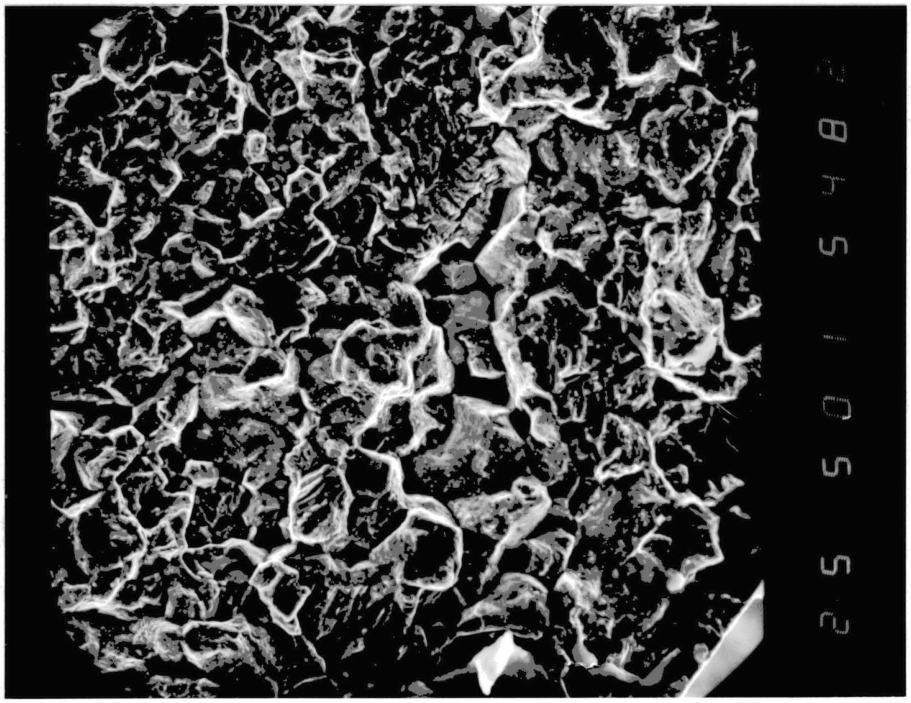
25 50 158 2

Figure 74. Fracture Surface of Small Grained Incoloy 800 Fatigued in Hydrogen at 70% of Tensile Strength (16X)

Figure 75. Origin Zone of Figure 74 Showing Intergranular Tearing (500X)

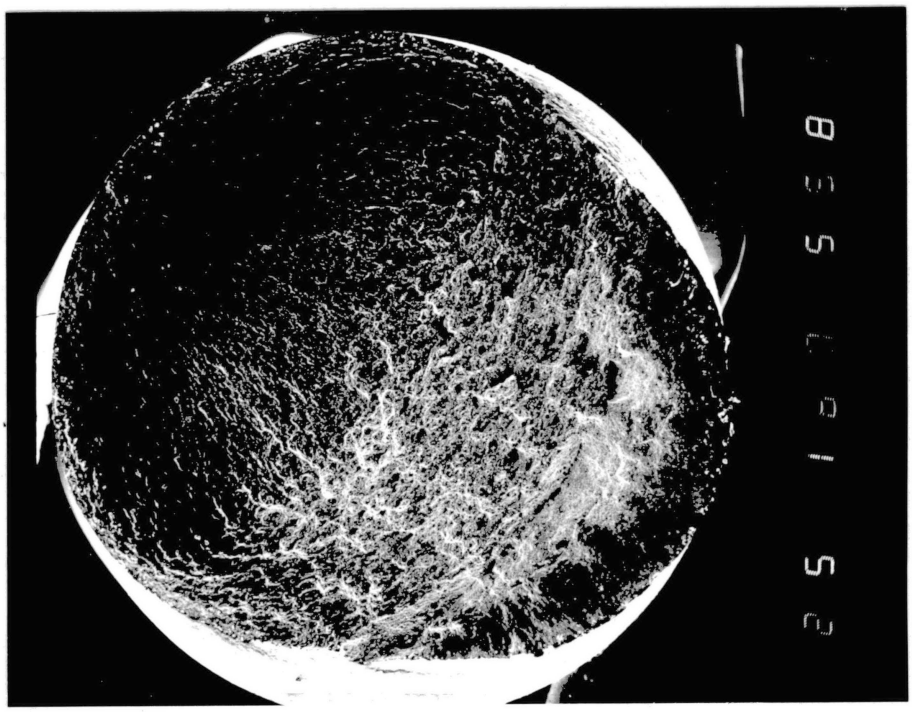

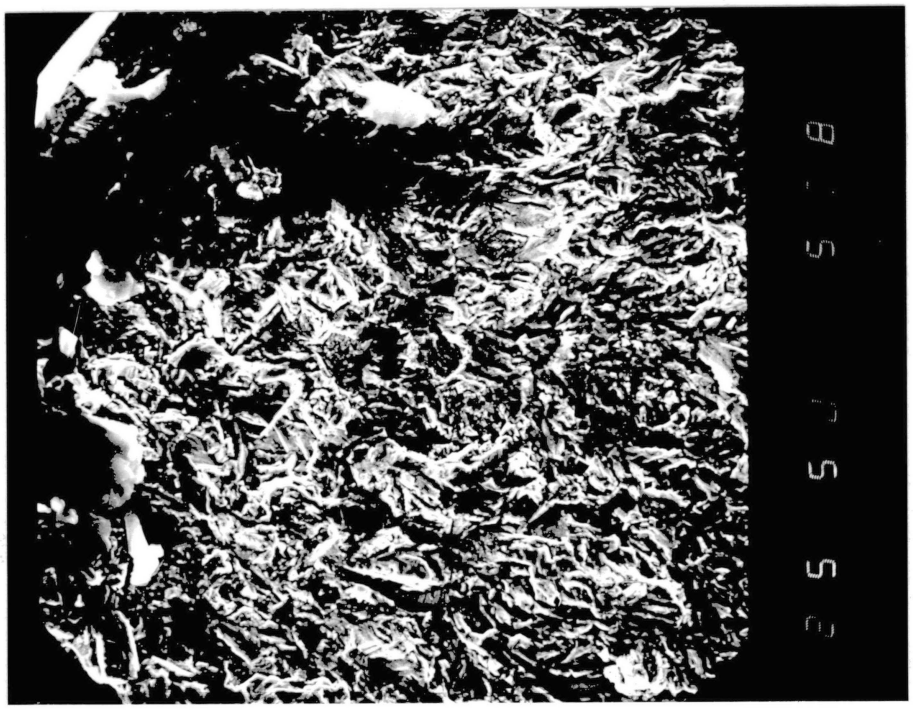

the fatigue life in hydrogen is enhanced more than the large grain size.

The next series of fatigue tests on Incoloy 800 investigated the environmental behavior at different peak stress levels. The 60 μm grain size samples were used. Stress levels tested were 70, 80, 90, and 95 percent of the tensile strength in air. The resulting fatigue lives shown in Table XX indicate some trends. As anticipated, the life in air decreases with increasing stress. This is also true in mercury and hydrogen, except for the samples tested at 70 percent of the tensile strength. Due to sample availability, these samples were of the constant cross section geometry rather than the waisted geometry like the others. The variation in stress field would surely have an effect on crack initiation and hence fatigue life. The constant cross section fatigue samples broke at the fillet. If we overlook the 70 percent tensile strength data, the remaining points are reasonable. Allowing for statistical variation, notice the lack of effect of mercury and enhancement of hydrogen. It appears that the amount of life enhancement is independent of stress level. As stress level was increased the fracture surfaced tended to become more transgranular and less intergranular, though not markedly. Otherwise, the general fracture surface character remains the same as the 70 percent tensile strength level.

Cold Worked Material

The final aspect of this thesis involved some tests on cold worked specimens of Incoloy 800 (UNS N08800) to determine whether the effects parallel those found in Nickel 200 and Monel 400 by Price and Good [1] and Traylor [3]. Both investigations found comparatively little embrittlement of the alloys in the cold worked state in either mercury or

TABLE XX

FATIGUE LIFE OF LARGE GRAIN (60 μm) INCOLOY 800

Fatigue Stress (kspi)	% Tensile Strength In Air	Life ($x10^3$ Cycles)		
		Air	Mercury	Hydrogen
64.2	70	142	98	155
73.6	80	131	168	509
82.8	90	105	84	307
87.4	95	52	60	187

hydrogen for tensile tests and fatigue tests. Consequently, cold worked (as received) samples of Incoloy 800 were fatigue tested in air, mercury, and hydrogen at 70 percent of the tensile strength in air. The results of these tests and the tests on the large grained material at the same stress level are shown in Table XXI. It appears that in all three environments the cold worked material performs slightly better than the large grained, annealed material. This effect might be due to work softening of the cold worked material.

Considering the relative fatigue lives and previous fractography, as expected the fracture surface characteristics were almost identical to the large grained sample except, of course, for the grain size. Once again, the samples from air and hydrogen environments were transgranular failures while the samples from mercury were transgranular with a tendency toward intergranular.

The fundamental result was that cold work decreased the relative embrittlement susceptibility in Incoloy 800 just as in the prior studies of the other alloys.

Discussion

Embrittlement Correlation

Several studies have attempted to correlate propensity for embrittlement with various factors such as stacking fault energy, strain hardening exponent, and slip character. Relative embrittlement is ambiguous in fatigue in either mercury or hydrogen. Monel 400 is extremely embrittled by both environments while the other alloys show very similar behavior. Except for Monel 400, the fatigue lives are reduced in mercury to 70 to 80 percent of that in air and are enhanced in hydrogen. This does

TABLE XXI

FATIGUE LIFE OF COLD WORKED AND ANNEALED INCOLOY 800 AT 82 KSPI

Condition	Hardness (R_B)	Grain Size (10^{-6} m)	Life (x 1000 Cycles)		
			Air	Mercury	Hydrogen
Cold Worked	92	20	154	105	546
Annealed	65	60	105	84	307

not appear to correlate with any material property. The relative ranking is the significant aspect. Table XXII lists an estimation of the stacking fault energy of each alloy as compiled from various sources [36, 37, 38]. Table XXIII is a ranking of various properties against relative embrittlement by mercury and by hydrogen. The highest strain hardening exponent, the highest stacking fault energy, the waviest slip character, and the least embrittled alloy are rank one; the other alloys follow by relative rank. Notice that the strain hardening exponent and relative embrittlement in mercury seem to correlate. Because of the small difference in value, the strain hardening exponent is not deemed a reliable property at this level of investigation. It was hoped that the stacking fault energy and slip character would correlate but this is not so. The lack of any correlation with hydrogen and embrittlement is also noted. It does not seem that propensity for embrittlement by hydrogen and mercury correlates with a single material property. A relationship might be found among several properties but that is beyond the scope of this study.

Relative Embrittlement of Hydrogen and Mercury

In tensile and fatigue tests on Monel 400, Fredell [5] found that mercury was a more potent embrittling agent than hydrogen. In tensile tests on Nickel 200, Traylor [3] found that hydrogen was somewhat more potent than mercury. For tensile tests, at least, the current study supports the findings of both studies. Furthermore, Inconel 600 and Incoloy 800 were found to be more embrittled by hydrogen than by mercury. Both Traylor [3] and Fredell [5] showed that relative embrittlement by hydrogen was not a result of inadequate hydrogen based on tests performed with different diameter specimens.

TABLE XXII

STACKING FAULT ENERGIES OF THE FOUR ALLOYS

Alloy	SFE ($erg\text{-}cm^{-2}$)
Nickel 200	130
Monel 400	80
Inconel 600	35
Incoloy 800	70

Source: Kotvall [36], Gallager [37], and Beeston [38].

TABLE XXIII

EMBRITTLEMENT CORRELATION WITH VARIOUS MATERIAL PROPERTIES

Alloy	Strain Hardening Exponent	Stacking Fault Energy	Slip Character	Embrittlement in Mercury	Embrittlement in Hydrogen
Nickel 200	2	1	2	2	3
Monel 400	4	2	3	4	4
Inconel 600	3	4	4	3	2
Incoloy 800	1	3	1	1	1

At least initially, embrittlement would seem a surface or near surface process. Mercury, with its large atom size, surely cannot penetrate below the surface of the metal. Hydrogen penetration should be minimal, since the diffusion rate of hydrogen in nickel is very low at 5×10^{-14} m^2/s at 25°C [39] and should be of the same order of magnitude for all four alloys. Depth of penetration is a function of the square root of the product of diffusivity and time [40]; hence the maximum penetration of hydrogen ahead of an advancing cracking is ~0.5 μm [39]. This does not seem significant for grain sizes greater than 25 μm. It would seem that the grain size would have to be less than 10 μm for hydrogen penetration to have a notable effect at room temperature.

A comparison of hydrogen embrittlement of the four alloys tested and hydrogen embrittlement of steels can be made. Due to the much higher diffusion rate of hydrogen into steels [41], cracking initiates below the surface in the plane strain zone and surface break, though it occurs later. If hydrogen penetration were significant, similar subsurface crack initiation would be expected. Fredell [5] found no evidence of subsurface crack initiation in Monel 400 and this study concurs. Furthermore, no evidence of subsurface crack initiation was found in any of the alloys tested.

Fracture Surface Characteristics

After Beachem [25] and precursory studies, a generalized fracture sequence was identified. If we extend the range of characteristics to include all four alloys in air, mercury, and hydrogen for tensile and fatigue tests, then the surface to center cracking sequence is intergranular, crystallographic transgranular, noncrystallographic

transgranular, and thence microvoid coalescence. Certainly, no one alloy exhibited the entire sequence but each may be fitted into the series for all testing conditions. Cracking in Monel 400 tends to begin at the intergranular level while Incoloy 800 tends to begin at the transgranular level. Cold work delays cracking to later in sequence, as does increasing grain size. For Monel 400, cracking due to hydrogen is a little later in the sequence than that due to mercury. The other alloys tend to start the sequence a little later. Since fatigue initiates cracking at lower stress, samples tested in fatigue initiate cracking earlier in the sequence than tensile tested samples. Beachem [25] correlated the transition in fractography with an increase in stress intensity factor, i.e., intergranular fracture at low stress intensity, going to transgranular and microvoids at higher stress intensity. The greater propensity of intergranular fracture in mercury indicates fracture at lower stress intensity. This is consistent with the findings by Traylor [3] for Nickel 200 and this study for Inconel 600 and Incoloy 800 that intergranular fracture may be found in fatigue but not in tensile tests. The propensity for clean intergranular fracture was greater in Inconel 600 than in Incoloy 800. This is also consistent with the significant loss of strength and ductility in Monel 400.

The stress intensity is proportional to the square root of the plastic zone radius [28]. Therefore, increasing stress gives increasing strain around the crack tip. It can be argued that at some critical stress intensity the plastic deformation and dislocation density reach threshold value where specific planes of atoms within the grain become more thermodynamically active than the grain boundary atoms and therefore react at least equally if not preferentially. This is consistent

with the results of the precursory studies and this study on cold worked (prestrained) Nickel 200, Monel 400, and Incoloy 800. The results have not been verified for Inconel 600 but contrary behavior is not likely. The threshold strain is probably different for each alloy.

Grain Size Effects

Kamdar [11] and Gordan and An [16] proposed that in LME the fracture strength of the metal is proportional to the inverse of the square root of the average grain diameter, the Petch relationship. The relationship has been verified for zinc [42] and cadmium [12] which have hexagonal close packed (HCP) crystal structures. The relationship has also been validated for BCC metals but not conclusively for the FCC alloys of this study. Fredell [5] found a slight increase in embrittlement for relatively small grain size samples and a decrease in embrittlement for very coarse grains (250 μm). In this study data for Inconel 600 and Incoloy 800 are available for two different grain sizes. In both alloys embrittlement by either mercury or hydrogen was less at the larger grain size. This does not support the Petch relationship. There are not enough data to detect a reversal of the trend as noted by Fredell [5] for Monel 400.

Side Damage Observations

It was noted that all four alloys show side cracking in tensile tests in air at slip bands, elongated grain boundaries, and presumably inclusions. Monel 400 is much more severely embrittled by both hydrogen and mercury than the other alloys. Perhaps it is pertinent that Monel 400 shows more side cracking when fractured in air than the other alloys. Presuming that air is not an active environment, something about Monel

400 makes it inherently the most susceptible to cracking. In tensile tests, Nickel 200, Inconel 600, and Incoloy 800 were more embrittled by hydrogen than by mercury but apparently Monel 400 differs, but even in Monel 400 the side cracking seems to be more extensive in hydrogen.

It appears, therefore, that hydrogen does not stimulate crack propagation once the mode ceases to be intergranular. An example of this is Inconel 600 tested in hydrogen which cracked very extensively, intergranularly well below the tensile strength, yet there was no significant loss of tensile strength (Figures 29 through 32). Also, for fatigue tests of Nickel 200, Inconel 600, and Incoloy 800, fatigue lives are improved in the presence of hydrogen, which presumably hinders crack propagation because cracks generally initiate early in fatigue.

Working Hypothesis of LME and HE

By utilizing concepts from several models by other investigators, combining the pieces, and extending the result, a working hypothesis has been developed consistent with most of the observations of this and the precursory studies, that may merit a follow up.

Initially, the embrittling atoms are chemisorbed at the metal surface as per Kamdar [11]. If, for the moment, we allow that boty hydrogen and mercury act by decreasing the cohesive stress as suggested by Kamdar, then the applied stress initially facilitates intergranular cracking, because intergranular failure is favored by one or more of the following:

1. Atoms in a higher energy state than surrounding atoms are more susceptible.

2. Preferential adsorption at grain boundaries due to less efficient packing.

3. Different atoms species due to segregation.

4. Grain boundary relaxation processes.

After initiation, as the crack advances, the stress intensity at the crack tip increases and this favors plastic deformation. If chemisorption leads to a decrease in cohesive strength, then it may also decrease the shear strength.

Again, allowing for the moment, that both hydrogen and mercury promote plastic deformation, perhaps by increasing dislocation initiation as proposed by Lynch [17], then extensive but localized plastic deformation will blunt the crack tip, thereby inhibiting grain boundary cracking. Plastic deformation can produce slip band cracking (recall the behavior of the specimens tested in air which developed cracks at the side of the neck). Therefore, we get shear for slip band cracking instead. More plastic deformation implies more work hardening; therefore, the crack does not grow unstably. Additionally, plastic deformation occurs in an enclave at the crack tip and total behavior is dominated by surrounding bulk material. Therefore, increased stress is needed to move the cardiodal zone of influence and advance the crack tip.

Both mercury and hydrogen can act at the crack tip, for example, to facilitate dislocation nucleation, but only hydrogen can diffuse ahead of the crack tip or channel along dislocation lines or along slip planes, thereby also influencing plastic deformation in a larger zone. Therefore, hydrogen is a more effective promoter of plastic deformation and consequently blunts the crack tip more than mercury. The mercury must be a surface effect; hydrogen can be, to a limited extent, a volume effect. Perhaps also, as Vehoff and Rothe [24] indicate, the smaller hydrogen atom can get closer to the tip of a sharp crack and thereby facilitate

blunting at a lower stress intensity. While hydrogen may cause more intergranular cracking initially, it will cause more blunting, hence less integranular cracking eventually. Given enough strain, enough stress intensity, voids can form ahead of the advancing crack tip and void coalescence mechanism takes over, as per Beachem [25].

Those conditions restricting plastic deformation promote intergranular embrittlement; conditions favoring plastic deformation restrict intergranular embrittlement, particularly in hydrogen. If the foregoing ideas are valid, they must be consistent with actual observations. Some of the consequences of this explanation are the following:

1. Plastic constraint conditions such as triaxial stresses and plane strain will promote transgranular fracture. From Good [1], for example, if a sample is broken quickly in mercury, the result is a cup-cone fracture with extensive longitudinal cracking. The effect is greater in cold worked materials.

2. Increasing grain size should have relatively little effect on stress levels to initiate intergranular cracking. Increasing grain size should decrease the yield strength and should encourage plastic deformation, thereby inhibit intergranular cracking and promote ductility as grain size increases.

3. Increasing strain rate should: (a) inhibit plastic deformation by increasing the yield strength; (b) allow less time for any hydrogen penetration ahead of the crack tip; and (c) if, like Gordon and An [16], there is an incubation period for crack initiation, intergranular or transgranular, it should inhibit initiation. Thus (a) and (b) would promote intergranular embrittlement, while (c), if operative, would decrease embrittlement. We know from Fredell [5] that increasing strain rate de-

creases mercury embrittlement and at a high enough strain rate we get cup-cone fracture. Likewise in hydrogen embrittlement but the effect is less conspicuous.

4. In fatigue, crack initiation is easy, rapid crack propagation behavior matters. Therefore, if hydrogen promotes plastic deformation and blunting while mercury does not, fatigue lives may be improved in hydrogen but worse in mercury. At the stress intensity levels of fatigue testing, the threshold for blunting has been reached in hydrogen but not in mercury. Fatigue fractures tend to be transgranular in hydrogen and intergranular in mercury.

The foregoing ideas seem to explain the observations of this and precursory studies but the detailed investigation necessary to validate the ideas is beyond the scope of this investigation. The concepts have merit and bear further scrutiny.

CHAPTER V

SUMMARY

1. All four alloys tested are embrittled by hydrogen and mercury. For Monel 400, mercury is the more severe environment, though loss of strength and ductility occurred in hydrogen as well. The other three alloys were more severely embrittled by hydrogen in tensile tests but not in fatigue testing.

2. A common fracture sequence of intergranular, crystallographic transgranular, noncrystallographic transgranular, and microvoid coalescence was identified for all four alloys in both environments. The initial cracking mode of each sample was governed by alloy, grain size, cold work, and environment. Strain rate effects were not investigated. This sequence was associated with an increasing stress intensity at the advancing crack tip.

3. All four alloys seem to eventually exhibit a decrease in embrittlement by hydrogen and by mercury for increasing grain size. It does not appear that changes in embrittlement occur at the same rate for each alloy.

4. The gatigue life of all four alloys was reduced in mercury and, except for Monel 400, fatigue lives were enhanced in hydrogen.

5. The foregoing were explained using aspects of embrittlement theories extant in the literature. Following chemisoption, both hydrogen and mercury promote intergranular embrittlement initially by a

reduction in bond strength but that eventually plastic deformation dissipates the localized stress intensities.

BIBLIOGRAPHY

1. Price, C. E. and J. K. Good. Unpublished Research, Okahoma State University, 1982.

2. Good, J. K. Unpuslished Research, Oklahoma State University, 1982.

3. Traylor, L. B., "A Comparison of Hydrogen and Mercury Embrittlement of Nickel Based Alloys." (Unpublished M.S. Thesis, Oklahoma State University, 1983.)

4. Traylor, L. B. Unpublished Research, Oklahoma State University, 1983.

5. Fredell, R. S., "A Detailed Comparison of Hydrogen and Mercury Embrittlement in Monel 400." (Unpublished M.S. Thesis, Oklahoma State University, 1983.)

6. Handbook of Huntington Alloys. The International Nickel Company, Inc., Number 20M 7-69 5-9, Huntington, West Virginia, 1969.

7. Tuttle, R. N. and R. D. Kane, "State-of-the-Art of H_2S Corrosion Problem Solving." Materials Performance, 1, 9-10, (1983).

8. Shunk, F. A. and W. R. Warke, "Specificity as an Aspect of Liquid Metal Embrittlement." Scripta Metallurgica, 8, 519-526, (1974).

9. Fontana, F. G. and N. D. Greene. Corrosion Engineering, 2nd. Ed., New York: McGraw-Hill Book Co., 1978.

10. Westwood, A. R. C. and M. H. Kamdar, "Concerning Liquid Metal Embrittlement, Particularly of Zinc Moncrystals by Mercury." Phil. Mag., 8, 787-804, (1963).

11. Kamdar, M. H., "Embrittlement by Liquid Metals." Progress in Materials Science, 15, 289-374, (1973).

12. Stoloff, N. S. and T. L. Johnston, "Crack Propagation in a Liquid Metal Environment." Acta Metallurgica, 11, 251-256, (1963).

13. Gilman, J. J. Plasticity. Oxford: Pergamon Press, 1960.

14. Kelly, A., W. R. Tyson, and A. H. Cottrell, "Ductile and Brittle Crystals." Phil. Mag., 15, 567, (1967).

15. Kristal, M. A., "The Formation of Dislocations in Metals on Diffusion of Surface-Active Substances in Connection with the Effect of Adsorption Embrittlement." Sov. Phys.-Doklady, 15, 614-617, (1970).

16. Gordon, P. and H. H. An, "The Mechanisms of Crack Initiation and Crack Propagation in Metal-Induced Embrittlement of Metals." Metallurgical Transactions, 3, 437-451, (1972).

17. Lynch, S. P., "Hydrogen Embrittlement and Liquid Metal Embrittlement in Nickel Single Crystals." Scripta Metallurgica, 13, 1051-1056, (1979).

18. Lynch, S. P., "Mechanisms of Hydrogen-Assisted Cracking." Metals Forum, 2, 189-199, (March, 1979).

19. Stoloff, N. S., S. Ashok, M. E. Glicksman, and T. Slavin, Technical Report, ONR Number N00014-79CD583, 1980.

20. Naguno, H. and T. Takahashi, "Hydrogen Embrittlement of Some Fe - Amorphous Alloys." Material Science and Engineering, 23, 257-259, (1976).

21. Kawashima, A., K. Hashimoto, A. Masuroto, "Fractographic Study of Amorphous Iron Based Alloys Embrittled by Hydrogen and Heat Treatment." Scripta Metallurgica, 14, 41-45, (1980).

22. Lynch, S. P., "A Fractographic Study of Gaseous Hydrogen Embrittlement in a Tempered-Martinsitic Steel." Acta Metallurgica, 1, 79-90, (1984).

23. Bernstein, I. M. and A. W. Thompson, "Hydrogen in Metals." (ASM) Metals Park, Ohio, 1974.

24. Vehoff, H. and W. Rothe, "Gaseous Hydrogen Embrittlement in F_eS_i - and N_i - Single Crystals." Acta Metallurgica, 11, 1781-1793, (1983).

25. Beachem, C. D., "A New Model for Hydrogen-Assisted Cracking." Metallurgical Transactions, 3, (437-451, (1972).

26. Zapffe, C. A., "Newman Bands and the Planar Pressure Theory of Hydrogen Embrittlement." Journal of the Iron and Steel Institute. 154, 123, (1946).

27. Tetelman, A. S. and W. D. Robertson, "The Mechanisms of Hydrogen Embrittlement Observed in Iron-Silicon Single Crystals." Transactions of the AIME, 224, 775, (1962).

28. Hertzburg, R. W. Deformation and Fracture Mechanics of Engineering Materials. 2nd Ed., New York: John Wiley and Sons, 1983.

29. Petch, N. J. and P. Stables, "Delayed Fracture of Metals Under Static Load." Nature, 169, 842-843, (1952).

30. Costas, L. P., "Effect of Phosphorus on the Embrittlement of Copper-Nickel Alloys by Mercury." Corrosion-NACE, 31, 11, (1975).

31. Funkenbusch, A. W., L. A. Heldt, and D. F. Stein, "The Influence of Grain Boundary Phosphorus Concentration on Liquid Metal and Hydrogen Embrittlement of Monel 400." Metallurgical Transactions, 13A, 611-618, (1982).

32. Parkins, R. N., "Development of Stress Corrosion Cracking Testing and Implications." ASTM STP 665, pp. 5-25.

33. Tegart, W. J. McG. The Electrolytic and Chemical Polishing and Metals. 2nd Ed., New York: Pergamon Press, Inc., 1959.

34. "Standard E8-Tension Testing of Metallic Materials." American Society for Testing and Materials, 1983 ed.

35. Datsko, J. Material Properties and Manufacturing Processes. New York: John Wiley and Sons, 1973.

36. Kotval, P. S., "The Microstructure of Superalloys." Metallography, 1, 251-285, (1969).

37. Gallagher, P. C. J., "The Influence of Alloying, Temperature, and Related Effects on the Stacking Fault Energy." Metallurgical Transactions, 1, 2429-2461, (1970).

38. Beeston, B. E. P. and L. K. France, "Stacking Fault Energy of Binary Nickel Alloys Fundemental to the Nimonic Series." Journal for the Institute for Metals, 96, 105-107, (1968).

39. Joosten, M. W., T. D. Lee, T. Goldenburg, and J. P. Hirth, "Hydrogen Effects in Metals." Third International Conference on Effect of Hydrogen on Behavior of Materials, AIME (1980), pp. 839-850.

40. Van Vlack, L. H. Elements of Materials Science and Engineering. 4th Ed. Reading, Mass.: Addison-Wesley Publishing Co., Inc., 1980.

41. Mashino, S. E., "The Diffusion of Hydrogen in Iron and Steel." (Unpublished M.S. Thesis, Oklahoma State University, 1982.)

42. Kamdar, M. H. and A. R. C. Westwood, "Effects of Alloying on the Brittle Fracture of Zinc in Liquid Mercury." Acta Metallurgica, 16, 1335-1341, (1968).

APPENDIX A

CALCULATION OF THE STRAIN HARDENING EXPONENT

This appendix reviews the conversion of engineering stress and engineering strain to true stress and true strain. Then the method used to obtain the strain hardening exponent and the strength coefficient is shown. Let

σ_E = engineering stress;

ε_E = engineering strain;

σ_T = true stress;

ε_T = true strain;

A_i = incremental cross sectional area;

A_o = original cross sectional area;

$\Delta\ell$ = change in length;

ℓ_o = original length; and

P = load.

Recall

$$\varepsilon_E = \frac{\Delta\ell}{\ell_o} \tag{A.1}$$

$$\varepsilon_T = \ell n\ (1 + \varepsilon_E) \tag{A.2}$$

$$\delta_T = \frac{P}{A_i} \tag{A.3}$$

Assume plastic deformation which is constant volume. Therefore,

$$A_i = \frac{A_o \ell_o}{\ell_i} \tag{A.4}$$

Hence

$$\sigma_T = \frac{P\ell_i}{A_o \ell_o} \tag{A.5}$$

which reduces to

$$\sigma_T = \sigma_E \ (1 + \varepsilon_E) \tag{A.6}$$

The resulting values for true stress and true strain were plotted on a log-log scale. This should result in a linear graph. Recall

$$\sigma_T = K\varepsilon_T^n \tag{A.7}$$

where

n = strain hardening exponent; and

K = strength coefficient, a material constant.

Taking the log of both sides,

$$\log \sigma_T = \log K + n \log \varepsilon_T \tag{A.8}$$

The form of the equation is linear with n being the slope and log K being the y intercept.

APPENDIX B

STRAIN HARDENING EXPONENT IN TERMS OF TRUE STRAIN

This analysis by Hertzberg [28] shows that the plastic true strain at necking is numerically equal to the strain hardening exponent.

Recall that

$$\sigma = K\varepsilon^{n} \tag{B.1}$$

where

σ = true stress;

ε = true strain;

n = strain hardening exponent; and

K = strength coefficient, defined as the true stress at a true strain of 1.0;

and

$$P = \sigma A \tag{B.2}$$

where

P = incremental load; and

A = incremental area;

also

$$dP = \delta dA + A d\delta \tag{B.3}$$

Recalling that necking occurs at maximum load,

$$dP = 0 \tag{B.4}$$

so that

$$\frac{d\sigma}{\sigma} = -\frac{dA}{A} \tag{B.5}$$

Recall that plastic deformation is a constant volume process such that

$$\ell_1 A_1 = \ell_2 A_2 = \text{constant} \tag{B.6}$$

hence

$$A d\ell + \ell dA = 0 \tag{B.7}$$

$$\frac{-dA}{A} = \frac{d\ell}{\ell} \tag{B.8}$$

Since $d\ell/\ell \equiv dE$, we find

$$\sigma = \frac{d\sigma}{d\varepsilon} \tag{B.9}$$

Using Equation (B.1)

$$K\varepsilon^n = Kn\varepsilon^{n-1} \tag{B.10}$$

Therefore,

$$n = \varepsilon \tag{B.11}$$

VITA 2

James Arthur Morris

Candidate for the Degree of

Master of Science

Thesis: HYDROGEN AND MERCURY EMBRITTLEMENT OF SELECTED NICKEL-BASED ALLOYS

Major Field: Mechanical Engineering

Biographical:

Personal Data: Born in Grants, New Mexico, November 10, 1959, the son of Mr. and Mrs. Wesley B. Morris.

Education: Graduated from Sapulpa High School, Sapulpa, Oklahoma, in May, 1978; received the Bachelor of Science degree in Mechanical Engineering from Oklahoma State University in May, 1982; completed requirements for the Master of Science degree at Oklahoma State University in May, 1984.

Professional Experience: Apprentice Pipefitter, summers of 1978 through 1982; Associate Engineer, Fife Corporation, 1982; Graduate Teaching Assistant, Oklahoma State University, 1982 and 1983; Engineer-in-Training, November, 1982.

Professional Organizations: American Society of Mechanical Engineers, National Society for Professional Engineers, Oklahoma Society for Professional Engineers.